BEST AVAILABLE IMAGES

Defective images within this document are accurate representations of The original documents submitted by the applicant.

Defects in the images may include (but are not limited to):

- BLACK BORDERS
- TEXT CUT OFF AT TOP, BOTTOM OR SIDES
- FADED TEXT
- ILLEGIBLE TEXT
- SKEWED/SLANTED IMAGES
- COLORED PHOTOS
- BLACK OR VERY BLACK AND WHITE DARK PHOTOS
- GRAY SCALE DOCUMENTS

IMAGES ARE BEST AVAILABLE COPY.

As rescanning documents *will not* correct images, please do not report the images to the Image Problem Mailbox.

PA 165034

THE UNITED STATES OF AMERICA

TO ALL TO WHOM THESE PRESENTS SHALL COME:

UNITED STATES DEPARTMENT OF COMMERCE

United States Patent and Trademark Office

October 22, 1999

THIS IS TO CERTIFY THAT ANNEXED HERETO IS A TRUE COPY FROM THE RECORDS OF THE UNITED STATES PATENT AND TRADEMARK OFFICE OF THOSE PAPERS OF THE BELOW IDENTIFIED PATENT APPLICATION THAT MET THE REQUIREMENTS TO BE GRANTED A FILING DATE UNDER 35 USC 111.

APPLICATION NUMBER: ***60/103,559***
FILING DATE: ***October 07, 1998***

PRIORITY DOCUMENT

SUBMITTED OR TRANSMITTED IN
COMPLIANCE WITH RULE 17.1(a) OR (b)

By Authority of the
COMMISSIONER OF PATENTS AND TRADEMARKS

P. SWAIN
Certifying Officer

PROVISIONAL APPLICATION COVER SHEET

This is a request for filing a PROVISIONAL APPLICATION under 37 CFR 1.53(c).

Docket Number	9820-0001-2 PROV	Type a plus sign (+) inside this box →	+

JC541 U.S. PTO 60/103559 10/07/98

INVENTOR(s)/APPLICANT(s)			
LAST NAME	FIRST NAME	MIDDLE INITIAL	RESIDENCE (CITY AND EITHER STATE OR FOREIGN COUNTRY)
~~Bevilacqua~~ Lepeursinge	Frederic Christian		Lausanne, Switzerland Lausanne, Switzerland

TITLE OF THE INVENTION (280 CHARACTERS MAX)

METHOD AND APPARATUS FOR MEASURING LOCALLY AND SUPERFICIALLY THE SCATTERING AND ABSORPTION PROPERTIES OF TURBID MEDIA

CORRESPONDENCE ADDRESS

OBLON, SPIVAK, MCCLELLAND, MAIER & NEUSTADT, P.C.
1755 Jefferson Davis Highway, Suite 400
Arlington

Phone: (703) 413-3000 Fax: (703) 413-2220

STATE	Virginia	ZIP CODE	22202	COUNTRY	USA

ENCLOSED APPLICATION PARTS (*check all that apply*)

- ■ Specification — *Number of Pages* 62
- ■ Drawing(s) — *Number of Sheets* 46
- □ Small Entity Statement
- □ Other (specify) _____

METHOD OF PAYMENT (*check one*)

■	A check or money order is enclosed to cover the Provisional Filing Fees	PROVISIONAL FILING FEE AMOUNT ($)	$150.00
□	The Commissioner is hereby authorized to charge filing fees and credit Deposit Account Number: _____		

The invention was made by an agency of the United States Government or under a contract with an agency of the United States Government.

■ No

□ Yes, the name of the U.S. Government agency and the Government contract number are:

Respectfully submitted,

SIGNATURE _____ Date October 7, 1998

TYPED or PRINTED NAME Gregory J. Maier REGISTRATION NO. 25,599
Vincent J. Sunderdick (*if appropriate*) 29,004

□ Additional inventors are being named on separately numbered sheets attached hereto.

PROVISIONAL APPLICATION FILING ONLY

METHOD AND APPARATUS FOR MEASURING LOCALLY AND SUPERFICIALLY THE SCATTERING AND ABSORPTION PROPERTIES OF TURBID MEDIA

Inventors: **Frédéric Bevilacqua**,
Swiss Federal Institute of Technology - Lausanne, Switzerland,
Christian Depeursinge,
Swiss Federal Institute of Technology - Lausanne, Switzerland.

References Cited

U.S PATENTS DOCUMENTS

5,284,137	2/94	Kessler et al.	128/633
5,517,987	5/96	Tsuchiya	128/633
5,630,423	5/97	Wang et al.	128/664
5,645,061	7/97	Kessler et al.	128/634
5,676,142	10/97	Miwa et al.	128/633

OTHER PUBLICATIONS

1. See "Welch, A. J.; van Gemert, M. J. C. *Optical Thermal Response of Laser Irradiated Tissue*; Plenum publishing Corp., New York, 1995", and references therein.

2. W.-F. Cheong, S.A. Prahl, and A.J. Welch, "A Review of the Optical Properties of Biological Tissues," IEEE J. Quantum Electron. 26, 2166-2185 (1990).

ABSTRACT

We present a method and apparatus for local and superficial measurement of the optical properties of turbid media. The depth probed is on the order of 1 transport mean free path of the photon. The absorption coefficient, reduced scattering coefficient and a phase function parameter are computed from a single measurement of the spatially resolved reflectance close to the source (around one transport mean free path). Measurements on biological tissues can be achieved using a probe of diameter less than 2 mm, and the average volume probed is on the order of 1 mm^3.

BACKGROUND AND SUMMARY OF THE INVENTION

1. Field of the invention

The present invention relates to a method and an apparatus to quantify the optical scattering and absorption properties of a turbid media. More precisely the present invention relates to a non-invasive measurement, over a small area of the sample surface. Local and superficial characterization of biological tissues *in vivo* is a major application of this invention.

2. Related Background Art.

Different techniques have already been proposed to quantitatively determine the absorption and reduced scattering coefficients of turbid media[1]. Most of the non-invasive methods are based on the measurement of spatially and/or temporally-resolved reflectance. The principle is as follows: the turbid medium is illuminated by a light source. The backscattered light is measured by one or several detectors. Different types of measurements are possible, depending on the time-dependence of the illuminating source: steady-state (continuous source), time-domain (short pulsed source) or frequency domain (amplitude modulated source). The present invention relates to the case of steady-state measurements, performed at different distance ρ between the source and the detectors.

The range of ρ values is an important point to consider, when comparing different methods based on the reflectance. First, the probed volume of the turbid medium is related to the source-detector separation ρ. The larger the source-detector separation, the deeper the average depth probed. Second, depending on the range of ρ, different mathematical processing must be used to obtain

the optical properties from the raw data.

At least two cases must be distinguished.

1) The first case corresponds to source-detector separations larger than several transport mean free paths. For biological tissues[2], this case correspond to source-detector separation of typically larger than 2 mm. An analytical form of the reflectance can be obtained from the diffusion equation, if the absorption coefficient μ_a is sufficiently lower than the scattering coefficient μ_s (typically at least ten times). In such a case, the relevant optical properties are the refractive index, the absorption coefficient and the reduced scattering coefficient. The average depth of probing is on the same order than the source-detector separation.

Such methods have been already published, and are the object of patents (Ref.1, Patent 517,987 Tsuchiya, Patent 5,676,142 Miwa et al.).

2) The second case corresponds to source-detector separations close to one transport mean free path. For biological tissues[2], source-detectors separation range typically between 0.1 to 2 mm, and the average depth probed is on the order of 1 mm. Such small source-detector separations enables to measure locally the optical properties.

In this case, light propagation can be modeled using Monte Carlo simulations. In contrast to the previous case 1), it was found that not only the first moment of the phase function must be considered, but also the second moment. Precisely, the relevant optical properties are the refractive index, the absorption, the reduced scattering coefficient and a parameter γ taking into account the two first moments of the phase function, and that we called the "phase function parameter".

Different methods have been proposed for local characterization of turbid media, and in particular of biological tissues. Wang et al. (Patent 5,630,423) proposed a method for the determination of the reduced scattering coefficient only, using an optical beam of oblique incidence. Moreover, their analysis does not include the effect of the phase function. Kessler et al. (Patents 5,284,137 and 5,645,0619) proposed a method for local dye concentration and scattering parameters in animal and human tissues, based on spatial and spectral measurements. However, their methods do not enable to the determine the absorption coefficient, reduced scattering coefficient and the parameter γ.

In the present invention we present a method and apparatus for the measurement of the absorption coefficient, the reduced scattering coefficient and the said phase function parameter γ, from the spatially-resolved reflectance data at short source detector separation. The parameters determination procedure is based on the analysis of the reflectance, at short source-detector separation, we performed with Monte Carlo simulations. These parameters, which can be measured at different wavelengths, enable us to characterize turbid media, such as biological tissues.

BRIEF DESCRIPTION OF THE DRAWINGS

Fig.1. Description of the principle of spatially-resolved reflectance measurement.

Fig.2. Density probability function for the mean depth of scattering event. Case of detected photons at distances 0.3, 1, 1.5 mfp'.

Fig.3. Examples of reflectance obtained with different phase functions. Case of matched refractive index (n=1.0).

Fig.4. Monte Carlo simulations and fits on the form $R(\rho) \equiv [A(\rho, \mu_s', \gamma) + \mu_s' B(\mu_a)]^2$. Case of γ=1.9, numerical aperture of the source and detectors = 0.37.

$$A = 0.0647\rho^{0.324}\exp(-0.161\rho),$$

$$B = 0.18653\,\mu_a - 0.8466\,\mu_a^2 + 1.836\mu_a^3$$

Fig.5.a. Basic description of the apparatus. Case of measurement with an optical fiber probe

Fig. 5.b Basic description of the apparatus. Case of measurement with sources and detectors directly in contact with the turbid medium.

Fig. 5.c. Basic description of the apparatus. Case of non-contact measurements with a 1D or 2D detector, coupled to an imaging device.

Fig. 5.d Basic description of the apparatus. Case of non-contact measurements with a scanning devices to illuminate and/or collect the backscattered light.

Fig.6. Examples of the sample ending of the fiber optical probe.

6a. simple arrangement for a single measurement.
6b. arrangement for symmetrical measurements.
6c.Arrangement for multiple measurements.
6d. Arrangement for multiple measurement, using an multicore fiber.

Fig.7. Example of a measured the spatially-resolved reflectance with the probe 2a. The measurement, performed on a microsphere suspension, is superimposed to a Monte Carlo simulation. The optical properties, computed from published water properties and Mie theory are: n=1.33, μ_a=0.0004 mm^{-1}, μ_s'=1.0 mm^{-1}, γ=2.2. The calibration was performed with a siloxane sample of known optical properties.

Fig.8. Relation between the parameters R(ρ=1 mm) and $|\partial_\rho \ln R(\rho=1\text{ mm})|$ and the optical coefficients μ_s' and μ_a. Case of γ=1.5 and 1.9. Probe of refractive index = 1.5, sample of refractive index = 1.4, optical fibers diameter = 200 μm, NA=0.37 (source and collection).

Fig.9. Plot of the parameter $\frac{\partial}{\partial\rho}\sqrt{R}$ for different γ values (1.0, 1.8, 2.5), different reduced albedo a' (1, 0.95, 0.9) and for fixed ρ=1 mm.. Mismatched refractive index n=1.4.

Fig.10 Plot of $\sqrt{R(a)'} - \sqrt{R(a'=1)}$ for different γ values and reduced albedo a', and for fixed ρ=1 mm. Mismatched refractive index n=1.4.

DETAILED DESCRIPTION OF THE INVENTION

1. Definitions

The concept of spatially resolved reflectance is illustrated in Fig.1. Consider light impinging on a turbid medium (through air or through a light guide), in a given solid angle ω_{source}. The spatially resolved reflectance R(ρ) is defined by the backscattered light power in a given solid angle $\omega_{detector}$ at a distance ρ from the source, per unit area and normalized by the source power. The distance ρ is referred as the source-detector separation (also in the case when light guides or imaging devices are used for the illumination and for the collection of the backscattered light).

R(ρ) depends on the optical properties of the turbid medium, defined below. Note that R(ρ) depends also on the source and detectors characteristics, i.e numerical aperture and sizes.

It is commonly admitted that the fundamental optical properties of a turbid medium is determined by the average index of refraction n of the medium, the absorption coefficient μ_a, the scattering coefficient μ_s, and the phase function p(θ) where θ is the scattering angle. The absorption coefficient μ_a [m^{-1}] is defined as the probability of absorption per unit infinitesimal pathlength. The scattering coefficient μ_s [m^{-1}] is the scattering probability per unit infinitesimal pathlength. The phase function p(θ) is the density probability function for the scattering

angle θ. The phase function is normalized as follows:

$$1 = 2\pi\int_0^{\pi} p(\theta)\sin\theta d\theta . \quad (1)$$

The n^{th} order moment g_n of the phase function is defined as:

$$g_n = 2\pi\int_0^{\pi} P_n(\theta)p(\theta)\sin\theta d\theta \quad (2)$$

where $P_n(\theta)$ is the Legendre polynomial of order n. The first moment of the phase function is also called the anisotropy factor, and is often simply noted g ($=g_1$). It represents the mean cosine of the scattering angle. The reduced scattering coefficient μ_s' is defined as:

$$\mu_s' = \mu_s(1-g_1) \quad (4)$$

The transport mean free path (or reduced mean free path) mfp' is defined as:

$$mfp' = (\mu_s'+\mu_a)^{-1} \quad (5)$$

The reduced albedo a' is the ratio:

$$a' = \mu_s'/(\mu_s'+\mu_a) \quad (6)$$

As a result of the present invention described in more details in the next section, it is also necessary to define another phase function parameter called γ:

$$\gamma = (1-g_2)/(1-g_1) \quad (7)$$

All the parameters listed above are referred as optical properties. They are wavelength dependent, and can vary in space and time.

2. Reflectance measurements at distances close to one transport mean free path

The methods described in the Patent 517,987 (Tsuchiya) are based on measurements with large range of source-detector separations, typically from 1 mfp' to 10 mfp'. In such cases, the volume probed is on the order of 10-1000 $(mfp')^3$. In contrast with such a large scale investigation, the present invention is directed to a novel approach where the volume probed is much smaller, on the order of 1 $(mfp')^3$. This is achieved by using *only* small source detector separations, typically from 0.1 to 2 mfp'. The lateral dimension of probing is limited to this range of distances.

A model of photon migration in tissues was necessary to predict the relationship between the measured reflectance and the optical properties. Analytical solutions from the diffusion equation are not appropriate in our case because we are interested in the reflectance close to the source, at distance comparable to the transport mean free path [mfp']. This is part of the invention to have performed Monte Carlo simulations to predict the measured reflectance of an homogeneous semi-infinite turbid media.

The exact diameter of the illuminating and collecting fibers, as well as their numerical apertures, have been taken into account in the simulations. The mismatch of index of refraction at the surface of the medium have been also taken into account in the simulation, by using the Fresnel law for each photon reaching the surface.

This is also one results of this simulation to compute the average depth of probing, illustrated in Fig.2. It is demonstrated that only the superficial part of the turbid medium is probed if small source-detector separation are used. The average scattering depth of scattering event was recorded for each photon detected in Monte Carlo simulations. We present in Fig.2 the probability density function of this quantity. Fig.2 shows that the average depth of scattering is approximately around 1 mfp'. Moreover it showed that the part located below 2 mfp' were not playing a significant role in the measured signal (for $\rho < 1.5$ mfp').

The spatially resolved reflectance R(ρ), with short source-detector separations is more complex than in the

case of large source-detector separations. Indeed, for small source detector-separation conditions, the inverse problem. i.e. calculating localized absorption and the reduced scattering coefficients, is necessarily sensitive to the scattering phase function. It is part of the present invention to have shown, from Monte Carlo simulations, that only the first and second moments of the phase function must be taken into account. Moreover, it was established that the influence of the these two moments are not independent. Indeed, it is a merit of this invention to demonstrate that only one new parameter γ, called "phase function parameter", which depends on the first and second moments can be used to characterize correctly the reflectance of tissues at short distance. Precisely, γ is defined as follows:

$$\gamma=(1-g_2)/(1-g_1) \qquad (8)$$

More, precisely, Fig.3 illustrates the fact that the parameter γ is the only predominant parameters of the phase function that must be taken into account (and not g_1 as frequently mentioned in literature). Reflectance curves, obtained from Monte Carlo simulations are shown in Fig.3. Four different phase functions were used for the simulations. Three phase functions are characterized by γ=1.25. For comparison, the results for a fourth phase function with γ=2.25 is also presented. For distances $\rho\mu_s'$ <0.3, the parameter γ appear clearly to be the important parameter of the phase function.

The parameter γ depend on the characteristics of the set of scatterers, inside the turbid medium: shape, distribution of sizes and refractive indices (medium and scatterers). Thus, the determination of γ can provide important information about the investigated sample.

In most cases, the refractive indices n and the source and detectors characteristics are fixed and known. In such case, a reduced set of three parameters only can be extracted from measurements at short source-detector separation: μ_a, μ_s' and γ.

It is important to note that the parameter γ, cannot be estimated if large source detector separations are used. Indeed, the reflectance is sensitive to γ, only at short source-detector separation.

It was also derived from Monte Carlo simulations that the reflectance R(ρ), for ρ≈1mfp', can be reasonably well approximated by the expression:

$$R(\rho) \equiv [A(\rho, \mu_s', \gamma) + \mu_s' B(\mu_a)]^2 \qquad (9)$$

it is important for the description of the invention to evidence the fact that the function A depends on ρ, the scattering properties (i.e. μ_s' and γ) but not on μ_a. In contrast, the function B depends on μ_a but neither on the phase function (i.e. γ) and nor ρ. An example of Equ.(9) is shown in Fig.4.

This formulation is of great help to solve the inverse problem, as described in section 5.3.

3. Apparatus

In the first embodiment, The apparatus can be divided in three parts, described in Fig.5.a.

The first part is the illuminating system. Different light sources can be used: a) white sources, such as halogen or xenon lights, metahalides or fluorescent or phosphorescent sources. b) the sources described in point a) where monochromators, filters or interference filters are added to select a given set of wavelengths c) sources such as laser, laser diodes, light emitting diodes or superluminescent diodes.

In the first preferred embodiment, The light power is conducted to the investigated sample by the probe, which is the second part of the apparatus. The probe is preferably made of optical fibers, to illuminate and to collect the backscattered light. Different possible

arrangements are illustrated in Fig.6. Two different modes of measurements can be chosen. First, one fiber is used to illuminate the sample and at least two others are used to collect the backscattered light at two different distances. Second, one fiber is used to collect the light and at least two others fibers, at two different distances from the first one, are used to illuminate sequentially the sample.

The arrangement of the different fibers can be replaced by any imaging system or image guide, such as multicore optical fibers.

The light collected by the probe is analyzed by the detection unit, which is the third part of the apparatus. If wide spectral light sources are used (such as halogen or xenon lights), a spectrograph should be put between the probe and the detector to get wavelength dependence of the backscattered signal (either in the source or detection unit). Different types of detectors, such as photodiodes, avalanche photodiodes or photomultipliers can be assigned to each collecting fibers. Simultaneous detection of each collecting fiber can also be achieved using linear or two-dimensional detectors such as Charge-Coupled Detectors (1D or 2D) or array of photodiodes.

The second embodiment is described in Fig. 5.b. The only difference with the first embodiment is that optionally no optical probe, based on the use of fibers or light pipes or grin rods is used. The light source unit is directly in contact with the turbid medium, as well as the detector unit. Collimating optics, microoptics or imaging optics (DOE for example) can be put between the turbid medium and the actual light sources and detectors. The different type of sources and detectors cited in example for the first embodiment can be used for the second embodiment. Hybrid design, such as arrangements involving both direct contacts sensors or detectors and fibers, light pipes or grin rods are also included in the present embodiment

The third embodiment is described in Fig. 5.c.and Fig. 5.d. The only difference with the first and second embodiment is that no contact measurements are performed. A collimating system allow for point illumination on the turbid medium. An imaging system enables to measure the spatial distribution of the reflectance. The detectors can be either an array (1D or 2D) of detectors (Fig. 5.c),or a single detector (Fig. 5.d). In this last case, an scanning device is used to obtain the spatially-resolved reflectance. A fiber bundle, multicore fiber or relay optics (grin rod or multiple lenses) can be put between the focal point of the imaging system and the detector(s). The different type of sources and detectors cited in example for the first embodiment can be used for the third embodiment

It must be also noted that multiple measurements at different locations allows to obtain an image of the different parameters μ_a, μ_s' and γ (the resolution is on the order on the mean source-detector separation used).

4. Normalization and calibration

The differences of transmission between each fiber are corrected using a measurement on a turbid phantom illuminated uniformly.

The background light, measured with the light source turned off, must be subtracted from the signal.

In order to perform absolute intensity measurements, calibration is performed on turbid medium of known optical properties. Examples of such media are: 1) solid turbid medium which properties have been measured by other standard techniques 2) water suspension of microsphere of know size distribution and refractive index. In case 2) the scattering properties are calculated from Mie

theory, and the absorption coefficient is assumed to be equal to the water absorption coefficient.

A Monte Carlo simulation is performed with the optical properties of the calibration sample. The experimental reflectance performed on the calibration sample is multiplied by a factor determined so as to fit the experimental to the simulated reflectance. This factor is defined as the calibration factor. Each new measurement is multiplied by the calibration factor.

5. Signal processing

5.1. Control of the homogeneity of the area probed

Artifacts during a measurement, for example due to bad contact between the probe and the sample, or heterogeneity of the sample, can be detected by the following procedure. Two illuminating fibers are disposed symmetrically in regard to the collecting fibers (see Fig.6b). If the sample is homogeneous, the reflectance curve should be identical with either illuminating fiber. Therefore, comparing the two curves tests the heterogeneity of the investigated tissue region or detects obstructions, beneath the fibers. If the two curves are sufficiently close, the measurement is validated and the average of the two curves is calculated.

5.2 Smoothing procedure and computation of the derivative of the curve.

Functions in the form $m_1\rho^{m_2}\exp(m_3\rho)$ were found to fit always well Monte carlo simulation results for restricted range of distances. Smoothing of the experimental reflectance $R(\rho)$ is obtained by fitting $R(\rho)$ to $m_1\rho^{m_2}\exp(m_3\rho)$.

The determination of the slope of the logarithm $\frac{\partial}{\partial\rho}(\ln R(\rho, \mu_s', a', \gamma))$ is also derived from this fit, using the following formula:

$$\frac{\partial}{\partial\rho}(\ln R(\rho, \mu_s', a', \gamma)) = \frac{m_1}{\rho} + m_2 . \qquad (10)$$

The slope of the square root of $R(\rho)$ is given by:

$$\frac{\partial}{\partial\rho}\sqrt{R(\rho, \mu_s', \mu_a, \gamma)} = \left(\frac{m_1}{\rho} + m_2\right)\left(\sqrt{m_1}\rho^{\frac{m_2}{2}}\exp\left(\frac{m_3\rho}{2}\right)\right) \qquad (11)$$

5.3. Inverse problem

We developed different methods to solve the inverse problem, which consists in extracting optical coefficients from the reflectance data.

Method 1.

Monte Carlo simulations show that measurements of the reflectance intensity $R(\rho)$ and the slope of $\ln R(\rho)$, determined at a fixed distance ρ, can be used to derive μ_s' and μ_a for a given γ value. Fig.8 shows graphically the relationship between μ_s' and μ_a and the two parameters $R(\rho=1\text{ mm})$ and $|\partial_\rho \ln R(\rho=1\text{ mm})|$ for $\gamma = 1.5$ and 1.9. We see in Fig.8 that μ_s' and μ_a can not be determined uniquely if γ is unknown. Further insight for optimizing the inversion strategy is provided by three additional features of Fig.8.

First, the determination of μ_s' is only weakly influenced by γ. Indeed in Fig.8 the errors induced by error in γ are typically 10% for μ_s' around 1 mm^{-1}. Second, although absolute determination of μ_a is not possible when γ is not precisely known, relative absorption changes can be still evaluated. Third, the indetermination of the parameter γ may be resolved by the values of $R(\rho)$ and/or $|\partial_\rho \ln R(\rho)|$ at other distances. Therefore the following procedure can be used:

(1) determination of μ_s' and μ_a from $R(\rho=1\text{ mm})$ and $|\partial_\rho \ln R(\rho=1\text{ mm})|$ for a set of values γ. For example: γ=1.0, 1.1, 1.2,...,2.5.

(2)simulations with the different sets of μ_s' and μ_a obtained

(3)comparison between the simulations and the reflectance profile for distances $0.3<\rho<2$ mm.

This last step allows us to determine the correct values

of γ, μ_s' and μ_a. Points 1 to 3 can be done iteratively to evaluate γ more precisely, using a finer discrimination of γ values.

Method 2.

The inverse problem can be optimized, considering properties of R(ρ) of Equ.(9).

Indeed, it can be derived from Equ.(9) that the quantity $\frac{\partial}{\partial\rho}\sqrt{R(\rho,\mu_s',\mu_a,\gamma)}$ does not depend on the absorption coefficient μ_a:

$$\frac{\partial}{\partial\rho}\sqrt{R(\rho,\mu_s',\mu_a,\gamma)}=2\frac{\partial A}{\partial\rho}(\rho,\mu_s',\gamma) \qquad (12)$$

This property is confirmed in Fig.9, where the quantity $\frac{\partial}{\partial\rho}\sqrt{R(\rho,\mu_s',\gamma)}$, evaluated at ρ=1 mm, is plotted as a function of μ_s' for γ=1, 1.9 and 2.5 and reduced albedo a'=1, 0.95 and 0.9. In Fig.9, the parameter $\frac{\partial}{\partial\rho}\sqrt{R(\rho,\mu_s',\gamma)}$ clearly depends on μ_s' and γ. In contrast, the dependence on a' is almost negligible.

Therefore, γ and μ_s' can be derived from the parameter $\frac{\partial}{\partial\rho}\sqrt{R(\rho)}$, calculated from the experimental reflectance R(ρ) (see section 5.2). Simultaneous determination of γ and μ_s' require values of $\frac{\partial}{\partial\rho}\sqrt{R(\rho)}$ at different distances ρ (at least two). If γ or μ_s' is already known, the determination of the unknown parameter can be obtained from the value of $\frac{\partial}{\partial\rho}\sqrt{R(\rho)}$ at a single distance. Convenient analytical approximation of $\frac{\partial}{\partial\rho}\sqrt{R(\rho)}$ can be obtained by fitting Monte Carlo results to polynomial functions. For example, in the case of fixed γ=1.9, we obtained:

$$\mu_s'=0.9162-52.89x+1795x^2-18155x^3+65428x^4 \qquad (13)$$

where $x=\frac{\partial}{\partial\rho}\sqrt{R(\rho)}$ at ρ=1 mm, expressed in [mm^{-2}].

This results is valid for a probe of refractive index of 1.5 and a sample of refractive index of 1.4, optical fibers of diameter 200 μm, NA=0.37 (source and collection).

Once μ_s' and γ are calculated from the procedure explained above, μ_a is calculated from the absolute value of R(ρ), which highly depends on μ_a. For given μ_s', γ and ρ values, the dependence of reflectance on μ_a is obtained by Monte Carlo results. From Equ.(9) we have:

$$\mu_a = h\left[\frac{\sqrt{R(\rho)}-f(\gamma,\mu_s')}{\mu_s'}\right] \qquad (14)$$

where f and h are functions given by Monte Carlo simulation. Particularly, they can be well approximated by polynomial functions. For example, for γ=1.9, probe refractive index of 1.5, sample refractive index of 1.4, optical fibers of diameter 200 μm, NA=0.37 (source and collection):

$$f=-0.002257-8.171\mu_s'+268.8\mu_s'^2 \qquad (15)$$

$$h=0.01311+0.05184x-0.01974x^2+ \qquad (16)$$

$$0.003217x^3-0.0001992x^4$$

where $x=\left[\frac{\sqrt{R(\rho)}-f}{\mu_s'}\right]$ (unitless).

Method 3

Equ.(9) also show that relative measurements of μ_a, i.e. variation of μ_a from a known value, is possible by the monitoring variation of the parameters $\sqrt{R(\rho)}$

Indeed, we have:

$$\sqrt{R(\rho,\mu_s',\gamma,\mu_a)}-\sqrt{R(\rho,\mu_s',\gamma,\mu_a=0)} = \mu_s'B(\mu_a)-\mu_s'B(\mu_a=0) \qquad (17)$$

This relation is illustrated in Fig.10 in the case of ρ=1, and for the same three γ values used in Fig.9 and for a'=1 to 0.83. Fig.10 confirms that the influence of γ is weak in the quantity $\sqrt{R(\rho,\mu_s',\gamma,\mu_a)}-\sqrt{R(\rho,\mu_s',\gamma,\mu_a=0)}$. For known μ_s', the function B(a') allows for the determination of a *relative* absorption change $\Delta\mu_a=\mu_a-\mu_{ao}$, from a known value μ_{ao}. Fig.10 illustrates the case $\mu_{ao}=0$, but any

other value of μ_{ao} is possible. The interesting point is that B(a') does not depend on the phase function.

We claim:

1.A method for local and superficial (on the order of one transport mean free path) characterization a turbid media using all the following parameters:

1) the refractive index n of the turbid media

2) the absorption coefficient μ_a of the turbid media

3) the reduced scattering coefficient μ_s' of the turbid media

4) the phase function parameter γ of the turbid media

and comprising the step of:

-measuring the spatially-resolved reflectance R(ρ) or any quantity which allow for the indirect determination of the said spatially-resolved reflectance R(ρ).

-mathematical processing to compute at least one of the said parameter (n, μ_a, μ_s', γ) or the relative variation of these said parameters.

2.The method of claims 1, wherein said spatially resolved reflectance is measured by an optical fiber probe as described by the first embodiment in section 3.

3.The method of claims 1, wherein said spatially resolved reflectance is measured by a device put directly in contact to the turbid media, as described by the second embodiment in section 3.

4.The method of claims 1, wherein said spatially resolved reflectance is measured by non contact detection unit, as described by the third embodiment in section 3.

5.The method of claims 1 to 4, wherein the following processing is performed:

- fit of the measured reflectance R(ρ) to the function:

$$m_1\rho^{m_2}\exp(m_3\rho) \qquad (18)$$

This fit give values for the parameters m_1, m_2 and m_3. The expression $R = m_1\rho^{m_2}\exp(m_3\rho)$ gives a smooth function R(ρ).

The slopes $\frac{\partial}{\partial\rho}\sqrt{R(\rho)}$ and $\frac{\partial}{\partial\rho}(\ln R(\rho))$, or any mathematical combinations of these two latter quantities and R(ρ), can be obtained directly from analytical functions using the parameters m_1, m_2 m_3, or by numerical procedures from the function $R = m_1\rho^{m_2}\exp(m_3\rho)$.

6. The method of claims 1 to 5, wherein the absorption coefficient μ_a, the reduced scattering coefficient μ_s' and the phase function parameter γ are determined on the basis of a fit of the spatially-resolved reflectance R(γ, μ_s', μ_a, ρ) to a Monte Carlo simulations, or functions approximating Monte Carlo simulations.

7.The method of claims 1 to 5, wherein the absorption coefficient μ_a, the reduced scattering coefficient μ_s' and the phase function parameter γ are determined on the basis of the following form of the reflectance:

$$R(\rho) = (A(\rho, \gamma, \mu_s') + \mu_s' B(\mu_a))^2 \qquad (19)$$

where the function $A(\rho, \gamma, \mu_s')$ and $B(\mu_a)$ taking into account the sources and detectors characteristics and the refractive index of the sample.

8. The method of claims 1 to 5, wherein the reduced scattering coefficient μ_s' and the phase function parameter γ are determined on the basis of the quantity $\frac{\partial}{\partial\rho}\sqrt{R(\rho, \mu_s', \gamma)}$, which depends weakly on the absorption coefficient μ_a for $0.3<\rho\mu_s'<5$.

9. The method of claims 1 to 5, wherein the absorption coefficient μ_a is determined based on the equation:

$$\mu_a = h\left[\frac{\sqrt{R(\rho)} - f(\gamma, \mu_s')}{\mu_s'}\right] \qquad (20)$$

where f and h are functions that approximate Monte Carlo simulations.

10. The method of claims 1 to 5, wherein variation of the absorption coefficient μ_a is possible computed from the variation of the parameters $\sqrt{R(\rho)}$.

11. The method of claims 1 to 5, wherein the μ_a value

can be obtained from a function B, derived from Monte Carlo simulation, such as:

$$\sqrt{R(\rho, \mu_s', \gamma, \mu_a)} - \sqrt{R(\rho, \mu_s', \gamma, \mu_a^*)} = \mu_s' B(\mu_a) - \mu_s' B(\mu_a^*) \quad (21)$$

where $\sqrt{R(\rho, \mu_s', \gamma, \mu_a^*)}$ is a obtained from measurement on a sample with a known μ_a^* value.

~~12. The method of claims 1 to 6, wherein said turbid~~ medium is a biological medium.

Monte Carlo study of diffuse reflectance at source-detector separations close to one transport mean free path

Frédéric Bevilacqua and Christian Depeursinge

Institute of Applied Optics, Microengineering Department,

Swiss Federal Institute of Technology Lausanne,

1015 Lausanne, Switzerland

Contact Address:

Christian Depeursinge,

Institute of Applied Optics, Microengineering Department, (IOA-DMT)

Bâtiment de Microtechnique

Swiss Federal Institute of Technology Lausanne (EPFL)

1015 Lausanne-Switzerland

Tel: +41 21 693 61 77

Fax: +41 21 693 37 01

e-mail christian.depeursinge@epfl.ch

ABSTRACT

The spatially resolved reflectance of turbid media is studied at short source-detector separation (around one transport mean free path), using Monte Carlo simulations. The role of the phase function is carefully assessed. Particularly, the importance of the first and second moment of the phase function is demonstrated for distances between 0.5 to 5 transport mean free paths, whereas the effect of moments of higher order is negligible. Similarity relations are tested and are found efficient to reduce the number of relevant parameters. Indeed, only the following parameters must be taken into account: the refractive index, the absorption coefficient, the reduced scattering coefficient, and a phase function parameter γ depending on the first and second moment of the phase function. Approximate analytical form of the reflectance at short source-detector separation are also derived from the simulations. It is based on the follwing findings for source-detectors separation between 0.5 to 2 transport mean free path: first the slope of the square of the reflectance depends weakly on the absorption, and second, differences of the square root of the reflectance weakly depends on the phase function parameter γ. These results give clues for the determination of scattering and absorption properties, using short short distances measurements.

1. INTRODUCTION

The spatially-resolved reflectance of turbid media has been studied experimentally and theoretically for many years. In particular, it has been shown that the measurement of the spatially resolved reflectance allows to determine the absorption and scattering properties of a turbid medium[1-9]. Such measurements have been applied for example in the medical field for oximetry[4], photodynamic therapy[3,6,9] or glucose monitoring[10]. Diffusion theory[1-7], Monte Carlo simulations[1,5-8] or random walk[11] have been used to describe theoretically the spatially-resolved reflectance. For source-detector separations larger than several transport mean free paths and high albedo, the diffusion equation gives accurate solutions for the reflectance, which depends in this case only on three parameters: the reduced scattering coefficient, the absorption coefficient and the index of refraction of the medium.

The reflectance at shorter distances has been less systematically investigated, although it is of great interest. Indeed, measurements of the reflectance close to the source interrogates a smaller volume of the sample, compared to large distances measurements. Therefore, a local determination of the optical properties is possible. For example small volumes of biological tissues can be optically characterized during *in vivo* investigations[12,26].

At source-detector separations of approximately one transport mean free path, diffusion theory fails to describe accurately the spatially resolved reflectance. The problem of modeling the propagation of photons is then more complex than far from the source. Indeed, Bolt et al.[13] have clearly shown experimentally that the absorption and reduced scattering coefficients are not sufficient to describe accurately the reflectance close to the source. In particular, the phase function has to be taken into account. This has also been demonstrated by Kienle et al.[7,14] and Mourant et al[15] using Monte Carlo simulations.

The first goal of this study is to assess the importance of the different moments of the phase function, in

the spatially-resolved reflectance. In earlier studies[7,13], only the first moment of the phase function, also called anisotropy factor, has been considered to quantify the effect of the phase function close to the source. We will show that this analysis is not correct. Indeed, the first *and* second order moments of the phase function have to be taken into account, whereas moment of higher order can be neglected.

The second goal of this study is to assess the validity of *similarity relations,* describing how the number of optical parameters can be reduced. We will show that, close to the source, only three parameters beside the index of refraction are needed: the absorption coefficient μ_a, the reduced scattering coefficient μ_s' and a third parameter γ, defined as a function of the first two moments of the phase function. Therefore, only the additional parameter γ is required compared to the case of large source-detector separations.

The third goal is to describe how of these three parameters, μ_a, μ_s' and γ can be determined from reflectance data. For this, the dependence the reflectance intensity, the slope of the log of the reflectance and the slope of the square of the reflectance is examined as a function of μ_a, μ_s' and γ. Interesting properties are derived from this study and are be presented.

The results of this theoretical study led us to the design of a probe measuring the scattering and absorption properties of tissues *in vivo,* with short source-detector separations[26,27]. Even if our main application target is the determination of the tissue optical properties, the results presented here have been obtained for a broad range of optical parameters, and can be applied to turbid media of various types.

2. THEORY

A. Geometry

The geometry used in our simulations is the semi-infinite space. As described in Fig.1, we consider a

light source and a detector placed normally to the surface and separated by a variable distance ρ. The spatially-resolved reflectance $R(\rho)$ is defined by the power received by the detector per unit area and normalized by the source power. The numerical aperture of the source and the detector is 0.38 (θ_{max}=43.6°). This value has been chosen to match closely experiments where optical fibers are used to illuminate the medium and to collect the backscattered light[12].

B. Optical properties

The medium has macroscopically homogeneous and isotropic optical properties: relative index of refraction n, absorption coefficient μ_a, scattering coefficient μ_s and phase function $p(\theta)$, where θ is the scattering angle. From these coefficients we can define the total attenuation coefficient $\mu_t=\mu_s+\mu_a$, the albedo $a = \mu_s/\mu_t$ and the mean free path $1/\mu_t$.

The phase function can be expanded in a series of Legendre polynomials[16,22,23] $P_n(\theta)$:

$$p(\theta) = \frac{1}{4\pi}\sum_n (2n+1) g_n P_n(\theta) \qquad (1)$$

g_n are the n^{th} order (Legendre) moment of the phase function:

$$g_n = 2\pi \int_0^\pi P_n(\theta) p(\theta) \sin\theta d\theta \qquad (2)$$

The zero-order moment g_0 is normalized to 1 for all phase functions. The first-order moment g_1 represents the mean cosine of the scattering angle θ. It is often called the anisotropy factor (or also asymmetry factor), and is usually simply noted g in optics. Thus, please note that $g=g_1$.

This parametrization of the phase function is interesting because, in most multiple scattering problems, only a limited number of moments need to be taken into account[16]. In particular we will examine the role of each moment on the reflectance, as a function of the source-detector separation.

C. Choice of the phase function

In this section we describe the different phase functions that we used for our study. Particularly, we define two phase functions, p_{MHG} and p_{MPC}, the moments g_1 and g_2 of which, can be conveniently adjusted. They allow to approximate a broad range of real phase functions found in optics (from this point we most often drop the "θ" dependence of the phase function for notation simplicity)

Before introducing these phase function, we need to recall the Henyey-Greenstein phase function[17] p_{HG}, which has been widely used for multiple-scattering problem. It allows to simulate highly forward scattering, and its mathematical form is simple:

$$p_{HG}(\theta) = \frac{1}{4\pi}\frac{1-g_{HG}^{2}}{(1+g_{HG}^{2}-2g_{HG}\cos\theta)^{3/2}} \tag{3}$$

The moment of p_{HG} are $g_n=g_{HG}^{n}$ where n is the order of the moment . The Henyey-Greenstein phase function is very convenient since its first moment can be easily adjusted. Nevertheless, fixing the value of g_1 determines also all the other moments. In order to investigate the effect of the second moment g_2 independently of g_1, we modified p_{HG} to a new phase function, we called p_{MHG}, by adding a term proportionnal $\cos^2\theta$ (thus p_{HG} is a particular case of p_{MHG}).

$$p_{MHG}(\theta) = \alpha p_{HG}(\theta) + (1-\alpha)\frac{3}{4\pi}\cos^2\theta \qquad \alpha = 0..1 \tag{4}$$

The weighting factor α guarantees the normalization of p_{MHG}. The term in $\cos^2\theta$ gives a contribution to g_2 only, as for Rayleigh scattering[16]. Thus, p_{MHG} can be interpreted as an average between two types of scattering events: one with anisotropic scattering (e.g. originating from large particles compared to the wavelength) and one with quasi-isotropic scattering (originating from small particles compared to the wavelength). Phase functions with such a structure have been actually measured in biological tissues[18-21].

The moments for p_{MHG} are given as follows:

$$g_1 = \alpha g_{HG},\ g_2 = \alpha g_{HG}^2 + 2(1-\alpha),\ g_3 = \alpha g_{HG}^3,\ g_4 = \alpha g_{HG}^4,\ \ldots \tag{5}$$

Equ.(5) shows that the parameters g_{HG} and α allow for the independent adjustment of g_1 and g_2. Nevertheless the choice of g_1 and g_2 is limited by the condition that $p(\theta) \geq 0$ for $0 \leq \theta \leq \pi$. Due to this condition, some values of g_1 and g_2, which are reached for example with Mie scattering[16], are not possible with p_{MHG}, as shown in Fig.2 In order to reach these values, we introduce a second phase function p_{MPC}, constructed in a similar way to p_{MHG}:

$$p_{MPC}(\theta) = \alpha p_{PC}(\theta) + (1-\alpha)\frac{3}{4\pi}\cos^2\theta \qquad \alpha = 0..1 \tag{6}$$

where p_{PC} is a phase function made of power of cosines (corresponding to particular cases of the expansion in Legendre polynomials of order N, see Van de Hulst[16]):

$$p_{PC}(\theta) = \frac{1}{4\pi}\frac{N+1}{2^N}(1+\cos\theta)^N \tag{7}$$

Similarly to p_{MHG}, the right term of p_{MPC} proportional to $\cos^2\theta$ in Equ.(6) allows to adjust g_2 independently of g_1. Indeed, the moments of p_{MPC} are then given by:

$$g_1 = \alpha g_{PC_1},\ g_2 = \alpha g_{PC_2} + 2(1-\alpha),\ g_3 = \alpha g_{PC_3},\ g_4 = \alpha g_{PC_4},\ \ldots \tag{8}$$

The value of g_{PC_n} g_{PC} depends on N:

$$g_{PC_1} = \frac{N}{(N+2)} \qquad g_{PC_n} = g_{PC_{n-1}}\frac{(N-n+1)}{(N+n+1)} = \frac{N(N-1)\ldots(N-n+1)}{(N+2)\ldots(N+n+1)} \tag{9}$$

In Fig.2, the regions of possible g_2 are plotted for p_{MHG} and p_{MPC} as a function of g_1. Values obtained from a broad set of Mie phase functions are plotted as well (relative refractive index from 0.9 to 2, and

size parameters from 1 to 25, from table 20 in Ref. 16). For high g_1 values, g_2 is generally characterized by $g_2 \leq g_1$. Note that the region covered by the Henyey-Greenstein phase function p_{HG} is only the line $g_2=g_1^2$, which represents therefore very limited cases of Mie phase functions.

Fig.2 clearly shows that p_{MHG} allows to cover most of the g_1 and g_2 values from Mie theory (and also the particular case of Raleigh scattering characterized by $g_1=0$, $g_2=0.1$). Nevertheless, some cases are cannot be obtained by p_{MHG}, but can be reached using p_{MPC}. Generally, the cases covered by p_{MHG} are also covered by p_{MPC}. For such cases, the use of p_{MHG} and p_{MPC} is complementary. Indeed, for identical g_1 and g_2 values, the higher oreder moments g_n (n>2) given by p_{MPC} are significantly lower than the ones given by p_{MHG}. This is shown in Fig.3, for the cases $g_1=0.9$, $g_2=0.81$ and $g_1=0.5$, $g_2=0.25$. Therefore, the use of either p_{MHG} or p_{MPC} is motivated depending on the choice of the moments of high order (> 2). In particular, we will use p_{MHG} and p_{MPC} to assess the role of moment of order higher than two on the reflectance.

D. Similarity relations and reduced coefficients

Consider a turbid medium with optical properties (μ_a, μ_s, $p(\theta)$). Is it possible to find a different set of optical properties (μ_a^*, μ_s^*, $p(\theta)^*$) that gives the same reflectance profile? If the answer is positive, the relations between these two sets of parameters are called the similarity relations. This concept, introduced by Van de Hulst[16], has been well discussed by Wyman et al.[22,23] The similarity relations are interesting because they allow for the reduction of the number of parameters necessary to describe the reflectance.

Wyman et al.[23] have shown that if the radiance $L(\mathbf{r}, \hat{\mathbf{s}})$ can be expressed as a finite spherical harmonics $Y_n^m(\theta, \varphi)$ expansion (φ is the azimuthal angle):

$$L(\mathbf{r}, \hat{\mathbf{s}}) = \sum_{n=0}^{N} \sum_{m=-n}^{n} a_{mn}(\mathbf{r}) Y_n^m(\theta, \varphi) \qquad (10)$$

then it is possible to define N+1 similarity relations:

$$\mu_a^* = \mu_a. \tag{11}$$

$$\mu_s^*(1 - g_n^*) = \mu_s(1 - g_n) \qquad n = 1,..., N \tag{12}$$

where g_n are the moments of order n of the phase function, as defined by Equ.(2).

If N=∞, the exact phase function has to be used to obtain the correct radiance distribution.

N=1 is the well known case of the diffusion approximation, where the radiance is only linearly anisotropic. Only two similarity relations are necessary (called first order similarity relations):

$$\mu_a^* = \mu_a. \tag{13}$$

$$\mu_s^*(1-g_{1*}) = \mu_s(1-g_1) \tag{14}$$

In this case, it is useful to define the following reduced coefficients:

- the reduced scattering coefficient: $\mu_s' = \mu_s(1-g_1)$,
- the reduced total attenuation coefficient: $\mu_t' = \mu_t(1-g_1)$,
- the reduced albedo $a' = \mu_s'/\mu_t'$.
- the transport or reduced mean free path $mfp' = 1/\mu_t'$

When the diffusion approximation holds, media with identical reduced coefficients lead to identical radiance distribution. For this reason, μ_s' and μ_a are commonly used to characterize optically thick turbid media.

The diffusion approximation (N=1) is generally valid for source detector separation larger than several transport mean free paths. For shorter distances, the case N=2 (radiance at most quadratically anisotropic) should be considered, then N=3 and so on.

For the case N=2, a third similarity relation should be added to Equ.(13) and Equ.(14):

$$\mu_s^*(1-g_2^*) = \mu_s(1-g_2) \tag{15}$$

Combining Equ.(14) and Equ.(15), the third similarity relations can be rewritten as:

$$\frac{1-g_2}{1-g_1} = \frac{1-g_2^*}{1-g_1^*} \equiv \gamma \tag{16}$$

Therefore in case N=2 (radiance at most quadratically anisotropic), three parameters have to be considered: μ_s', μ_a, and $\gamma = (1-g_2)/(1-g_1)$. The validity of these similarity relations will be assessed by simulations.

The γ value depends on the balance between the first and second moment of the phase function. Examples of γ values, computed from Mie scattering, are given in Fig.4 for monodisperse spheres. In this figure, γ is plotted versus the parameter diameter/wavelength, for three different index of refraction ratios $n = n_{sphere}/n_{medium}$: 1.05, 1.1 and 1.2. For very small particles, γ decreases if the size of the particle decrease and has a limit value of 0.9 for Rayleigh scattering. In such a case, the first moment $g_1=0$, but the second moment is $g_2=0.1$. For poydisperse scatterers, the parameter γ is also sensitive to size distribution. In the particular case of two populations of scatterers, one of very small size (Rayleigh scattering) and one with large particles, the average phase function can be approximated by p_{MHG} or p_{MPC}. From Equ.(5) and Equ.(8), it can be easily shown that γ is very essentially sensitive to the ratio of the concentration between large particles and small particles (this ratio is equal to $\alpha/(1-\alpha)$).

E. Monte Carlo model

The Monte Carlo method is well known to give accurate solutions for the light propagation in turbid media, if interference effects are negligible. The Monte Carlo code we used has been extensively tested and compared with other codes.[24-26]

The source and detector characteristics follow the description given in Fig.1. Boundary conditions are taken into account using Fresnel and Snell laws for each photon reaching the surface.

Taking advantage of the semi-infinite geometry and cylindrical symmetry, scaling procedures can be used to limit the number of simulations. The idea is simply to express the source-detector separation by the unitless quantity $\rho \cdot \mu_s'$. Indeed, for a given reduced albedo a', the unitless quantities $(\mu_s')^{-2}R(\rho\mu_s', a')$ computed from a single simulation (for example choosing $\mu_s' = 1\ mm^{-1}$, $a' = 0.99$), allows to derive the reflectance $R(\rho)$ for any μ_s' values (but constant reduced albedo a'). This is explained as follows. Consider the spatially resolved reflectance $R(\rho, \mu_s', a')$ obtained with a medium of coefficient μ_s' and reduced albedo a'. The reflectance $R(\rho, k\,\mu_s', a')$, obtained with a medium of the same albedo but with a scaled coefficient $k\,\mu_s'$, is simply related to the previous one by rescaling ρ by $k\rho$ and by renormalizing the reflectance (because of the rescaling of the area of the detectors):[28]

$$R(\rho, k\mu_s', a') = \frac{1}{k^2}R(k\rho, \mu_s', a') \tag{17}$$

We present our results of the reflectance using such unitless quantities $(\mu_s')^{-2}R(\rho \cdot \mu_s', a')$ or $\rho^2 R(\rho \cdot \mu_s', a')$, in order to obtain the most general results. Similarly, the dependence of slope of the log of the reflectance as a function of μ_s' or ρ can be derived the unitless quantity $\rho\frac{\partial}{\partial\rho}\ln R(\rho \cdot \mu_s', a')$.

3. SIMULATION RESULTS

A. Effect of the moments g_n on the reflectance

First we examine the effect of the different moments g_n on the reflectance. Results for the reduced albedo a'=0.99 are plotted here. Such albedo are found in biological tissue for red and near-infrared wavelengths. The effect of the absorption on the reflectance is examined later (section C and section D). A relative refractive index n=1.4 of the medium is considered. When indicated, the results obtained with

n=1.4 are compared to the case n=1.

The effect of g_1 is first examined. For this, g_2 is held constant and g_1 is varied. In Fig.5, the reflectance is computed with p_{MHG} with g_1=0.9, g_2=0.81 and p_{MHG} with g_1=0.81, g_2=0.81. Fig.5 shows clearly that the influence of g_1 is important at distances around $\rho\mu_s' \approx 1$. Note that such differences are much larger than if the Henyey-Greenstein phase function was used for this test, as it has been performed by some authors[7,29]. This is due to the fact that when p_{HG} is used, g_2 is not held constant when g_1 is changed, but varies as g_1^2. In such a case, as it will be clarified by the similarity relations shown in section B, the effect of g_1 is underestimated.

The role of the second moment g_2 is examined in Fig. 6.a and Fig.6.b (Fig.6.b is a close view of Fig. 6.a, for $0<\rho\mu_s'<2$). All the reflectance curves are obtained with phase functions of identical $g_1 = 0.9$ but different g_2 values: 0.75, 0.81, 0.9. p_{MHG} was used for $g_2 = 0.9$ and 0.81 ($p_{HG}=p_{MHG}$ in this case), and p_{MPC} in the case of $g_2 = 0.75$. As shown in Fig.2, these g_2 values correspond, to extreme cases found when considering Mie phase functions with high g_1. The solution of the diffusion equation given by Kienle et al.[30] is also presented in these figures, in order to quantify the limit of validity of the diffusion theory. The angular distribution of the reflectance was assumed as Lambertian[7].

Fig. 6.a clearly shows that all the reflectance curves converge to the diffusion solution for $\rho\mu_s' > 10$. It demonstrates that for such distances the diffusion approximation is valid. Nevertheless the divergence between the diffusion solution and simulations depends highly on the second moment g_2. For example, in the case of $g_2 = 0.9$, the reflectance is approximately 25% smaller than the diffusion solution at $\rho\mu_s'$=2. In contrast, the diffusion solution matches closely the reflectance obtained with p_{HG}, where differences smaller than 5% are found for distances as close as $\rho\mu_s' = 0.5$. The importance of g_2 is clearly demonstrated in Fig.6.b g_2 can induce differences in the reflectance up to 30% at distances $0.5<\rho\mu_s' < 2$.The role of g_2 is found here to be similar to that of g_1 shown previously. Therefore, the

combination of both g_1 and g_2 is responsible for the reflectance curve shape at $\rho\mu_s' \approx 1$.

One could suspect that the differences found in Fig.5 or Fig.6.b are not only due to differences in g_1 or g_2, but also to differences between the moments of higher order. To study the role of the moments g_n (n>2), two sets of phase functions with identical g_1 and g_2, but different higher moments are used. Two cases were investigated: g_1=0.5, g_2 = 0.25 and g_1=0.9 and g_2=0.81. For this test, p_{MHG} and p_{MPC} are used, because their moments g_n exhibit important differences for n≥3 (see Fig.39). Such differences are close to maximum values that can be found between different Mie phase functions. Fig. 7.a and Fig.7.b show that the reflectances curves computed using these two phase functions are very close for $\rho\mu_s'$>0.5 (differences smaller than 5% in Fig. 7.a and 15% in Fig.7.b). For smaller distances, the differences become important (>50% for $\rho\mu_s'$<0.1). Compared to the effect of g_1 in Fig.5 or g_2 found in Fig.6.b, the effect of g_n with n≥2 is weak for the reflectance at distances $\rho\mu s'$>0.5, whereas the g_n values (n≥2) have definitely to be taken into account to compute the correct reflectance at smaller distances.

B. Similarity relations

The fact that only the two first moments play a significant role for the reflectance at distances larger than 0.5 mfp' suggests that the second order similarity relation may be valid. In such a case, the similarity relations given by Equ.(13), Equ.(14) and Equ.(16) indicate that the reflectance should depend only on the parameters: $\gamma=(1-g_2)/(1-g_1)$, μ_s' and μ_a. To demonstrate the validity of these similarity relations we report in Fig. 8.a the reflectance computed with three phase functions characterized by identical γ = 1.25, but with g_1 = 0.2, 0.5, 0.9 and g_2= 0, 0.375, 0.875 respectively.

Fig. 8.a shows that these similarity relations are satisfied within only 2% error margin for $\rho\mu_s'$> 0.5, in the case n = 1.0. For the case n=1.4, slightly higher differences are found: <10% for $\rho\mu_s'$> 0.5. Note that these differences are much lower that differences found in Fig.5 and Fig.6.b, where g_1 and g_2 where varied independently.

Using these similarity relations, isotropic scattering (g_n=0 for all n, γ = 1.0) can also be approximated by a phase function characterized by γ = 1.0, even with high g_1. This is illustrated in Fig.8.b, where the reflectance produced by isotropic scattering (g_n=0), and p_{MHG} with g_1=g_2=0.9 are compared. As before, the similarity relations are found efficient. The differences found are of the same order than in Fig. 8.a

In view to these results, the hypothesis of quadratically anisotropic radiance for μ_s'> 0.5, on which is based the similarity relations we used, appear to be well satisfied. For n=1.4, the mismatch of refractive index modified the angular distribution of the radiance, which explains that the similarity relations are less perfectly satisfied for n=1.4 compared to the case of n=1.0 .

In summary, Fig. 8.a and Fig.8.b clearly show that the effect of the phase function can be quantified by only the parameter γ only, for distances $\rho\mu_s$'>0.5, constant μ_s' and a'. For shorter distances, the moments of order higher than two must be taken into account, which would involve other similarity relations to be considered.

C. Effect of the albedo on the reflectance.

We study in this section the effect of the albedo on the reflectance at short distance. Increasing the absorption induces changes in the intensity and in the slope of the reflectance. To examine this effect quantitatively, we derived from the reflectance the two unitless parameters $\rho^2 R(\rho\mu_s', a')$ and $\rho\partial_\rho \ln R(\rho\mu_s', a')$. For ρ=1 mm, these parameters represent respectively the intensity of the reflectance and the slope of the $\log_e$ (noted ln) of the reflectance, measured at 1 mm. Scaling relationships allow to derive easily these latter quantities for other distances.

The parameters $\rho^2 R(\rho\mu_s', a')$ and $|\rho\partial_\rho \ln R(\rho\mu_s', a')|$ are plotted in Fig.9 for reduced albedo from a'=1 to a'=0.83 and for distance $\rho\mu$s' from 0.28 to 5, and for two different phase function with the same first moment g_1 = 0.916 (p_{HG} with g_1=0.916, γ=1.92 and p_{Mie} with g_1=0.916, γ=2.23).

For distance μ_s'ρ larger than approximately 5, the difference induce by these phase function are

negligible. This is in agreement with the results presented in section A. At shorter distance significant differences can be found, depending on the phase function used. As shown in the previous section, γ is the important parameter of the phase function to consider, if the distance is larger than approximately $\mu_s'\rho = 0.5$.

Fig.9 shows that, for a fixed phase function and a fixed distance ρ, the two parameters $\rho^2 R(\rho\mu_s')$ and $\rho\partial_\rho \ln R(\rho\mu_s')$ of the are related uniquely to $\rho\mu_s'$ and a'. Therefore, for a given value of ρ, $\rho^2 R(\rho\mu_s')$ and $\rho\partial_\rho \ln R(\rho\mu_s')$ allow to determine the parameters a' and μ_s' (or equivalently μ_a and μ_s') of the medium with known phase function. If the phase function is not known, the determination of a' and μ_s' require the measurements of $\rho^2 R(\rho\mu_s')$, $\rho\partial_\rho \ln R(\rho\mu_s')$ at a given distance ρ and at least an additional parameter. This latter one could be for example $\rho^2 R(\rho\mu_s')$ or $\rho\partial_\rho \ln R(\rho\mu_s')$ measured at a second distance ρ. This point is discussed further in the section 4.

D. Approximate form of the reflectance close to the source.

We present in this section empirical properties of the reflectance close to the source, obtained by simulations. They may be used to determine the optical properties form reflectance data. For reduced albedo $a' \geq 0.9$ (corresponding to tissue reduced albedo found for red and near-infrared wavelengths) and $\rho\mu_s' < 4$, we found empirically that the reflectance can be expressed in the form:

$$R(\rho, \mu_a, \mu_s', \gamma) \cong [A(\rho, \mu_s', \gamma) + B(\mu_s', \mu_a)]^2 \qquad (18)$$

where A and B are functions that are described in Fig. 10.a and Fig.10.b. The function A depends on the scattering properties (i.e. μ_s' and γ) but not on the absorption. In contrast, the function B depends on the absorption but not on the phase function (i.e. γ). Equ.(18) is interesting because it shows that it is possible to uncouple the effect of the phase function and of the absorption. We illustrate this approximation in two steps, by deriving two property of Equ.(18).

First, the slope of the square root of the reflectance $\frac{\partial}{\partial\rho}\sqrt{R}$ does not depend on the absorption coefficient μ_a:

$$\frac{\partial}{\partial\rho}\sqrt{R}=\frac{\partial A}{\partial\rho}(\rho,\mu_s',\gamma) \tag{19}$$

The dimensionless quantity $\rho^2\frac{\partial}{\partial\rho}(\sqrt{R})$ is plotted in Fig. 10.a as a function of $\rho\mu_s'$ for γ=1, 1.9 and 2.5 and reduced albedo a'=1, 0.95 and 0.9.

Fig. 10.a shows that $\rho^2\frac{\partial}{\partial\rho}(\sqrt{R})$ depends highly on $\rho\mu_s'$ and γ. In contrast, the dependence on a' is almost negligible. If γ is known, μ_s' can be simply monitored by the parameter $\rho^2\frac{\partial}{\partial\rho}(\sqrt{R})$, independently of the variation of μ_a. Moreover, the inversion procedure, i.e determining μ_s' from the reflectance curve is simple using $\rho^2\frac{\partial}{\partial\rho}(\sqrt{R})$, because this parameter can be well approximated by polynomial functions (of order 4 or 5) (for the range $0.4<\rho\mu_s'<4$).

The second properties derived from Equ.(18) is as follows:

$$\sqrt{R(\rho,\mu_a,\mu_s',\gamma)}-\sqrt{R(\rho,\mu_a=0,\mu_s',\gamma)}=B(\mu_a,\mu_s')-B(\mu_a=0,\mu_s') \tag{20}$$

The difference $\sqrt{R(\rho,\mu_a,\mu_s',\gamma)}-\sqrt{R(\rho,\mu_a=0,\mu_s',\gamma)}$ can be transformed in dimensionless quantity by multiplying it by ρ. This dimensionless difference illustrated in Fig.10.b for the same three phase functions that we used in Fig. 10.a and for a'=1 to 0.83. Fig.10.b shows that the influence of the phase function is weak in the quantity $\rho(\sqrt{R(\rho\mu_s',a')}-\sqrt{R(\rho\mu_s',a'=1)})$. Moreover the relation found in Fig.10.b is very close to a linear function. Therefore, the further approximation can be made:

$$(\sqrt{R(\rho\mu_s',a')}-\sqrt{R(\rho\mu_s',a'=1)})\cong\mu_s'f(a') \tag{21}$$

where f(a') is a function depending only on a'. For known μ_s', the function f(a') allows the determination of a *relative* absorption change $\Delta\mu_a=\mu_a-\mu_{ao}$, from a known value μ_{ao}. Fig.10.b illustrates

the case μ_{ao} =0, but any other value of μ_{ao} is possible. The interesting point is that f(a') does not depend on the phase function.

The two properties given by Equ.(19) and Equ.(20), proven by simulations examples in Fig. 10.a and Fig.10.b, respectively, confirm the form of the reflectance (close to the source) given by Equ.(18).

4. DISCUSSIONS AND CONCLUSIONS

The study of the spatially resolved reflectance is easier if distinct ranges of distances are considered, corresponding to different regimes of the photon propagation. Each regime is related to a specific angular distribution of the radiance, which varies from a highly anisotropic distribution (close to the source) to a quasi-isotropic distribution (far from the source)[31]. In this discussion we consider three different regimes.

The first regime occurs where the diffusion approximation holds and corresponds to a linearly anisotropic radiance. Its range of validity can be determined indirectly by testing the validity of the first order similarity relations (μ_a=cte, μ_s' = cte). Simulations performed with a set of different phase functions show that their effect on the reflectance is less than 5% for distances defined by $\rho\mu_s'$>10 as long as μ_s' and μ_a are kept constant (Fig. 6.a). The different phase functions we used for this test approximate phase functions that can be obtained from Mie theory or phase functions that have been measured in biological tissues.

This limit of the diffusion regime is comparable to other estimations obtained when studying other quantities such as the spatially resolved transmittance[24] or the radiance angular distribution inside a turbid medium[32]. Nevertheless, this estimation is quite conservative. As demonstrated by other authors[5,30,33], solutions of the diffusion equation can still be accurate much closer to the source. In particular, in agreement with Kienle et al[30], we found that the diffusion solution is very close to

simulations down to distances $\rho\mu_s' \approx 1$, if Henyey-Greenstein phase functions with high anisotropy factors are used. However, this not true for other phase functions. Thus, diffusion theory should be used with care for distance $\rho\mu_s'<10$, if the actual phase function is not known.

The second regime is delimited approximately by $0.5<\rho\mu_s'<5$ range, and corresponds to the region where the radiance is approximately quadratically anisotropic. In this case, a third similarity relation can be used: the reflectance depends on the parameter $\gamma = (1-g_2)/(1-g_1)$, which must be kept constant in addition to μ_s' and μ_a. Therefore, both the first moment g_1 and the second moment g_2 of the phase function must be taken into account. In this regime, the effect of moments of higher order is weak on the reflectance, compared to the effect of g_1 and g_2.

The third region corresponds to distances $\rho\mu_s'<0.5$. The anisotropy of the radiance becomes high, and more moments must be taken into account. In such a case, computations with accurate phase functions should be performed.

Our analysis also demonstrated that it is not possible to determine the value g_1 alone by the measurement of reflectance close to the source, if no other parameter of the phase function is known. In view of this, we believe that the errors found by Jones and Yamada[29], in the measurement g_1 by such a technique, are explained by the fact that they neglected the effect of the second and higher moments in their theoretical analysis. It also shows that testing the effect of g_1 using the Henyey-Greenstein phase function alone is not correct. Indeed, in this case, both g_1 and $g_2=g_1^2$ are varied simultaneously. For g_1 between 0.8 and 1, γ varies then only from 1.8 to 2.0. This explains that the influence of g_1 on the reflectance has been reported[7,34] to be weak for $g_1>0.8$. However, as shown in Fig.5, the effect of g_1 can be much larger if g_2 remains constant.

The three coefficients μ_s', μ_a, and γ can be determined if measurements are performed in the diffusive regime and close to the source ($\rho\mu_s'>0.5$ mfp') on homogenous samples. μ_s', μ_a can be obtained by

fitting the diffusion solution to the measurement at large distance[5,7,33], in order to avoid the dependence of γ. The γ value can be then determined by comparison between the reflectance measurement close to the source ($\rho\mu_s \approx 1$) and a set of simulations performed with various γ values.

If the measurement is performed only close to the source, the determination of the μ_s', μ_a, and γ are possible by fitting simulations to the measured curve, but with a lower degree of precision. Note that non-linear regression could also be performed using the method proposed recently by Kienle et al.[34], which consists in using ad hoc analytical functions fitting the reflectance simulations and scaling relationships.

At short distance, the problem of computing the optical properties is facilitated if γ or μ_s' is known. If γ is known, μ_s' and μ_a can be derived from the reflectance intensity $R(\rho)$ and the slope of the logarithm of the reflectance $\partial_\rho \ln R(\rho)$ at one distance ρ close to the source. From Fig.9, the precision of such determination can be estimated. For an optical distance of 1 mfp', a precision better than ±1.5% is achievable on the determination of μ_s' if these two parameters are measured with an accuracy of ±1%. The accuracy on μ_s' is weakly dependent on μ_a and μ_s', for typical tissues properties ($0.5 < \mu_s' < 2$ mm^{-1}, $\mu_a < 0.2$ mm^{-1}). In contrast, the accuracy achievable on μ_a is highly dependent of the μ_a value. At a distance of 1 mfp' and $\mu_a \approx 0.1$ mm^{-1}, the error on μ_a is approximately ±5%, taking into account uncertainties of ±1% on $\partial_\rho \ln R(\rho)$ and $R(\rho)$. For μ_a around 0.02 mm^{-1}, the errors increases to approximately ±20%.

If μ_s' is known, but not the phase function, relative measurements of μ_a can be still achieved using the empirical property demonstrated in section D (Equ.(21)). This feature is very interesting for absorption monitoring in tissue for example.

In conclusion we showed that the spatially-resolved reflectance region at distances close to one transport mean free path can be accurately predicted with only three parameters: μ_a, μ_s', $\gamma = (1-g_2)/(1-g_1)$. These

results were applied for the determination of μ_a and μ_s' of biological tissues[26], using spatially-resolved measurements at distances $0.5<\rho<1.5$ mm, corresponding in tissue typically to distances of approximately one transport mean free path.

ACKNOWLEDGMENT

We would like to thank Olivier Coquoz, Laure Montandon, Pierre Marquet and Alwin Kienle for critical reviews of the manuscript. This work was supported by the Swiss National Science Foundation (N0 2053-049628.96).

5. REFERENCES

1. R. A. J. Groenhuis, J. J. Ten Bosch, and H. A. Ferwerda, "Scattering and absorption of turbid materials determined from reflection measurements. 1: Theory," Appl.Opt. 22, 2456-2462 (1983).

2. R. A. J. Groenhuis, J. J. Ten Bosch, and H. A. Ferwerda, "Scattering and absorption of turbid materials determined from reflection measurements. 2:Measuring method and calibration," Appl.Opt. 22, 2463-2467 (1983).

3. B.C. Wilson, T.J. Farrell, and M.S. Patterson, "An optical fiber-based diffuse reflectance spectrometer for non-invasive investigation of photodynamic sensitizers in tissue in vivo," Proc. SPIE, vol. IS06, 219-231 (1990).

4. J.M. Schmitt, "Simple photon diffusion analysis of the effects of multiple scattering on pulse oximetry," IEEE trans. Biomed. Eng. 38, 1194-1203 (1991).

5. T. J. Farrell, M. S. Patterson, and B. C. Wilson, "A diffusion theory model of spatially resolved, steady -state diffuse reflectance for the noninvasive determination of tissue optical properties in vivo," Med.Phys. 19 (1992).

6. R. Bays, G. Wagnières, D. Robert, D. Braichotte, J.-F. Savary, P. Monnier, and H. van den Bergh, "Clinical determination of tissue optical properties by endoscopic spatially resolved reflectometry," Appl.Opt. 35, 1756-1766 (1996).

7. A. Kienle, L. Lilge, M.S. Patterson, R. Hibst, R. Steiner, and B.C. Wilson, "Spatially resolved absolute diffuse reflectance measuremnts for noninvasive determination of the optical scattering and absorption coefficients of biological tissue.," Appl.Opt. 35, 2304-2314 (1996).

8. L Wang and S.L. Jacques, "Use of a laser beam with an oblique angle of incidence to measure the reduced scattering coefficient of a turbid medium," Appl.Opt. 34, 2362-2366 (1995).

9. R.A. Weersink, J.E. Hayward, K.R. Diamond, and M.S. Patterson, "Accuracy of noninvasive in vivo measurements of photosentizer uptake based on a diffusion model of reflectance spectroscopy," Photochem. Photobiol. 66, 326-335 (1997).

10. J.T. Bruulsema, J.E. Hayward, T.J. Farrell, M.S. Patterson, L. Heinemann, M. Berger, T. Koschinsky, J. Sandahlchristiansen, and H. Orskov, "Correlation Between Blood-Glucose Concentration in Diabetics and Noninvasively Measured Tissue Optical-Scattering Coefficient," Opt. Lett. 22, 190-192 (1997).

11. R.F. Bonner, R. Nossal, S. Havlin, and G.H. Weiss, "Model for photon migration in turbid biological media," J. Opt. Soc. Am. A 4, 423-432 (1987).

12. F Bevilacqua, D. Piguet, P. Marquet, J. D. Gross, B. J. Tromberg, and C. Depeursinge, "*In vivo* local optical determination of tissue optical properties," Proc. SPIE, Vol. 3194, 262-268 (1998).

13. JR.A. Bolt and J.J. ten Bosh, "Method for measuring position-dependent volume reflection," Appl.Opt. 32, 4641-4645 (1993).

14. A.Kienle, "Lichtausbreitung in biologischem Gewebe", PhD Dissertation, Universität Ulm, 1994.

15.J.R. Mourant, J. Boyer, A.H. Hielscher, and I.J. Bigio, "Influence of the Scattering Phase Function on Light Transport Measurements in Turbid Media Performed with Small Source-Detector Separations," Opt. Lett. 21, 546-548 (1996).

16. H.C. van de Hulst, *Multiple Light Scattering, Tables, Formulas, and Applications*, vol. II, (Academic Press. inc., London, 1980).

17. L. G. Henyey and J. L. Greenstein, "Diffuse Radiation of the Galaxy," Astrophys. J. 93, 70-83 (1941).

18. S. T. Flock, B. C. Wilson, and M. S. Patterson, "Total attenuation coefficient and scattering phase functions of tissues and phantom materials at 633 nm," Med. Phys. 14, 835-841 (1987).

19. S. L. Jacques, C. A. Alter, and S. A. Prahl, "Angular Dependence of HeNe Laser Light Scattering by Human Dermis," Lasers in Life Sciences 1, 309-333 (1987).

20. R. Marchesini, A. Bertoni, S. Andreola, E. Melloni, and A.E. Sichirollo, "Extinction and absorption coefficients and scattering phase functions of human tissues in vitro," Appl. Opt. 28, 2318-2324 (1989).

21. P. van der Zee, M. Essenpreis, and D.T. Delpy, "Optical properties of brain tissue," proc. SPIE, Vol. 1888, 454-465 (1993).

22. D.R. Wyman, M.S. Patterson, and B.C. Wilson, "Similarity Relations for anisotropic Scattering in Monte Carlo Simulations of Deeply Penetrating Neutral Particles,". of Comput.Phys. 81, 137-150 (1989).

23. D.R. Wyman, M.S. Patterson, and B.C. Wilson, "Similarity relations for the interaction parameters in radiation transport," Appl.Opt. 28, 5243-5249 (1989).

24. P. Marquet, F. Bevilacqua, C. Depeursinge, and E. B. de Haller, "Determination of reduced

scattering and absorption coefficients by a single charge-coupled-device array measurement, part I: comparison between experiments and simulations," Opt.Eng. 34, 2055-2063 (1995).

25. F. Bevilacqua, P. Marquet, C. Depeursinge, and E. B. de Haller, "Determination of reduced scattering and absorption coefficients by a single charge-coupled-device array measurement, part II: measurements on biological tissues," Opt.Eng. 34, 2064-2069 (1995).

26. F. Bevilacqua, *Local optical characterization of biological tissues in vitro and vivo,* PhD dissertation n°1781, Swiss Federal Institute of Technology Lausanne, 1998.

27. F. Bevilacqua, D. Piguet P. Marquet, J.D. Gross, B.J. Tromberg and C. Depeursinge· "*In vivo* local determination of tissue optical properties: Applications to human brain", to be submitted to Appl. Opt.

28. A.K. Kienle and M.S. Patterson, "Determination of the optical properties of turbid media from a single Monte Carlo simulation," Phys.Med.Biol. 41, 2221-2227 (1996).

29....M.R. Jones and Y. Yamada, "Determination of the asymmetry parameter and scattering coefficient of turbid media from spatially resolved reflectance measurements," OSA TOPS on Advances in optical imaging and photon migration, Vol. II, 379-382 (1996).

30. A. Kienle and M.S. Patterson, "Improved solutions of the steady-state and the time-resolved diffusion equations for reflectance from a semi-infinite turbid medium," J. Opt. Soc. Am. A. 14, 246-254 (1997).

31. J.R. Zijp and J.J. ten Bosch, "Anisotropy of volume-backscattered light," Appl. Opt. 36, 1671-1680 (1997).

32. S. T. Flock, M. S. Patterson, B. C. Wilson, and D. Wyman, "Monte-Carlo Modeling of Light Propagation in Highly Scattering Tissues-I: Model Predictions and Comparison with Diffusion Theory," IEEE Trans. Biomed. Eng. 36, 1169-1173 (1989)

33. M.G. Nichols, E.L. Hull, and T.H. Foster, "Design and Testing of a White-Light, Steady-State Diffuse-Reflectance Spectrometer for Determination of Optical-Properties of Highly Scattering Systems," Appl. Opt. 36, 93-104 (1997).

34. A.K. Kienle and M.S. Patterson, "Determination of the optical properties of turbid media from a single Monte Carlo simulation," Phys.Med.Biol. 41, 2221-2227 (1996).

FIGURE CAPTIONS

Fig.1 Geometry of the study. Photons are emitted at $\rho=0$ isotropically in a solid angle defined by the angle θ_{max}. They are detected at variable distances ρ in the same solid angle defined by θ_{max}.

Fig.2 Possible values of g_2 as a function of g_1 for Mie phase functions and p_{MHG} and p_{MPC}. The region covered by the p_{HG} is represented by the line $g_2=g_1^2$. The line $g_2=g_1$ represent the phase function formed by isotropic scattering added of a purely forward peak[16]. The dots represent a broad choice of Mie phase functions (relative refractive index from 0.9 to 2, and size parameters from 1 to 25, from table 20 in Ref. 16)

Fig.3 Values of the moment g_n for p_{MPC} and p_{MHG}. The values of the moment g_o, g_1 and g_2 are identical for both phase functions. Two cases are shown: $g_1=0.9$, $g_2=0.81$ (upper curves) and $g_1=0.5$, $g_2=0.25$ (lower curves).

Fig.4 $\gamma=(1-g_2)/(1-g_1)$ from Mie theory. $\gamma=(1-g_2)/(1-g_1)$ is shown as a function of the ratio sphere diameter/wavelength, for different index of refraction ratios $n = n_{sphere}/n_{medium}$.

Fig.5 Effect of the first moment $g=g_1$ for constant second moment g_2.

Fig. 6.a Role of the second moment on the reflectance, for a fixed first moment $g_1 = 0.9$.

Fig.6.b Role of the second moment on the reflectance, for a fixed first moment $g_1 = 0.9$. This graph is a close view of Fig. 6.a

Fig. 7.a Effect of the third and higher order moments on the reflectance. The first two moments are fixed: $g_1= 0.5$, $g_2=0.25$.

Fig.7.b Effect of the third and higher order moments on the reflectance. The first two moments are

fixed: $g_1 = 0.9$, $g_2=0.81$

Fig. 8.a Illustration of the second order similarity relations. All phase function have identical parameter $\gamma = (1-g_2)/(1-g_1) = 1.25$

Fig.8.b Illustration of the second order similarity relations. The isotropic scattering can approximated by a phase function with high g_1 if $g_1=g_2$. In such a case $\gamma = (1-g_2)/(1-g_1) = 1$.

Fig.9 Relationship between the parameters $\rho^2 R(\rho\mu_s')$ and $\rho\partial_\rho \ln R(\rho\mu_s')$ and the reduced scattering coefficient μ_s' and the reduced albedo a', for p_{HG} with g=0.9 (γ=1.9). Mismatched boundary condition n=1.4.

Fig. 10.aPlot of the parameter $\rho^2 \frac{\partial}{\partial \rho}(\sqrt{R})$ for different phase functions and different reduced albedo. The following phase functions were used: p_{MHG} with g_1=0.9, g_2=0.9 (γ=1.0), p_{HG} with g_1=0.9, g_2=0.81 (γ=1.8) and p_{MPC} with g_1=0.9, g_2=0.75 (γ=2.5). Mismatched refractive index n=1.4.

Fig.10.b Plot of $\rho(\sqrt{R(\rho\mu_s', a')} - \sqrt{R(\rho\mu_s', a'=1)})$ for different phase function and reduced albedo a'.

fig 1

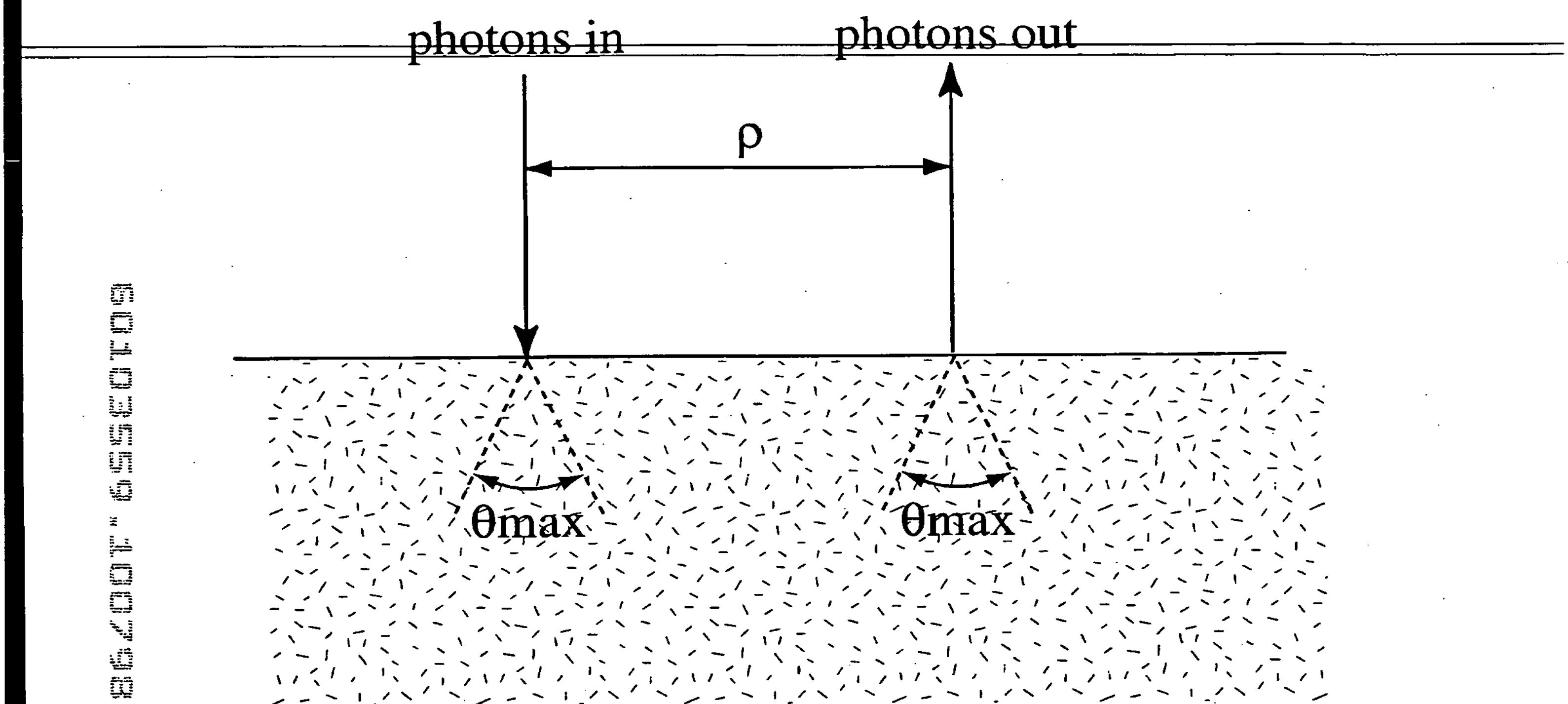

fig2

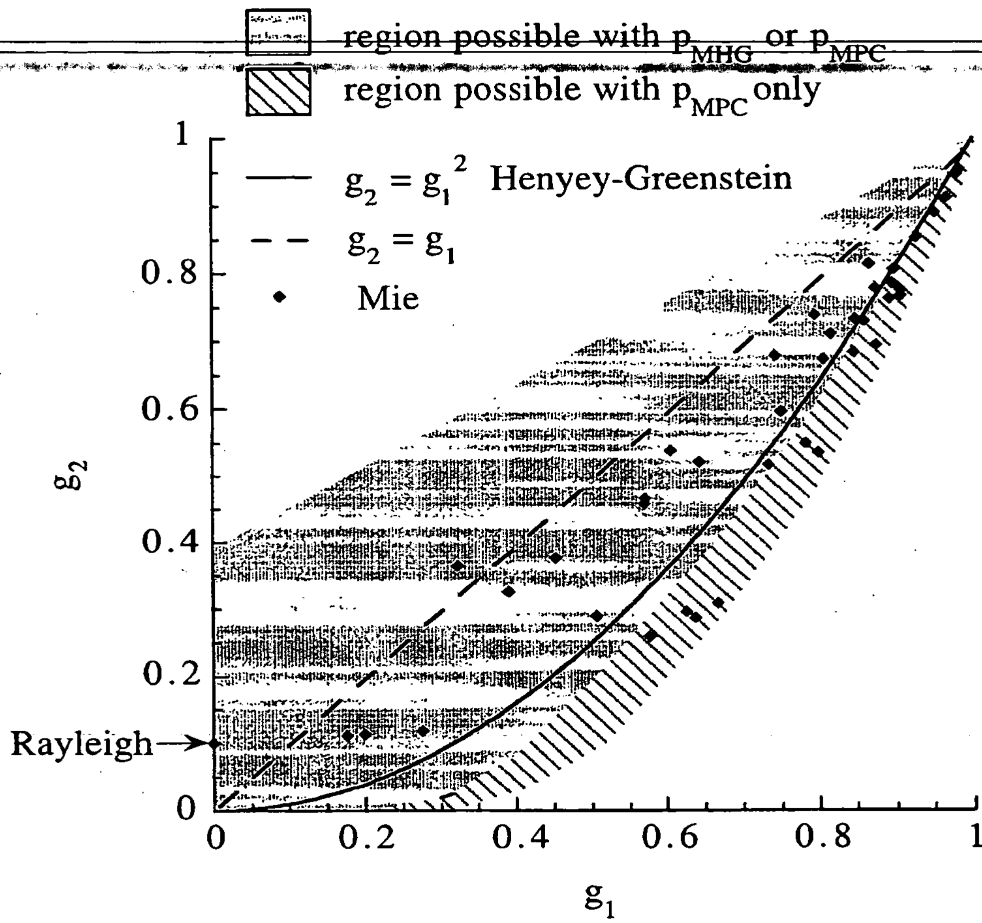
region possible with p_{MHG} or p_{MPC}
region possible with p_{MPC} only
$g_2 = g_1^2$ Henyey-Greenstein
$g_2 = g_1$
Mie
Rayleigh
g_2
g_1
0
0.2
0.4
0.6
0.8
1

fig 3.

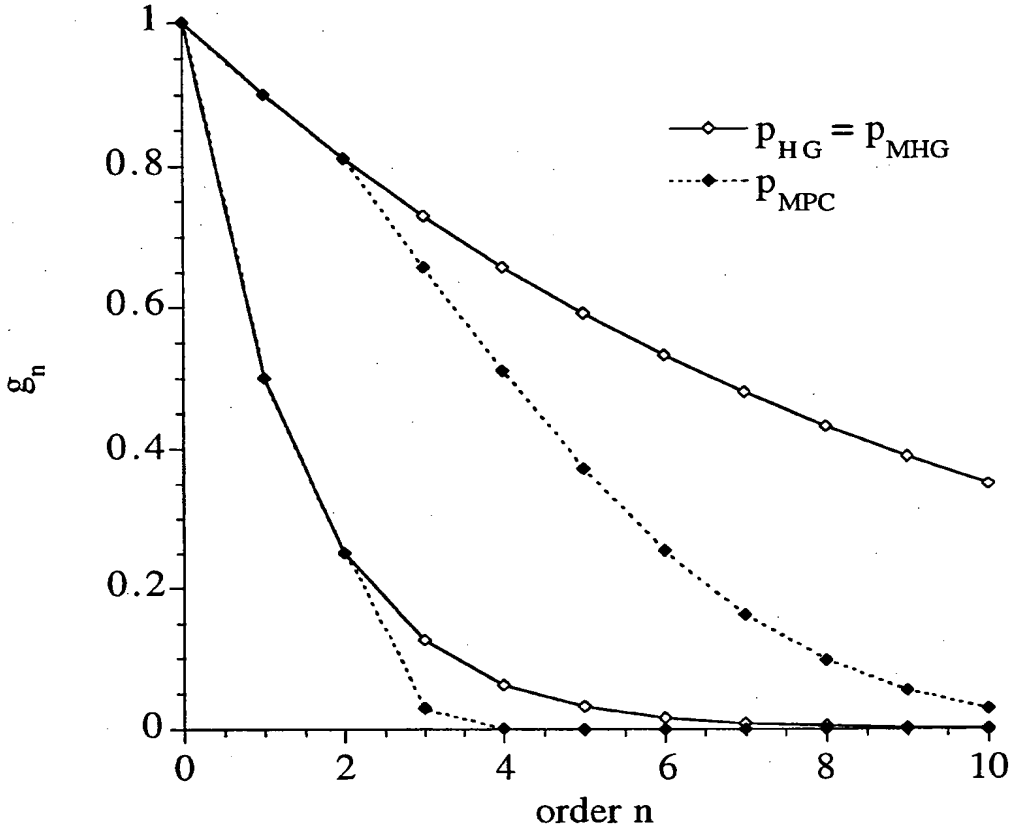

fig 4

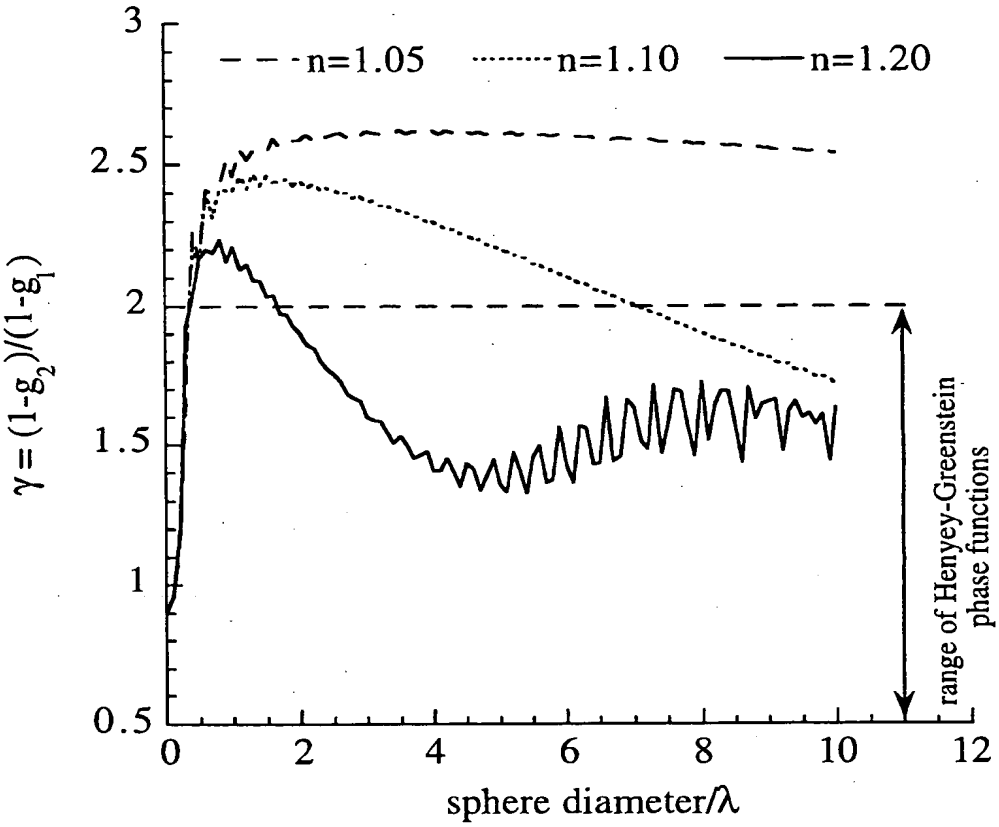

Fig 5

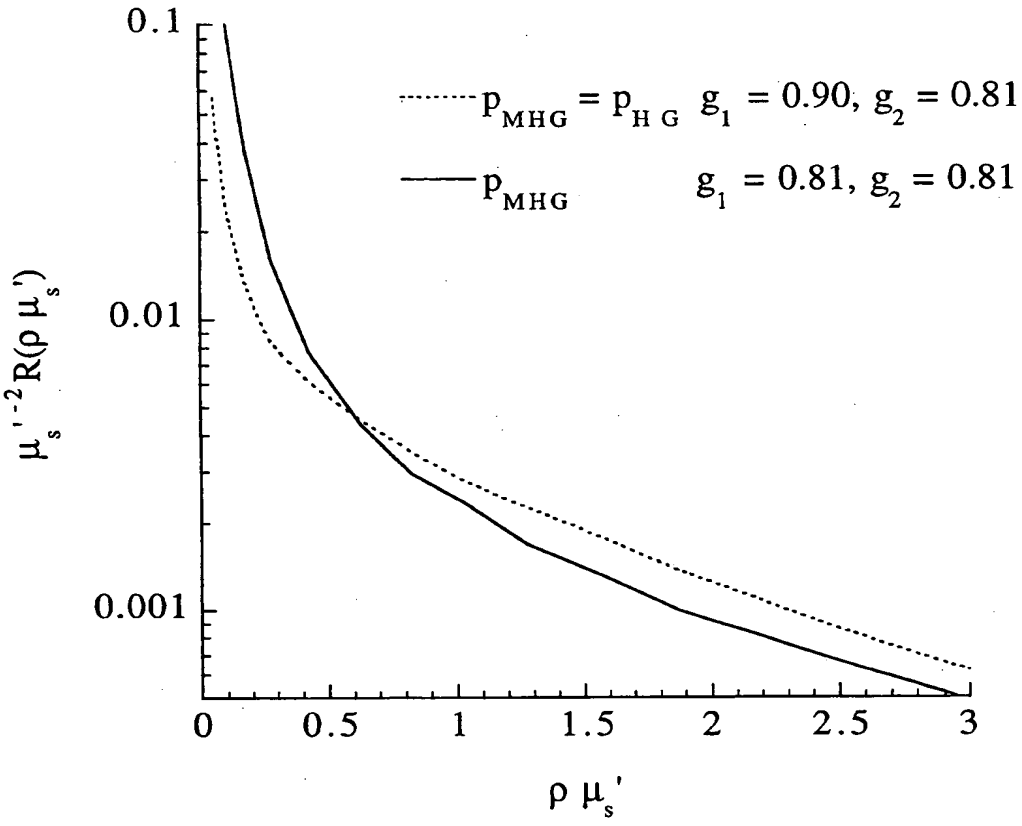

fig 6a

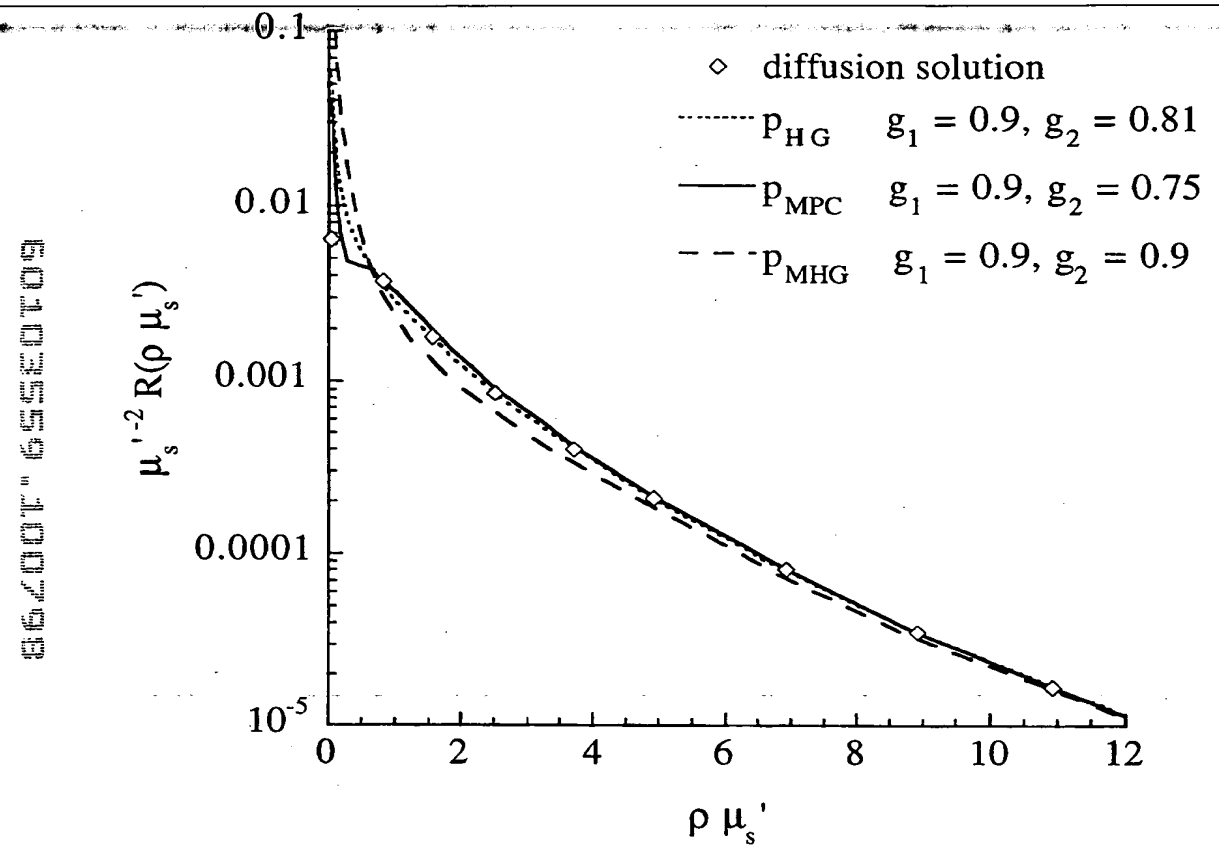

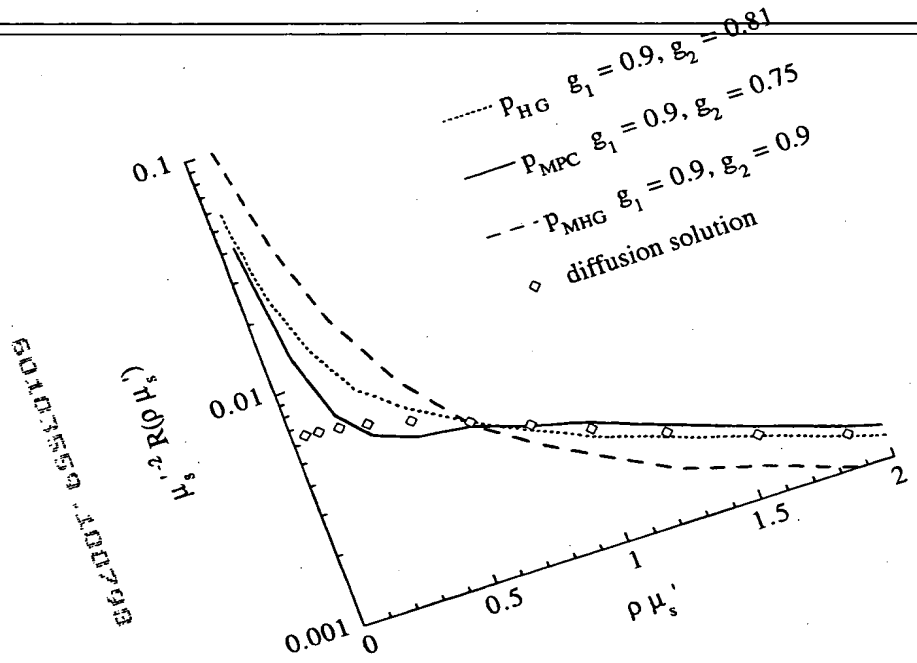
p_{HG} $g_1 = 0.9, g_2 = 0.81$
p_{MPC} $g_1 = 0.9, g_2 = 0.75$
p_{MHG} $g_1 = 0.9, g_2 = 0.9$
diffusion solution
0.1
0.01
0.001
0
0.5
1
1.5
2
$\rho\mu_s'$
$\mu_s'^2 R(\rho\mu_s')$

fig 7a

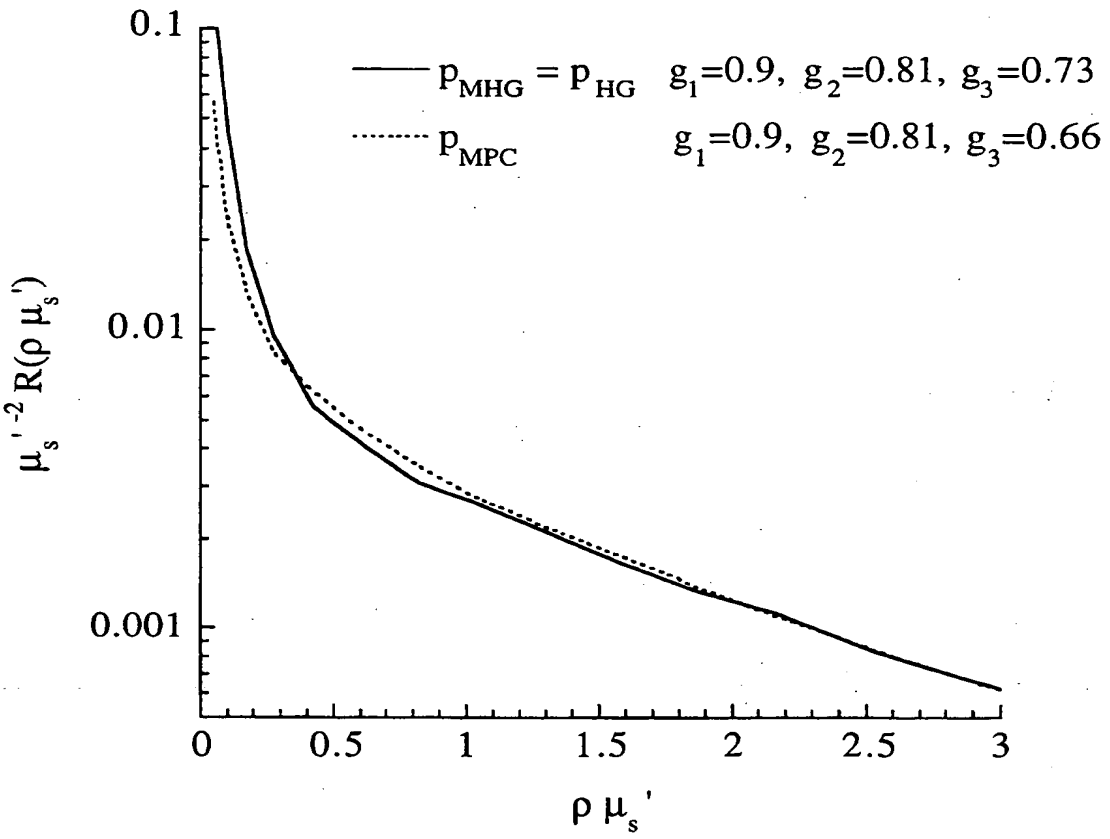

fig 7b

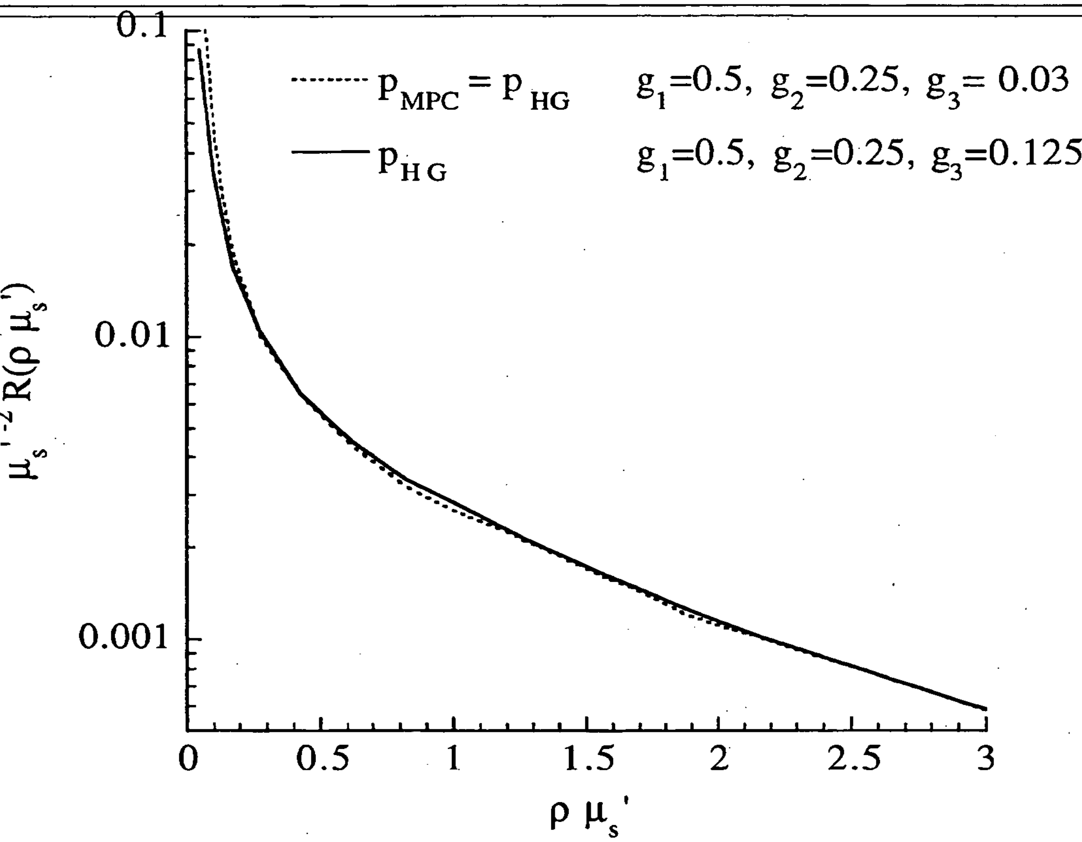

$p_{MPC} = p_{HG}$ g_1=0.5, g_2=0.25, g_3= 0.03
p_{HG} g_1=0.5, g_2=0.25, g_3=0.125
0.1
0.01
0.001
0
0.5
1
1.5
2
2.5
3
$\mu_s'^{-2} R(\rho \mu_s')$
$\rho \mu_s'$

Fig 8a

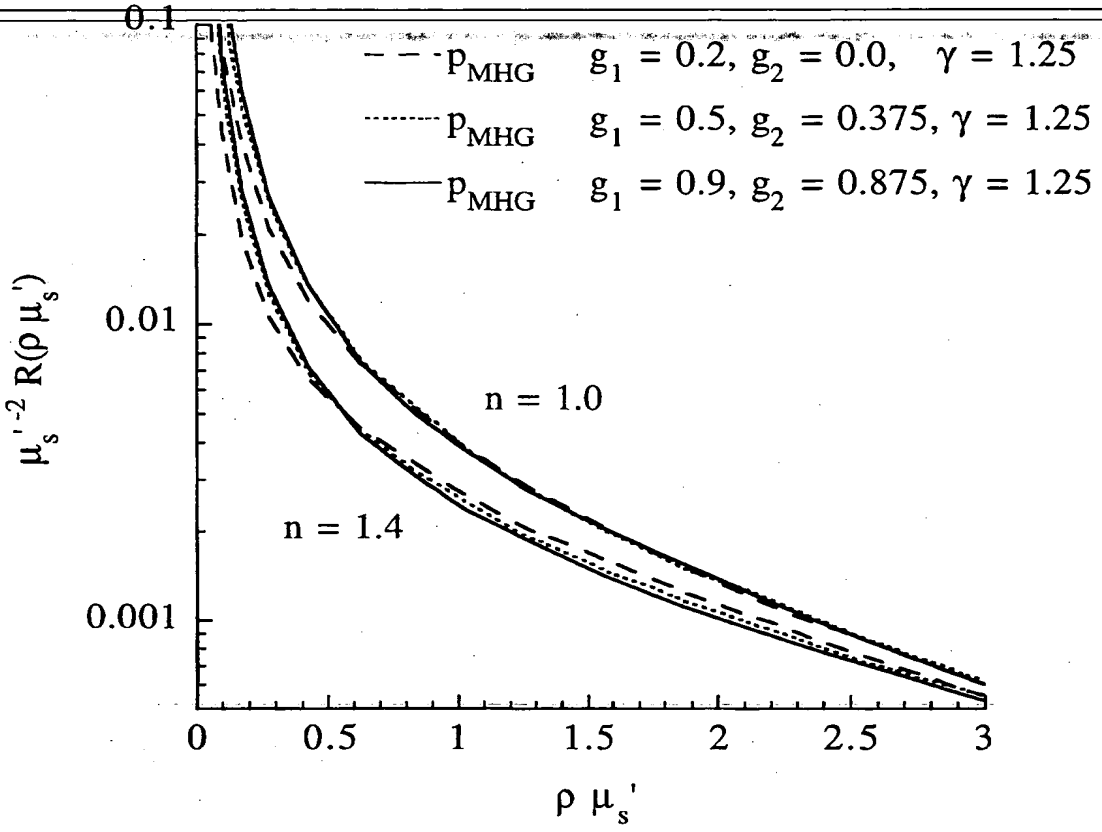

fig 8b

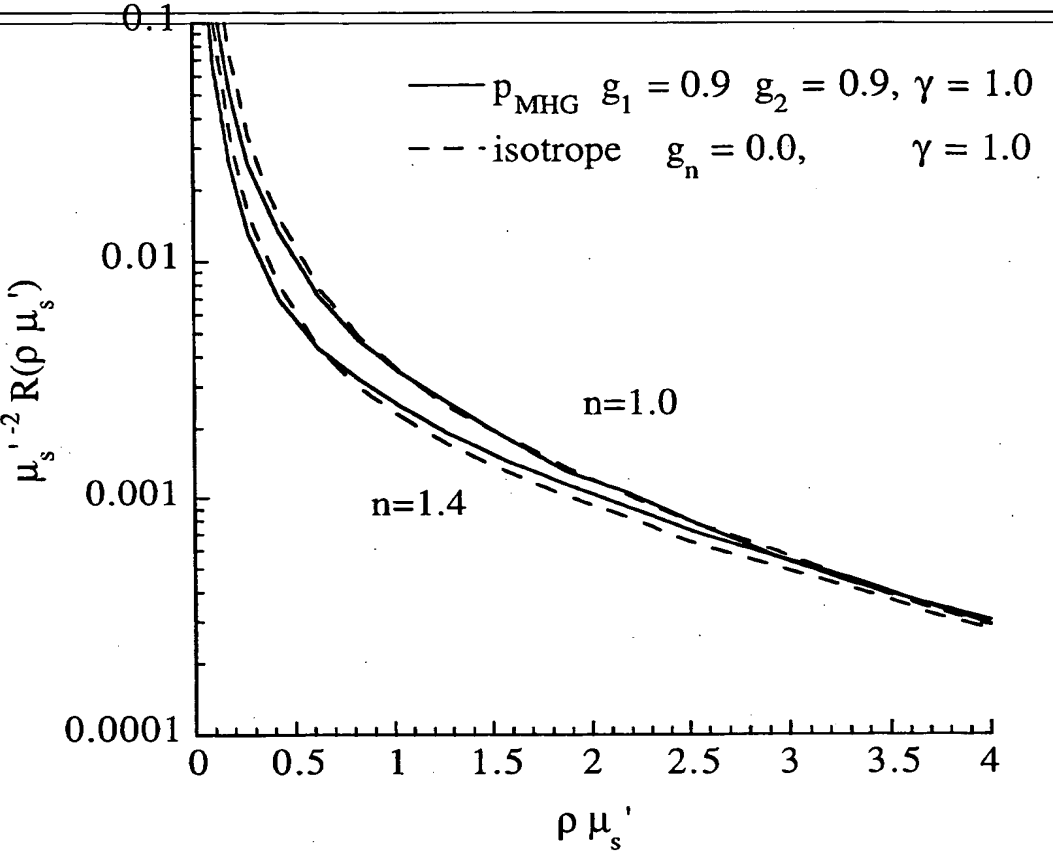

fig 9

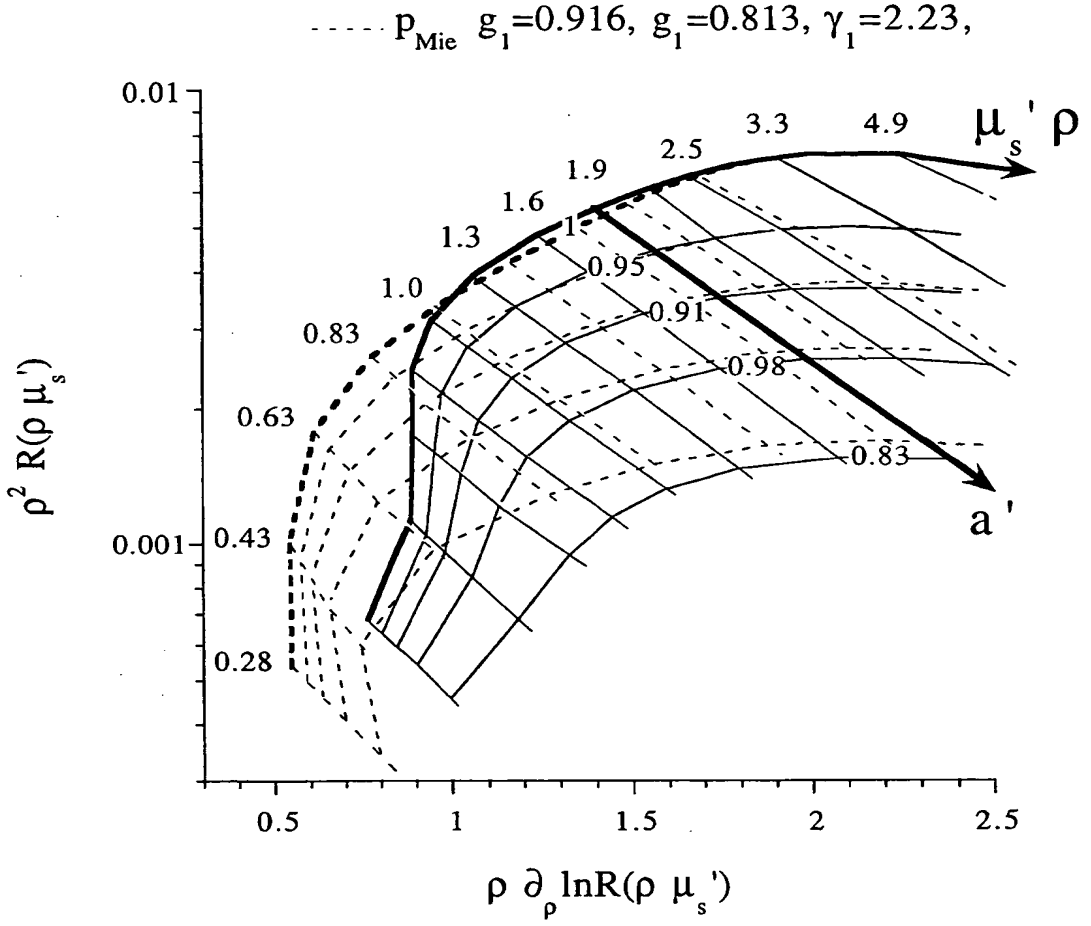

fig 10a

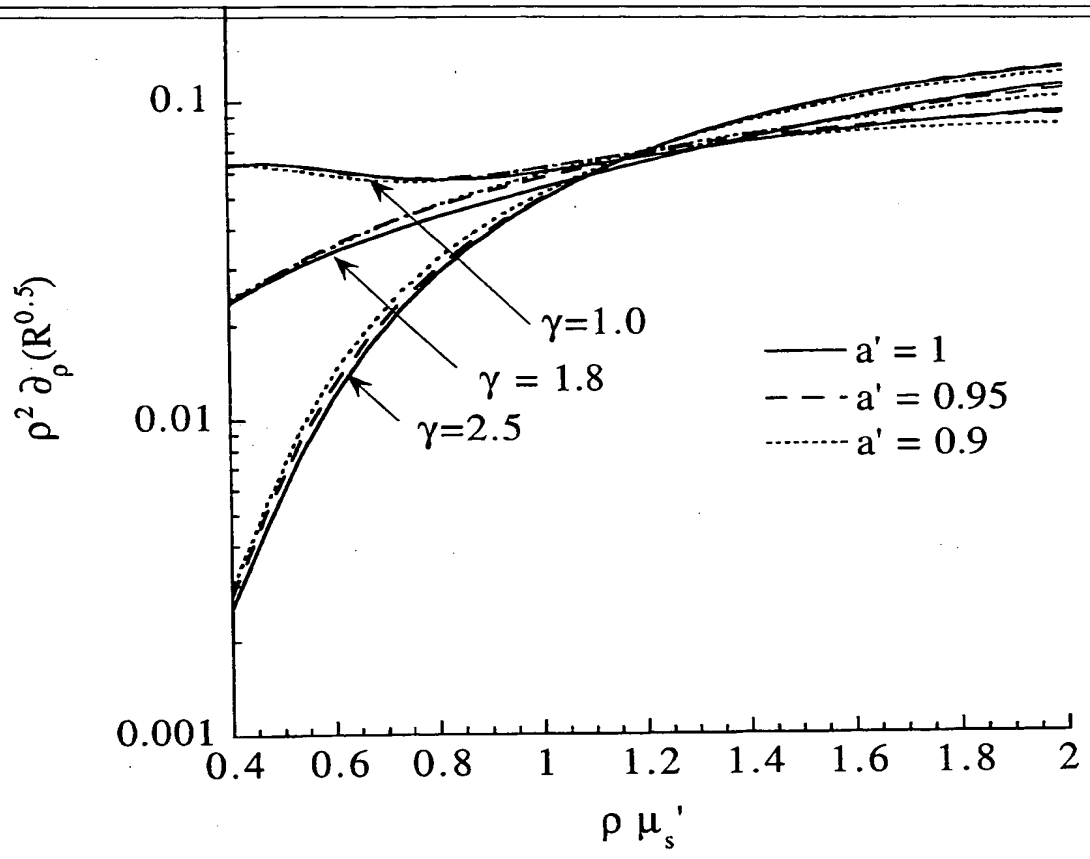

In vivo local determination of tissue optical properties: Applications to human brain

F. Bevilacqua[a], D. Piguet[a], P. Marquet[a], J.D. Gross[c], B.J. Tromberg[b] and C. Depeursinge[a]

[a]Institut d'Optique Appliquée, Département de Microtechnique,
Ecole Polytechnique Fédérale de Lausanne, CP 127, 1015 Lausanne, Switzerland
e-mail: frederic.bevilacqua@epfl.ch

[b]Laser Microbeam and Medical Program, Beckman Laser Institute and Medical Clinic,
University of California at Irvine
1002 Health Sciences Road
Irvine CA 92612, USA

[b,c]Division of Neurological Surgury
University of New Mexico School of Medicine
Albuqueruqze, NM 87131, USA

ABSTRACT

Local and superficial near infrared (NIR) optical property characterization of turbid biological tissues can be achieved by measuring spatially resolved diffuse reflectance at small source-detector separations (<1.4 mm). However, under these conditions, the inverse problem. i.e. calculating localized absorption and the reduced scattering coefficients, is necessarily sensitive to the scattering phase function. This effect can be minimized if a new parameter of the phase function γ which depends on the first and second moments of the phase function, is known. If γ is unknown, an estimation of this parameter can be obtained by the measurement, but the uncertainty on the absorption coefficient is increased. A spatially-resolved reflectance probe employing multiple detector fibers (0.3 to 1.4 mm from the source) is described. Monte Carlo simulations are used to determine γ the reduced scattering and absorption coefficients from reflectance data. Probe performance is assessed by measurements on optical phantoms, the optical properties of which was measured by other techniques (frequency domain photon migration (FDPM) and spatially-resolved transmittance) and reasonable agreements are found. However, the spatially resolved probes shows optimum measurement sensitivity in the measurement volume immediately beneath the probe, while FDPM typically samples larger regions of tissues. In vivo measurements performed intraoperatively on human skull and brain are reported for 4 NIR wavelength (674, 811, 849, 956 nm), using both methods. Optical property values for human skull, white matter, scar tissue, optic nerve and tumors are reported, which show distinct absorption and scattering differences between structures and a clear dependence on the phase function parameter γ.

Keywords: turbid media, tissue optics, optical biopsy, neural tissue, absorption coefficient, scattering coefficient.

1. INTRODUCTION

Probing the optical properties of biological tissues has a major impact in several medical applications for diagnosis and therapy. For example, the knowledge of these properties is necessary for optimizing techniques such as near infrared spectroscopy or photodynamic therapy. The scattering and absorption characteristics of many different kinds of tissues have been reported in the literature[1]. However they have been mostly measured *in vitro*. Because of unavoidable alterations of excised samples, such as blood drainage, structural alterations, and temperature changes, these values are questionable and *in vivo* measurements are preferable.

The measurement of optical properties performed *in vivo* could be also used as a diagnostic tool, which is complementary to other optical biopsy techniques, e.g. tissue autofluorescence. Indeed, light scattering and absorption can provide information both on tissue structure and chromophore content, features which can be used to distinguish between normal tissues, malignant lesions and other pathologies. For example hemoglobin and water content have been found to be significantly different in normal and cancerous tissues[2,3]. Differentiation between normal and malignant bladder tissues[4] have found to be possible from the elastic scattering and absorption properties.

Different methods have already been proposed to quantitatively determine the absorption and reduced scattering coefficients *in vivo*, using spatially-[5-7] and/or temporally-resolved measurements[2,3,8,9]. Besides organs such as breast or brain which can be transilluminated, measurements of thick tissues can be made in reflectance geometry. The case where the source-detector separations are larger than several transport mean free paths, corresponding typically to distances larger than 5 mm for biological tissues, has been extensively studied theoretically and experimentally. Diffusion theory or Monte Carlo simulations have been commonly used to relate the measured light intensity to the optical coefficients. In particular, optimized source-detector separations have been calculated by different authors[6,10] in order to ensure the best sensitivity to absorption and scattering coefficients from spatially-resolved reflectance data. For typical turbid tissues, optimal determination of both absorption and scattering properties requires reflectance measurement at small and large distances. For example, measurements were performed by Patterson and co-workers using distances from 1 to 10 mm, and by Bays and co-workers using distances from 3.6 to 15 mm or 2 to 14 mm.

Nevertheless, all these studies consider the turbid medium as homogeneous, or made of homogeneous layers. Our approach is different. We wish to optically characterize a small volume of tissue, on the order of a few cubic millimeters, possibly distinct from the surrounding tissues. Therefore, our goal is to differentiate a small tissue heterogeneity instead of determining average optical properties of a large volume of tissue. To achieve this we chose to perform spatially resolved reflectance measurements with only small source-detector separations, from 0.3 to 1.4 mm, even if these distances are not optimal for absorption determination.

Mourant et al[4,11] have shown that the absorption coefficient can be estimated with a measurement at a single distance of approximately 1.7 mm, assuming the scattering coefficient to be in a certain range. They have also shown that measurements at a single shorter distance (approximately 0.3- 0.4 mm) allows monitoring of spectroscopic variations in the scattering properties of tissues. In this work, we address a general case where both tissue scattering and absorption properties are simultaneously estimated, from measurements at distances smaller than 1.4 mm.

A previous study we performed using Monte Carlo simulations gives the theoretical framework for the interpretation of the measured profile in terms of absorption and scattering properties[12,13]. The role of the phase function at short source detector separations were carefully studied. In particular, we showed that, beside the absorption and reduced scattering coefficients, a parameter depending on the first and second moment of the phase function must be taken into account, for source detector separation ranging from 0.3 to 5 transport mean free path. This analysis is more complete compared to previous work which considered only the first moment of the phase function (anisotropy factor).

We first describe the probe design and the Monte Carlo model developed to simulate the measured profile. Second the average tissue volume probed, and sensitivity to medium boundaries are discussed from experiments and simulations. Third we describe how the scattering and absorption properties of tissues can be deduced from reflectance data. The accuracy of the proposed procedure is demonstrated on phantoms, the optical properties of which are measured by others techniques. Finally measurements of human brain and cervix tissues obtained *in vivo* are presented and discussed. These clinical measurements were performed in parallel with a complementary method, frequency domain photon migration (FDPM)[2,3], which probes a

larger tissue volume. Optical properties from FDPM measurements are compared with values obtained by the spatially-resolved method described here, using small source-detector separations.

2. MATERIALS AND METHODS

A. Definitions

The spatially resolved reflectance is denoted $R(\rho)$ where ρ is the source-detector separation. It is defined by the power received by a detector per unit area for a source of power unity. In our measurements ρ ranges between 0.3 and 1.4 mm.

The optical properties of tissues are the average index of refraction n of the medium, the absorption coefficient μ_a, the scattering coefficient μ_s, and the phase function $p(\theta)$ where θ is the scattering angle. The phase function is the density probability function for θ. We consider the index of refraction of tissues[14] as a constant n=1.4.

It is also useful to define the reduced scattering coefficient $\mu_s' = \mu_s(1-g)$ and the transport mean free path *mfp'* $= (\mu_s'+\mu_a)^{-1}$ where g is called the anisotropy factor and is defined as the average of $\cos\theta$. Generally the reduced scattering coefficient μ_s' and the absorption coefficient μ_a are used to characterize optically thick tissue. Indeed, the light fluence rate depends only on μ_s' and μ_a at distances of several transport mean free paths (typically ρ>5mm) from the source (diffusion approximation). Therefore the use of μ_s' and μ_a is a natural choice if measurements are performed at such distances. As we want to make measurements at closer distances, in the range of one transport mean free path, we expect that some parameters of the phase function have to be taken into account. This theoretical problem was fully studied with Monte Carlo simulations and reported in reference 12. We consider below only the main implications of this work.

For distances between than 0.3-5 [mfp'], we found that the reflectance curve depends on μ_a, μ_s' and a third parameter $\gamma = (1-g_2)/(1-g_1)$, where g_1 and g_2 are respectively the first and second moment of the phase function. The parameter γ is derived from the second order similarity relations derived by Wyman et al[15], which are valid for a quadratically anisotropy radiance. For comparison, note that the diffusion approximation and first order similarity relation correspond to a linearly anisotropy radiance.

Generally, the n^{th} moment g_n is defined as[16]:

$$g_n = 2\pi \int_0^{\pi} P_n(\theta) p(\theta) \sin\theta d\theta \qquad (1)$$

where P_n is the Legendre polynomial of order n. Note that the first moment g_1 is the anisotropy factor g. The role of the parameter $\gamma=(1-g_2)/(1-g_1)$ implies that the anisotropy factor g ($=g_1$) alone is not sufficient to predict correctly the reflectance curve close to the source.

From this analysis, each tissue can be potentially characterized by three parameters: μ_a, μ_s' and γ. However, due to the restricted range of the source-detector distances we want to use, the simultaneous determination of μ_a, μ_s' and γ is not always possible with high degree of accuracy. The achievable accuracy depends on the optical properties themselves and on the experimental uncertainties. This problem is addressed in the results section 3. for both phantom and tissue measurements.

The parameter γ may give interesting information about the tissue structure. Indeed, as measured by several authors[17-20], tissue phase function can be seen as a sum of a highly forward phase function $p_{HA}(\theta)$, due to large particles, plus a low anisotropy phase function $p_{LA}(\theta)$, due to small particles.

$$p_{tissue}(\theta) = (1-\alpha)p_{HA}(\theta) + \alpha\, p_{LA}(\theta) \qquad (2)$$

The coefficient α is introduced to guaranteed the normalization of $p_{tissue}(\theta)$.

The first term $p_{HA}(\theta)$ has been often fitted to the Henyey-Greenstein phase function:

$$p_{HG}(\theta) = \frac{1}{4\pi} \frac{1-g_{HG}^2}{(1+g_{HG}^2 - 2g_{HG}\cos\theta)^{3/2}} \qquad (3)$$

The moments of the Henyey-Greenstein phase function are given by $g_n = g_{HG}^{\ n}$ (n>0).

The second term $p_{LA}(\theta)$ can be interpreted by Raleigh scattering, valid for very small scatterers compared to the wavelength. It has been approached by a purely isotropic term[17] or an Henyey-Greenstein phase function with a low negative g value[18]. We propose to use the exact Rayleigh phase function[16]:

$$p_{Rayleigh}(\theta) = \frac{3\pi}{16}(1+\cos^2\theta) \quad (4)$$

The moments of the Rayleigh phase function are: $g_1 = 0$, $g_2 = 0.1$, $g_3 = 0$, $g_4 = 0$, ...

Rayleigh scattering give no contribution to first moment g_1, but only to the second moment g_2. The moments of the tissue phase function $p_{tissue}(\theta)$ given by Equ.(2) are therefore:

$$g_1 = (1-\alpha)g_{HG},\ g_2 = (1-\alpha)g_{HG}^2 + 0.1\alpha \quad (5)$$

Therefore, we see that the parameter γ is influenced by the relative concentration of Rayleigh scatterer α, which should depends on the tissue structure.

Published phase function data suggest possible values of γ for biological tissues[17-20]. They have been performed by goniometric experiments of thin samples. Many artifacts can affect these measurements, such as the tissue preparation and the tissue thickness, and these results should be used with caution. The phase function reported by Jacques et al.[17] for human dermis at 633 nm leads to $\gamma = 1.4$. The phase functions of white and grey matter at $\lambda = 750$ nm measured by van der Zee et al.[19] give values of approximately 1.5. Therefore we performed p_{MHG} simulations with $\gamma = 1.5$ as a starting point. As will be discussed, fitting our experimental data to simulations performed with different values of γ estimation, permits reasonable parameter estimation.

B. Experimental setup

The probe used for the measurement of the spatially resolved reflectance is described in Fig.1. It is a linear array of optical fibers (core diameter of 200 µm, N.A. = 0.37 in air). Two source fibers can be used to illuminate the tissue. They are disposed symmetrically in regard to the collecting fibers. If the sample is homogeneous, the reflectance curve is identical with either illuminating fiber. Therefore, comparing the two curves tests the heterogeneity of the investigated tissue region or detects obstructions, beneath the illuminating fibers. If the two curves are close (typically differences less than 10%), the measurement is validated and the average of the two curves is calculated.

The illuminating fibers are slid in small stainless steel tubes in order to avoid direct light coupling with the collecting fibers. The coupling between each collecting fiber has been experimentally measured and found to

be less than 2%. The fiber array is set in a stainless steel tube of 2.2 mm diameter and 20 cm long. The tube is filled with an optically clear adhesive. The probe is rigid, which allows for easier handling by the physician, during surgery for example. The whole probe can be sterilized.

The experimental setup is shown in Fig.2. An optical switch (Dicon, model GP700) is used to select the illuminating fiber from different sources. For the brain measurements, four laser diodes emitting at 674 nm, 811 nm, 849 nm and 956 nm were used (SDL, Inc. models 7421, 5420, 5421 and 6321, respectively). Two other laser diodes were used for the phantom measurements, emitting at 675 nm and at 828 nm (ILEE LDA 2011 and 1805 respectively). The six fibers used to collect the backscattered light are imaged on a linear Charge-Coupled-Device (CCD) (Hamamatsu S3921). The signal is digitized by a 12 bit A/D card. Only one measurement, which takes approximately 0.1 s, is then needed to measure simultaneously the intensity collected by the six fibers. The entire system is controlled by a personal computer.

Transmission differences between each fiber are corrected using a measurement on a turbid phantom illuminated uniformly. Immediately after each reflectance measurement, a measurement of the background light is automatically performed and then subtracted from the reflectance signal. To minimized the background light, a long pass filter ($\lambda > 650$ nm) is put between the end of the bundle and the CCD. Even during open surgery where the ambient light is substantial, the measured background was less than 5% of the signal.

C. Monte Carlo Simulations

A model of photon migration in tissues is necessary to define the relationship between the measured reflectance and the optical properties. Analytical solutions from the diffusion equation are not appropriate in our case because we are interested in the reflectance close to the source, at a distance comparable to the transport mean free path [mfp']. [5,7] We performed Monte Carlo simulations to predict the measured reflectance of an homogeneous semi-infinite turbid media. The code we used was extensively tested[21,22]. Any phase function can be implemented in discretized form.

Our simulations take into account the exact diameter of the illuminating and collecting fibers, as well as their numerical apertures (NA=0.28 in tissue). However, the distortion of the signal due to the size of the fibers we used (200 nm) has an almost negligible influence on the reflectance curve.

The mismatch of index of refraction at the surface of the medium is also taken into account in our simulation, by using the Fresnel law for each photon reaching the surface. Simulations have been performed with the exact geometry of the probe as described in Fig.1, taking into account the mismatch of index of refraction between the probe adhesive ($n = 1.5$) and the sample, as well as the mismatch of index of refraction between the air and the sample outside the probe ($\rho > 1.8$ mm) (see Fig.3 and Fig.4). Nevertheless we found that the effect of the boundaries located at $\rho<1.4$ mm have a weak influence on the intensity collected by the fibers. To illustrate this, the reflectance obtained with the exact probe configuration is compared in Fig.4 to the simplified case of the semi-infinite space ($n_{medium} = 1.4$, $n_{probe} = 1.5$). As expected, there are important differences between the exact and simplified cases for $\rho>1.5$ mm, close to the limit of the probe. The decreased reflectance at $\rho > 1.8$ for the exact case is due to the increase of internal reflection at the interface between the medium and the air. However, the differences between the exact and simplified cases are less than few percents for $\rho < 1.4$ mm, corresponding to the region where the measurements are performed.

The simplified case, assuming a cylindrical symmetry, is computationally much less time-consuming than the "exact configuration". "Exact configuration" simulations require approximately ten times the number of photons to achieve statistical errors comparable for the simplified case. Following the result illustrated in Fig.4, we decided to employ only the simplified semi-infinite condition and restrict to $\rho < 1.4$ mm.

3. RESULTS AND DISCUSSION

A. Boundary effects

During *in vivo* investigations the ideal case of a medium with a perfect plane surface is never realized. Moreover, the probe could be slightly pushed inside the tissue. Therefore the effect of the medium boundary on the measured reflectance is important to quantify experimentally. In Fig.5, we show two measurements in Intralipid ($\lambda = 675$ nm), one at the surface and the second inside the medium. The difference between these

two measurements is less than 5%, which could seem very surprising at first glance. However, as it was shown by simulation in Fig.4, the boundary condition outside the probe has only a weak effect on the intensity measured by the six fibers. The boundary condition created by the probe itself, i.e. the index of refraction mismatch between the medium and the adhesive inside the probe, is much more critical.

The negligible effect of the tissue boundaries shown in this section is an important advantage for clinical investigation. This experiment also clearly demonstrates that the sample volume investigated is principally confined to the region just beneath the probe surface. This point is developed further in the next section.

B. Depth of tissue investigated

To quantify more precisely the volume of tissue probed by our technique, the average depth of scattering events was recorded for each photon detected in Monte Carlo simulations (backscattered photons). To allow more general statements, distances are expressed in mfp' units. For typical turbid tissue[1] and near infrared wavelengths, μ_s' is around 1 mm^{-1} and μ_a less than 0.1 mm^{-1}, which means that 1 mfp'≈ 1mm. Fig.6 shows that the average depth of scattering is approximately around 1 mfp'. Moreover it shows that for typical tissue optical properties, structures greater than 2 mfp', located beneath the probe are not likely to contribute significantly to the measured signal (for $\rho < 1.5$ mfp').

To evaluate experimentally the average depth probed, we performed experiments in Intralipid placing the probe at the liquid surface, and moving an absorbing plate placed horizontally, as described in Fig.7. The reflectance $R(\rho, d)$ was measured for varying thickness d. The ratio $R(\rho, d)/R(\rho, d=\infty)$ is reported in Fig.7. This figure shows that the intensity of the reflectance is decreased by approximately 20% if the medium is 2 [mfp'] thick, and by 10% if it is 3 [mfp'] thick (for the albedo and the range of ρ considered). These results imply that 80% or 90% of the photons do not penetrate deeper than 2 [mfp'] or 3 [mfp'], respectively, into the medium. This confirms our simulation results (Fig.6) where the average depth of scattering was estimated to be approximately 1 mfp'. Thus, for typical biological tissues, our measurements are mainly sensitive to the region of tissue located within 2 mm of the surface and the investigated volume is on the order of 1 mm^3.

C. Calibration and test on microsphere suspension.

In order to perform absolute intensity measurements, calibration is performed on a solid turbid siloxane phantom of known optical properties (determined independently by frequency domain photon migration [2,3]). As shown in Fig.8, these measurements, multiplied by a factor independent of the fibers, fit well the Monte Carlo simulations performed with the phantom coefficients. This factor is defined as the calibration factor for a given wavelength. It is derived from measurements on the standard tissue phantom obtained at the end of each set of clinical measurements. The calibration was performed at the end of each set of clinical measurements.

Experiments on microsphere suspensions (polystyrene sphere Ø 1.072 ±0.019 μm) were performed to assess the accuracy of our theoretical model and the calibration method. The scattering coefficient and the phase function of such turbid media can be precisely known using Mie theory[23]. As no dye was added to the suspension, μ_a was considered to be equal to the water absorption. In Fig.8, a measurement of the reflectance is compared to a simulation computed with the microsphere suspension coefficients (μ_s' = 1.0 mm^{-1}, μ_a = 0.00041 mm^{-1}, γ = 2.2). The excellent agreement found here between experiments and simulation confirms the accuracy of our simulations, and the validity of our calibration procedure.

D. Inverse problem

Our goal is to solve the inverse problem which consists of extracting optical coefficients from the reflectance data. The measurements of the reflectance intensity R(ρ) and the slope of lnR(ρ), determined at a distance ρ = 1 mm, can be used to derive μ_s' and μ_a for a given γ value. Fig.9 shows graphically the relationship between μ_s' and μ_a and the two parameters R(ρ=1 mm) and $|\partial_\rho \ln R(\rho=1 \text{ mm})|$. To illustrate the influence of the parameter γ, two examples are superimposed: γ = 1.5 and γ = 1.9. We see clearly in Fig.9 that μ_s' and μ_a can not be determined uniquely from the two parameters R(ρ=1 mm) and $|\partial_\rho \ln R(\rho=1 \text{ mm})|$ if γ is unknown. This indetermination may be resolved by the values of R(ρ) and/or $|\partial_\rho \ln R(\rho)|$ at other distances. Therefore the following procedure was defined for tissue measurements:

(1) determination of μ_s' and μ_a from R(ρ=1 mm) and $|\partial_\rho \ln R(\rho=1 \text{ mm})|$ for discrete values of γ (for example γ=1.0,1.5, 1.9, 2.2)

(2) simulations with the different sets of μ_s' and μ_a obtained

(3) comparison between the simulations and the reflectance profile for distances $0.35<\rho<1.4$ mm.

This last step allows us to determine the value of γ which gives the best fit. Points 1 to 3 can be done iteratively to evaluate γ more precisely. The precision that can be obtained depends on the optical coefficients themselves, and on the experimental uncertainties. Nevertheless two important technical points should be noted here:

First, the determination of μ_s' is only weakly influenced by γ, for μ_s' close to 1 mm^{-1}. Indeed in Fig.9 the differences induced by $\gamma = 1.5$ or $\gamma = 1.9$ are typically 10% for μ_s'.

In contrast, absolute determination of μ_a is critically sensitive to by γ. However, if γ remains constant, relative variations of μ_a can be still precisely evaluated. This point is discussed with the results obtained of Intralipid measurements in the next section. Metabolism monitoring or drug monitoring could be therefore a potential application of such a probe.

Second, the experimental determination of $|\partial_\rho \ln R(\rho=1 \text{ mm})|$ requires measurements at different distances close to 1 mm. To minimize errors on $|\partial_\rho \ln R(\rho=1 \text{ mm})|$ due to experimental artifacts, we perform a fit of the reflectance curve (0.5 mm $<\rho$ 1.4 mm) with the function $m_1\rho^{m_2}\exp(-m_3\rho)$ which was always found to fit well to Monte carlo simulations for this restricted range of distances (the same function was also proposed by Bolt and ten Bosh[24]). The parameters $R(\rho=1 \text{ mm})$ and $|\partial_\rho \ln R(\rho=1 \text{ mm})|$ are then derived from the fit. Once the optical coefficients μ_a and μ_s' are derived, the validity of this procedure is double-checked, by comparing the curve obtained from the Monte Carlo simulation to the experimental profile.

E. Phantom measurements

We present in this section measurements on tissue-like phantoms (Intralipid™ and on microsphere suspensions). The value of γ is *a priori* not known for Intralipid. Measurements of Intralipid phantoms with varying μ_a and μ_s' values were used to test the inversion procedure. Phantom optical properties were calibrated by the FDPM technique, (performed at large source-detector separations and therefore insensitive to γ). For Intralipid measurements, reflectance profiles were found to be fit best when the parameter γ was

between 1.6 and 1. 8 for λ =674 to 849 nm. μ_a values derived from our method are plotted in Fig.10.a versus the values obtained by the FDPM technique. Fig.10.a shows that γ=1.8 leads to an overestimation of μ_a by approximately 0.005 mm^{-1}, whereas γ=1.6 leads to an underestimation of μ_a by approximately 0.01 mm^{-1}. This confirms that exact value of γ is between 1.6 and 1.8. This example clearly illustrates that absolute values of μ_a are sensitive to γ. However relative measurements of $\Delta\mu_a$ are achievable with a sensitivity of 0.005 mm^{-1} using our system. The accuracy of the inversion procedure on μ_s' is illustrated in Fig.10.b. In the case of μ_s', as already mentioned above, the influence of γ is weaker than in the case of μ_a. A difference of only 5% is found on the μ_s' if γ=1.6 is used instead of 1.8. This is also approximately the variation in μ_s' values obtained by multiple FDPM measurements. We also found that in the case of a constant Intralipid concentration, the measured values of μ_s' vary less than 2% when μ_a is increased by adding dye, which proves that the data inversion procedure effectively uncouples μ_a and μ_s'.

Further assessments of the inversion procedure were performed on microsphere suspensions. In this case the value of γ is known: γ=2.22. The optical coefficients derived from our local reflectance measurements are compared to values obtained with a spatially-resolved transmittance method described elsewhere[21,22].

Fig.11.a and Fig.11.b. show μ_a and μ_s' values obtained by both methods: spatially resolved transmittance and reflectance. Phantoms made of microsphere suspensions and ink, at different concentrations, were used. An excellent correlation is found between the μ_a and μ_s' values, obtained by the two methods. Small systematic differences (typically 10%) are found when comparing absolute values. They are mainly due to errors occurring in the calibration procedures (for both methods).

The relatively small errors we found here are typical of errors found when different techniques for measuring turbid media optical properties are compared[25]. Such errors could be avoided by multiple calibrations on several turbid samples of different known optical properties. However, the accuracy of tissue measurements is subject to other major limitations, due for example to their structure and heterogeneity[26]. Therefore, more accurate calibration is not necessarily required for absolue tissue measurements, since we are mainly interested in observing optical property differences between tissue physiological states.

F. In vivo measurements on brain tissues

Clinical measurements of normal and malignant neural tissues were recorded *in vivo* during brain surgery[27]. Two different cases are reported here. Case 1 was a 3 year old male and case 2 was an 8 year old male. Different types of tissues were investigated in each case. Several measurements (typically 6) were always performed successively at a given location. The intensity fluctuations (typically on the order of 10%) for these measurements were mainly due to tissue heterogeneity and slight probe movements. The average reflectance was calculated for each location, as well as the standard deviation. Note that the uncertainty due to the apparatus, estimated from measurements on a phantom, are much lower (< 5%). Before each set of measurements, the blood from the surgical site was carefully irrigated away with saline, and the probe cleaned with a saline damped sponge. The measurements presented here were performed in parallel with frequency domain measurements (FDPM)[2,3] using a source-detector separation of 10 to 14 mm.

Fig.12.a and Fig.12.b. show the measured parameters $R(\rho=1 \text{ mm})$ as a function of $|\partial_\rho \ln R(\rho=1 \text{ mm})|$ obtained for cases 1 and 2, respectively. These graphs are similar to Fig.9, except that the relationship between the parameters $R(\rho=1 \text{ mm})$ and $|\partial_\rho \ln R(\rho=1 \text{ mm})|$ and the optical coefficients μ_a and μ_s' is indicated only qualitatively by two arrows for better clarity (different grids corresponding to different γ values should be superimposed). Quantitative results are reported in Table 1 and Table 2.

In case 1, measurements were performed on normal cerebral cortex (frontal lobe and temporal lobe), optic nerve astrocytoma (size≈1.3 cm) and normal optic nerve. In case 2, measurements were performed on the skull, deep cerebellar white matter with scar tissue (from a previous surgery), medulloblastoma (size≈3.8 cm), and deep cerebellar white matter (normal). Tumor dimensions were estimated from conventional imaging techniques (i.e. Computed Tomography and/or Magnetic Resonance Imaging).

As discussed in section B, the depth probed is less than about 3 mm. For each type of tissue that we investigated, the influence of surrounding tissues on the measurement is weak. In particular, only gray matter is investigated during the cerebral cortical surface measurements.

Fig.12.a and Fig.12.b. show that the parameters $R(\rho=1 \text{ mm})$ and $|\partial_\rho \ln R(\rho=1 \text{ mm})|$ provide an excellent discrimination between tissue types. The spectroscopic signature on $R(\rho=1 \text{ mm})$ and $|\partial_\rho \ln R(\rho=1 \text{ mm})|$ should also be noted. The cortex and the skull exhibit less significant spectroscopic differences compared to

tumor tissues such as the astrocytoma and the medulloblastoma. Thus, the parameters R(ρ=1 mm) and $|\partial_\rho \ln R(\rho=1 \text{ mm})|$ could be useful for optical biopsy. Nevertheless we believe that in order to fully exploit these results, the differences found must be explained in terms of scattering and absorption parameters. These factors, in turn, can be used to understand physiological and structural variations. The procedure described in the section D was used to determine the coefficients μ_s', μ_a and γ from the measured curves. This procedure is fully illustrated for measurements of the temporal lobe and astrocytoma. Results of optical coefficient calculations are summarized for all tissues in Table 1 and Table 2. Values obtained in parallel by the FDPM technique are also indicated.

Fig.13.a shows that the best fit to the cortex (temporal lobe) data is obtained with γ=1.9. Lower values, such as γ=1.5, led to impossible values for R(ρ=1 mm) and $|\partial_\rho \ln R(\rho=1 \text{ mm})|$ m) and should be therefore rejected. Larger values, such as γ=2.2 do not fit the reflectance data for distances $\rho < 0.8$ mm. The γ value is then estimated to be γ=1.9±0.2. The coefficients found with γ=1.9 are: $\mu_s' = 1.0$ mm^{-1} and $\mu_a = 0.02$ mm^{-1} at $\lambda = 674$ nm, and $\mu_s' = 0.82$ mm^{-1} and $\mu_a = 0.025$ mm^{-1} at $\lambda = 956$ nm. Note that $\gamma = 2.2$ would lead to almost identical μ_s' (differences less than 5%) and an overestimation of μ_a of approximately 0.02 mm^{-1}. Taking into account the uncertainties on the measurements (approximately 5% on R(ρ=1 mm) and $|\partial_\rho \ln R(\rho=1 \text{ mm})|$ for this tissue), and the uncertainty on γ (±0.2), the error on the absolute value of μ_s' is estimated to be 5%.

The astrocytoma reflectance obtained at 674 nm and 956 nm are plotted in Fig.13.b. with simulations performed with $\gamma = 1.5$ and 1.9. Both values of γ can fit well the reflectance at distance $\rho > 0.8$. For shorter distances $\rho < 0.8$, the experimental curve falls between the simulations with γ=1.5 and 1.9. The γ value is then estimated to 1.7±0.2. Taking into account this uncertainty on γ, $\mu_s' = 1.25 \pm 0.10$ mm^{-1}, $\mu_a = 0.14 \pm 0.03$ mm^{-1} at $\lambda = 811$ nm and $\mu_s' = 0.73 \pm 0.1$ mm^{-1}, $\mu_a = 0.15 \pm 0.05$ mm^{-1} at $\lambda = 956$ nm. As reported in Table 1, the absorption coefficients at 811 and 849 nm are lower than those obtained at $\lambda = 674$ nm or λ =956 nm. This result is consistent with the fact that the main near-infrared tissue chromophores, hemoglobin and water, have absorption maximum at approximately at $\lambda < 700$ nm and $\lambda = 970$ nm, respectively[28]. The overall absorption is much higher in the tumor than the cortex presumably due to the greater hemoglobin

abundance of these components, particularly hemoglobin in the tumor. Tumors generally grow more new blood vessels and thus have a higher blood flow.

The μ_s' of the tumor is similar to the cortex at λ = 956 nm. However the variation of μ_s' between λ = 674 nm and λ = 956 nm is much larger for the tumor than for the cortex: $\mu_s'(\lambda=956\text{ nm}) - \mu_s'(\lambda=674\text{ nm}) \approx 0.57\ mm^{-1}$ for tumor, $\mu_s'(\lambda=956\text{ nm}) - \mu_s'(\lambda=674\text{ nm}) = 0.10\ mm^{-1}$ for the cortex. Such spectroscopic variations may be attributable to structural differences between tissue types. Indeed such differences may depend on the average size or size distribution of scattering structures within or between cells.

Higher scattering is found for the normal optic nerve compared to all the other tissues in case 1. This is likely due to the presence of myelin. *In vitro* measurements have also shown that myelin containing white matter exhibits a higher scattering coefficient compared to other tissue[12,22]. The accuracy of the measurement on the optic nerve tissue can be affected by the high anisotropy of this type of tissue. Indeed, it has been reported that light propagation depends on whether the direction considered is parallel or perpendicular to the nerve fibers[29-31]. Interestingly, comparison between measurements with the two symmetric sources reveals larger differences than for the other tissues. This variation is represented in Fig.12.a by the relatively large uncertainties associated with the optic nerve measurements.

In case 2, the first measurements were acquired directly from the skull. The difference in reduced scattering properties between λ = 674 and 956 nm is very small (μ_s' = 0.9 and 0.85 mm^{-1}, respectively) as shown in Fig.12.b. Previously determined *in vitro* values[32] for pig skull were approximately twice as large. Such differences may be due to variations in water content and sample preparation between *in vivo* and *in vitro* studies.

Case 2 data were also obtained from, in series deep cerebellar white matter with scar tissue, tumor (medulloblastoma) and cerebellar white matter in the excavated tumor bed. Fig.12.b. shows that scar tissue is well differentiated from other structures and is characterized by high γ value (γ = 2.2) and low absorption ($\mu_a < 0.02\ mm^{-1}$), which is consistent with the low vascularization of such tissue. In contrast, larger μ_a, smaller γ and large spectroscopic differences in μ_s' are found in white matter and medulloblastoma. As in case 1, the large μ_a values obtained for the tumor can be related to higher hemoglobin content, as is often found for cancerous tissues. Taking into account measurement variability, no significant differences are found between

the tumor and the "normal" white matter. However it is not clear that the so-called "normal" tissue, measured at the surgical boarder could be considered disease-free and unaffected by the tumor vasculature.

The different type of tissue examined here showed and a clear dependence on the phase function parameter γ. This confirms that γ may be a valuable parameter for tissue characterization. Nevertheless, an improvement of the accuracy would be necessary to conclude about the importance of this parameter.

The optical coefficients we obtained can be compared to the measurements performed simultaneously with the FDPM technique. One should keep in mind that the depth investigated by FDPM technique is larger compared to the spatially-resolved technique described here. Generally the μ_s' values are similar between the two methods, whereas more differences are found for μ_a. For the cortex and skull measurements, both μ_s' and μ_a values are in excellent agreement. The decrease of μ_s' from λ = 674 to 956 nm, is slightly more pronounced in the FDPM data. In contrast, important differences are found for μ_a results where tumor values (astrocytoma and medulloblastoma) obtained by FDPM are significantly lower. This can be explained by the sensitivity of the spatially-resolved probe to the high local hemoglobin content which can be resolved only by the small source-detector separations. In contrast, the large source detector separation employed by the FDPM probe interrogates much greater larger tissue volumes and hence measures average optical properties from multiple structures (e.g. normal + malignant).

4. CONCLUSION

The purpose of this work was to assess the performance of spatially resolved reflectance using short source-detector separations (< 1.4 mm). Monte Carlo simulations, the accuracy of which were confirmed by experiments on microsphere suspensions, were used to establish the correspondence between the measured reflectance and the optical properties.

Optical properties which can be determined by this technique are the absorption coefficient μ_a, the reduced scattering coefficient μ_s', and a parameter of the phase function $\gamma=(1-g_2)/(1-g_1)$, where $g_1(=g)$ and g_2 are the first and second moment of the phase function. Experiments on calibrated Intralipid solutions showed that μ_s' and μ_a can be determined with a precision of ± 0.05 mm^{-1} and ± 0.005 mm^{-1} respectively, and γ can be determined with a precision of typically 10%. Systematic errors are possible if the parameter γ is not

determined with sufficient accuracy. These performances could be improved with by lowering the uncertainty on reflectance measurements.

Experiments and simulations helped to define the average volume probed by this technique. For typical tissues, the average probe depth is about typically 1 mm and the influence of layers located below 3 mm is negligible.

Finally, *in vivo* measurements on human brain showed that excellent discrimination can be obtained between different types of neural tissues, normal and abnormal. Good correlation has been found between spatially-resolved reflectance and simultaneous measurements performed by frequency domain photon migration (FDPM). These two techniques offer interesting complementary features. The spatially resolved probe can potentially provide better differentiation between different types of tissue, due to its sensitivity to local structure. This is due to the fact that substantially smaller volume of tissue is probed. On the other hand, due to physical limitations imposed by large NIR mean absorption lengths in tissue, the precision for μ_a estimate is likely to be worse. Consequently, the short distance, spatially-resolved technique appears to be well suited for clinical settings, which require rapid localized tissue identification, such as endoscopic or needle-based "optical biopsy", and intraoperative tissue mapping for surgical guidance.

ACKNOWLEDGMENT

We would like to thank Prof. P. Fankhauser for his help in the design of the probe. We acknowledge the Microengineering Departement, Swiss Federal Insitute of Technology-Lausanne for the Visiting Faculty Fellowship Program. This work was supported by the Swiss National Science Foundation (N0 2053-049628.96 National Institutes of Health (NIH) Laser Microbeam and Medical Program (LAMMP) and Optical Biology facilities (grants, RR-01192 and CA-62203, respectively); NIH grant GM-50958, and DOE grant DE-FG03-91ER61227.

5. REFERENCES

1. W.-F. Cheong, S.A. Prahl, and A.J. Welch, "A Review of the Optical Properties of Biological Tissues," IEEE J. Quantum Electron. 26, 2166-2185 (1990).

2. J.B. Fishkin, O. Coquoz, E.R. Anderson, M. Brenner, and B.J. Tromberg, "Frequency-domain photon migration measurements of normal and malignant tissue optical properties in human subject," Appl. Opt. 36, 10-20 (1997).

3. B.J. Tromberg, O. Coquoz, J.B. Fishkin, T. Pham, E.R. Anderson, J. Butler, M. Cahn, J.D. Gross, V. Venugopalan, and D. Pham, "Non-invasive measurements of breast tissue optical properties using frequency-domain photon migration," Phil.Trans.R.Soc.Lond. B. 352, 661-668 (1997).

4. J.R. Mourant, I.J. Bigio, J. Boyer, R.L. Conn, T. Johnson, and T. Shimada, "Spectroscopic Diagnosis of Bladder-Cancer with Elastic Light-Scattering," Lasers Surg. Med. 17, 350-357 (1995).

5. T. J. Farrell, M. S. Patterson and B. C. Wilson, "A diffusion theory model of spatially resolved, steady -state diffuse reflectance for the non invasive determination of tissue optical properties in vivo," Med.Phys. 19, 879-888 (1992).

6. R. Bays, G. Wagnières, D. Robert, D. Braichotte, J.-F. Savary, P. Monnier and H. van den Bergh, "Clinical determination of tissue optical properties by endoscopic spatially resolved reflectometry," Appl.Opt. 35 (10), 1756-1766 (1996).

7. A. Kienle, L. Lilge, M.S. Patterson, R. Hibst, R. Steiner, and B.C. Wilson, "Spatially resolved absolute diffuse reflectance measurements for noninvasive determination of the optical scattering and absorption coefficients of biological tissue.," Appl.Opt. 35, 2304-2314 (1996).

8. J.S. Fantini, M.A. Franceschini, J.B. Fishkin, B. Barbieri, and E. Gratton, "Quantitative determination of the absorption spectra of chromophores in strongly scattering media: a light-emitting based techniques," Appl.Opt. 33, 5204-5213 (1994).

9. G. Mitic, J. Kölzer, J. Otto E. Plies, G. Sölkner and W. Zinth, "Time-gated transillumination of biological tissues and tissuelike phantoms," Appl.Opt. 33, 6699-6710 (1994).

10. G. Kumar and J.M. Schmitt, "Optimal probe geometry for near-infrared spectroscopy of biological tissue," Appl. Opt. 36, 2286-2293 (1997).

11. J.R. Mourant, I.J. Bigio, D.A. Jack, T.M. Johnson, and H.D. Miller, "Measuring absorption coefficients in small volumes of highly scattering media: source detector separations for which path lengths do not depend on scattering properties," Appl. Opt. 36, 5655-5661 (1997).

12. F.Bevilacqua, "Optical characterization of biological tissues *in vitro* and *in vivo*", PhD dissertation N° 1781, Swiss Federal Institute of Technology Lausanne (1998).

13. F.Bevilacqua and C.Depeursinge, "Monte Carlo study of diffuse reflectance at source-detector separations close to one transport mean free path", submitted.

14. F.P. Bolin, L.E. Preuss, R.C. Taylor and J. Ference, "Refractive index of some mammalian tissues using a fiber optic cladding method," Appl. Opt. 28, 2297-2296 (1989).

15. D.R. Wyman, M.S. Patterson, and B.C. Wilson, "Similarity relations for the interaction parameters in radiation transport," Appl.Opt. 28, 5243-5249 (1989)..

16. H.C. van de Hulst, *Multiple Light Scattering, Tables, Formulas, and Applications*, Academic Press. Inc., London, 1980.

17. S. L. Jacques, C. A. Alter, and S. A. Prahl, "Angular Dependance of HeNe Laser Light Scattering by Human Dermis," Lasers in Life Sciences 1, 309-333 (1987).

18. R. Marchesini, A. Bertoni, S. Andreola, E. Melloni, and A.E. Sichirollo, "Extinction and absorption coefficients and scattering phase functions of human tissues in vitro," Appl. Opt. 28, 2318-2324 (1989).

19. P. van der Zee, M. Essenpreis, and D.T. Delpy, "Optical properties of brain tissue," SPIE, Vol. 1888, 454-465 (1993) .

20. S. T. Flock, B. C. Wilson, and M. S. Patterson, "Total attenuation coefficient and scattering phase functions of tissues and phantom materials at 633 nm," Med. Phys. 14, 835-841 (1987).

21. P. Marquet, F. Bevilacqua, C. Depeursinge, and E. B. de Haller, "Determination of reduced scattering and absorption coefficients by a single charge-coupled-device array measurement, part I: comparison between experiments and simulations," Opt.Eng. 34, 2055-2063 (1995).

22. F. Bevilacqua, P. Marquet, C. Depeursinge, and E. B. de Haller, "Determination of reduced scattering and absorption coefficients by a single charge-coupled-device array measurement, part II: measurements on biological tissues," Opt.Eng. 34, 2064-2069 (1995).

23 F. Bohren and D.R. Huffman, *Absorption and Scattering of Light by Small Particles*, Wiley, New York, 1983.

24. JR.A. Bolt and J.J. ten Bosh, "Method for measuring position-dependant volume reflection," Appl.Opt. 32, 4641-4645 (1993).

25. S.J. Madsen, B.C. Wilson, M.S. Patterson, Y.D. Park, S.L. Jacques, and Y. Hefetz, "Experimental tests of a simple diffusion model for the estimation of scattering and absorption coefficients of turbid media from time-resolved diffuse reflectance measure," Appl.Opt. 31, 3509-3517 (1992).

26. F. Bevilacqua, P. Marquet, O. Coquoz, and C. Depeursinge, "Role of tissue structure in photon migration through breast tissues," Appl.Opt., 36, 44-51 (1997).

27 Protocol and informed consent was obtained for the patient undergoing neurological surgery for an intra-axial brain tumor as demonstrated on conventional neuroimaging. The protocol and informed consent documents were approved by the UCI review board (HS#96-495).

28. M Cope, "The developement of a near infrared spectroscopy system and its application for non invasive monitoring of cerebral blood and tissue oxygenation in the the newborn infant," Ph.D. Dissertation, University College London, 1991.

29. K. M. Hebeda, T. Menovsky, H.Van Staveren , J. F. Beek, and J. C. van Gemert, "Light propagation in the brain depends on nerve fiber orientation," Neurosurgery , 720-722 (1994).

30. D. R. Sandeman, T. Mills and S. G. Bown, "Enhancement of light penetration by white matter tracts in the normal mouse brain", Lasers Med. Sci., 3, 47, (1986).

31. J. G. Wolbers, W. Kamphorst, H. J. M. Sterenborg, M. J. C. van Gemert and W. Hogervorst, "Dose response of rat brains interstitially irradiated by argon light", Lasers Med. Sci., 2, 255-260, (1987).

32. M. Firbank, M. Hiraoka, M. Essenpreis, and D.T. Delpy, "Measurements of the optical properties of the skull in the wavelength range 650-950 nm.," Phy.Med.Biol. 38, 503-510 (1993).

FIGURE CAPTIONS

Fig.1. Probe for the measurement of the spatially resolved reflectance

Fig.2. Experimental set-up.

Fig.3. Boundary condition for exact probe configuration.

Fig.4. Comparison between the exact and simplified boundary conditions (The numerical aperture was slightly increased to NA=0.37 instead of NA=0.28 for this graph, because of the small amount of detected photons in the exact configuration). The optical coefficient are: $\mu_s' = 1$ mm^{-1}, $\mu_a = 0.01$ mm^{-1} and $\gamma=1.9$.

Fig.5. Comparison between measurements in a semi-infinite and an infinite media. The medium is Intralipid. The optical coefficients were measured by the FDPM technique $\mu_s' = 1.2$ mm^{-1}, $\mu_a = 0.0005$ mm^{-1} (λ=675 nm).

Fig.6. Average depth of scattering events was recorded for each photon detected in Monte Carlo simulations (backscattered photons). Case of $\gamma = 1.9$.

Fig.7. Effect of the Intralipid thickness on the reflectance. The set-up for the investigation on Intralipid with varying thickness is illustrated on right of the graph. The optical coefficients of the Intralipid were measured by the FDPM technique (λ = 956 nm). The reduced albedo is $a'=\mu_s'/(\mu_s'+\mu_a) = 0.98$

Fig.8. Calibration measurement on a siloxane phantom and measurement test on a microsphere suspension. The calibration measurement is multiplied by the calibration factor to fit the corresponding simulation. The phantom optical properties were measured with frequency-domain photon migration: $\mu_a=2.4\pm 0.2\ 10^{-4}$ mm^{-1}, $\mu_s'=1.82 \pm 0.007$ mm^{-1}(λ=674 nm). The measurement on microsphere suspension is multiplied by the calibration factor derived from the phantom measurement. corresponding simulation is performed using the optical properties derived from Mie theory: $\mu_s' = 1.0$ mm^{-1}, $\mu_a = 0.0005$ mm^{-1}, Mie phase function (g=0 .916, $\gamma = 2.2$).

Fig.9. Relation between the parameters R(ρ=1 mm) and $|\partial_\rho \ln R(\rho=1 \text{ mm})|$ and the optical coefficients μ_s' and μ_a Case of γ=1.5 and 1.9.

Fig.10.a. Comparison between μ_a obtained by the frequency domain photon migration technique (FDPM) and by the probe measurements. Measurements on Intralipid and dye.

Fig.10.b. Comparison between μ_s' obtained by the frequency domain photon migration technique (FDPM) and by the probe measurements. Measurements on Intralipid

Fig.11.a. Comparison between μ_a obtained from spatially-resolved transmittance (method described in references 21 and 22) and μ_a from by the probe measurements. Measurements on microsphere suspension.

Fig.11.b. Comparison between μ_s' obtained from spatially-resolved transmittance (method described in references 21 and 22) and μ_s' from by the probe measurements. Measurements on microsphere suspension.

Fig.12.a. Clinical measurements *in vivo* on human brain. Case 1. $R(\rho=1)$ and $|\partial_\rho \ln R(\rho=1 \text{ mm})|$ for different types of brain tissues: normal cortex (frontal and temporal lobe), astrocytoma of optic nerve and normal optic nerve.

Fig.12.b. Clinical measurements *in vivo* on human brain. Case 2. $R(\rho=1)$ and $|\partial_\rho \ln R(\rho=1 \text{ mm})|$ for different types of brain tissues: skull, deep cerebellar white matter, deep cerebellar white matter with scar tissue and cerebellum tumor.

Fig.13.a. Comparison between the spatially reflectance curve measured on normal cortex (temporal lobe) and simulations.

Fig.13.b. . Comparison between the spatially reflectance curve measured on astrocytoma of optic nerve and simulations.

TABLE CAPTIONS

Table 1. Optical properties of normal and malignant human brain tissue. Case1

Table 2. Optical properties of normal and malignant human brain tissue. Case2

October 22, 1999

OBLON SPIVAK MCCLELLAND MAIER ET AL
ATTN: ROBERT F. GRUSE
PSF BOX: 37

This is to inform you that the document requested in your order dated 10-19-1999 is a true reproduction of the official office record copy of that document:

60103559 CERTIFIED PAT APP AS FILED-EXPEDITE-PSF

draw figs missing

☑ The enclosed Patent Application as Filed is a reproduction of the application as originally filed and has been recorded using high quality scanning or microfilm equipment. Copies of page/papers that were not scannable have not been included, nor have pages/papers received after the original filing date. Copies of these pages/papers may be ordered separately.

☐ The enclosed document is a reproduction of the best available source of the official office record copy of that document.

If you have any questions or need additional information, please contact our Customer Service Department.

Mailing Address:
U.S. Patent and Trademark Office
Office of Public Records, Customer Service
Crystal Gateway 4, Suite 300
Washington DC 20231

Delivery Address:
U.S. Patent and Trademark Office
Office of Public Records, Customer Service
1213 Jefferson Davis Highway, Suite 300
Arlington VA 22202

For faster processing of new orders, please specify as appropriate:
Box 9 (Copy Sales) for Uncertified copies, or Box 10 for Certified copies of PTO Documents

Voice: (703) 308-9726 Fax: (703) 308-7048 E-Mail: PTCS@USPTO.GOV or Certdiv@USPTO.GOV

Ref:PS 165034

Fig. 1

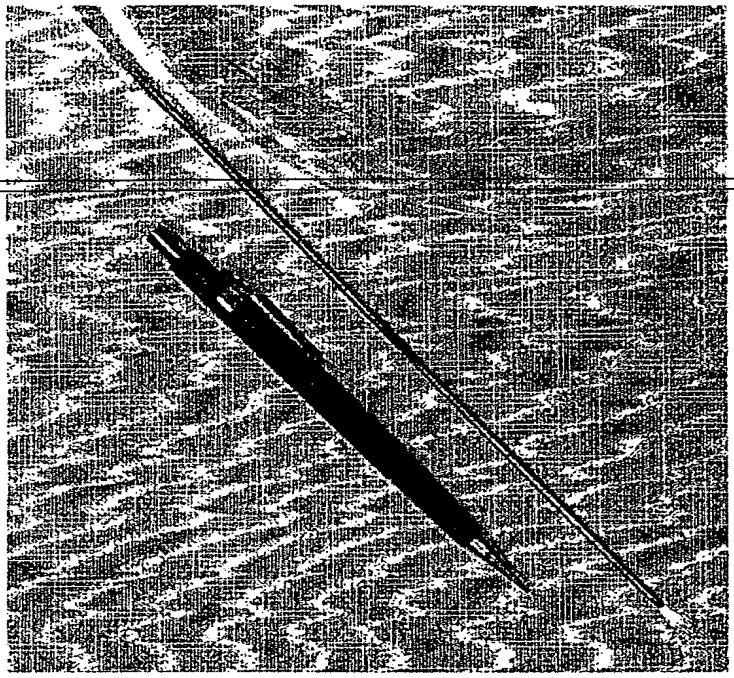

illuminating fibres (used alternatively)
in a stainless steel tube Ø 0.3 mm

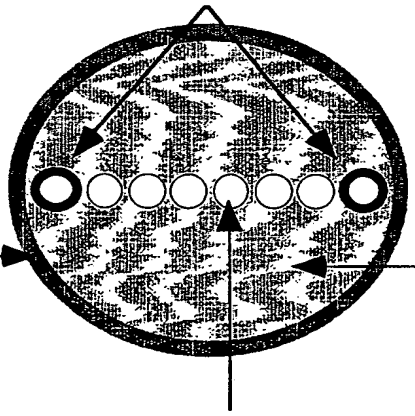

stainless steel tube
Ø 2-2.5 mm

adhesive
(clear)

collecting fibres core
Ø 0.2 mm

Fig. 2

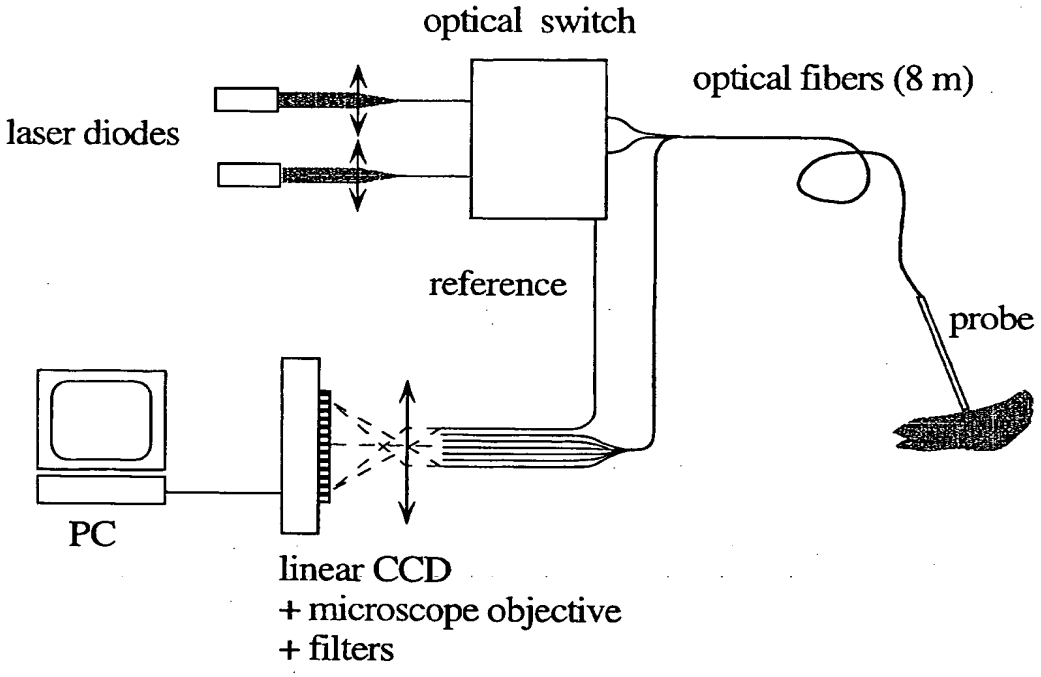

Fig. 3

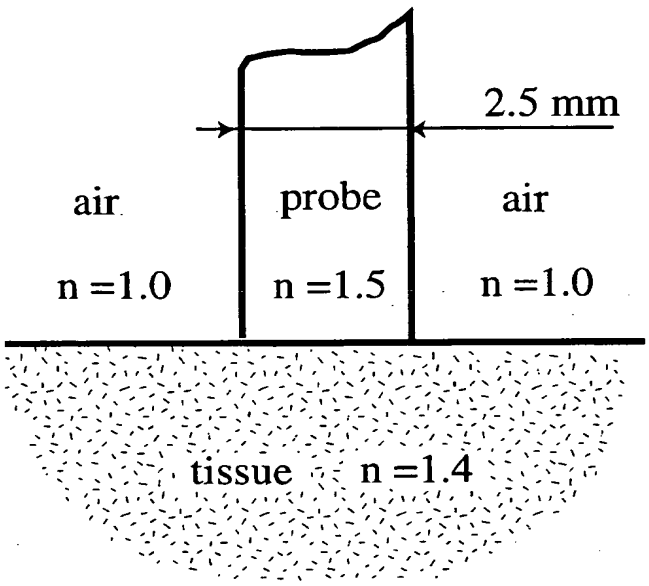

Fig. 4

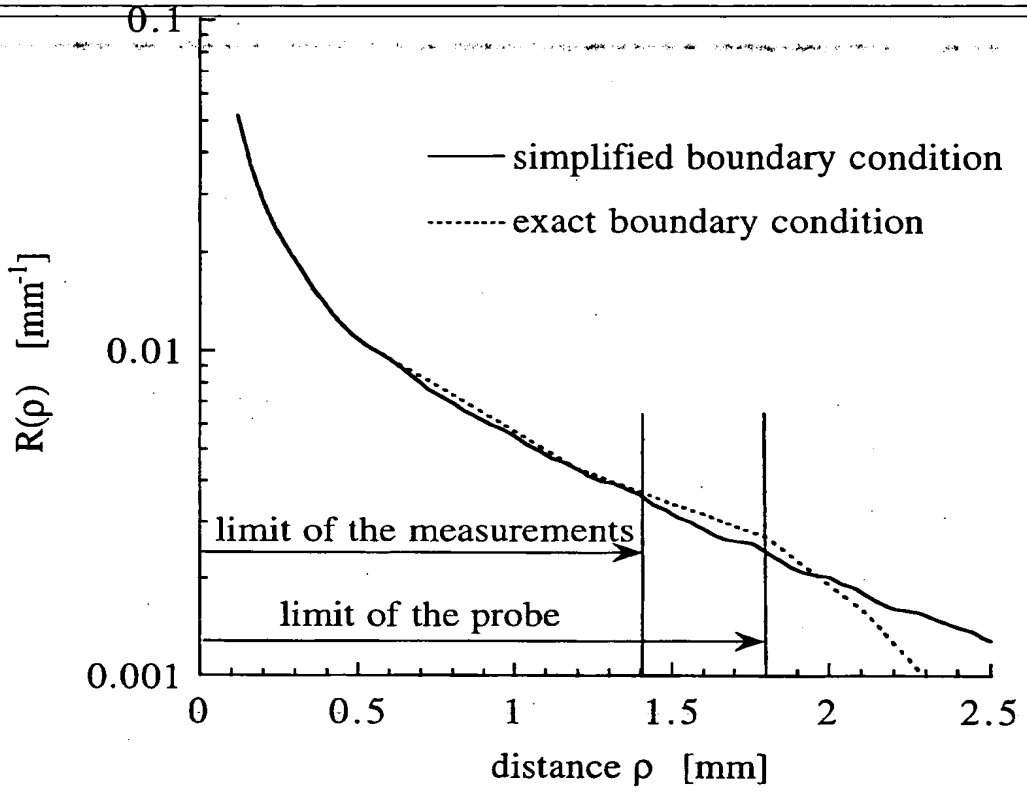
0.1
0.01
0.001
R(ρ) [mm⁻¹]
simplified boundary condition
exact boundary condition
limit of the measurements
limit of the probe
0
0.5
1
1.5
2
2.5
distance ρ [mm]

Fig. 6.

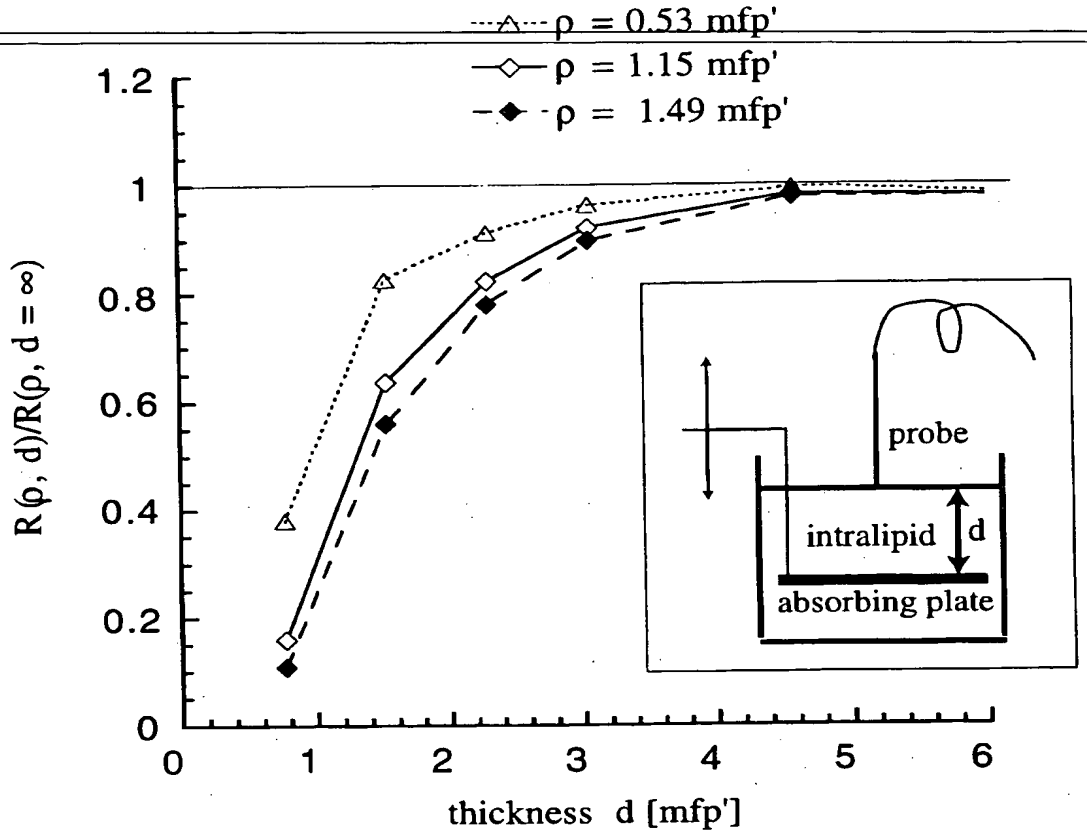

Fig. 7

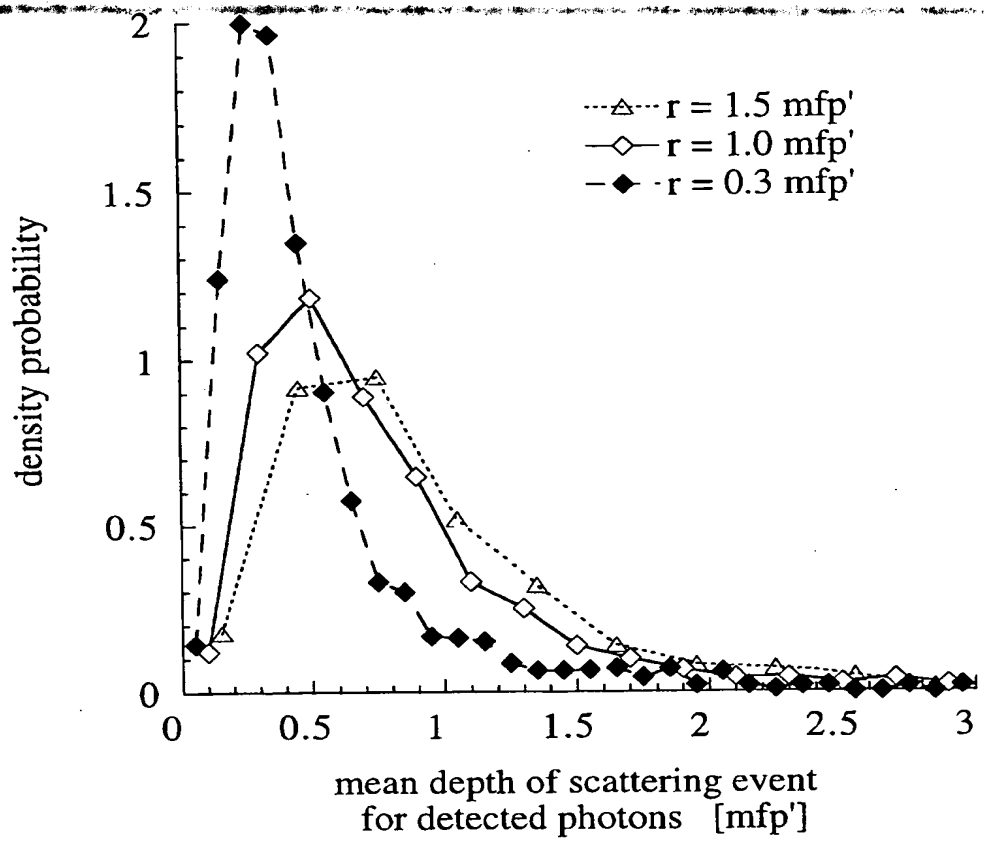

Fig. 8

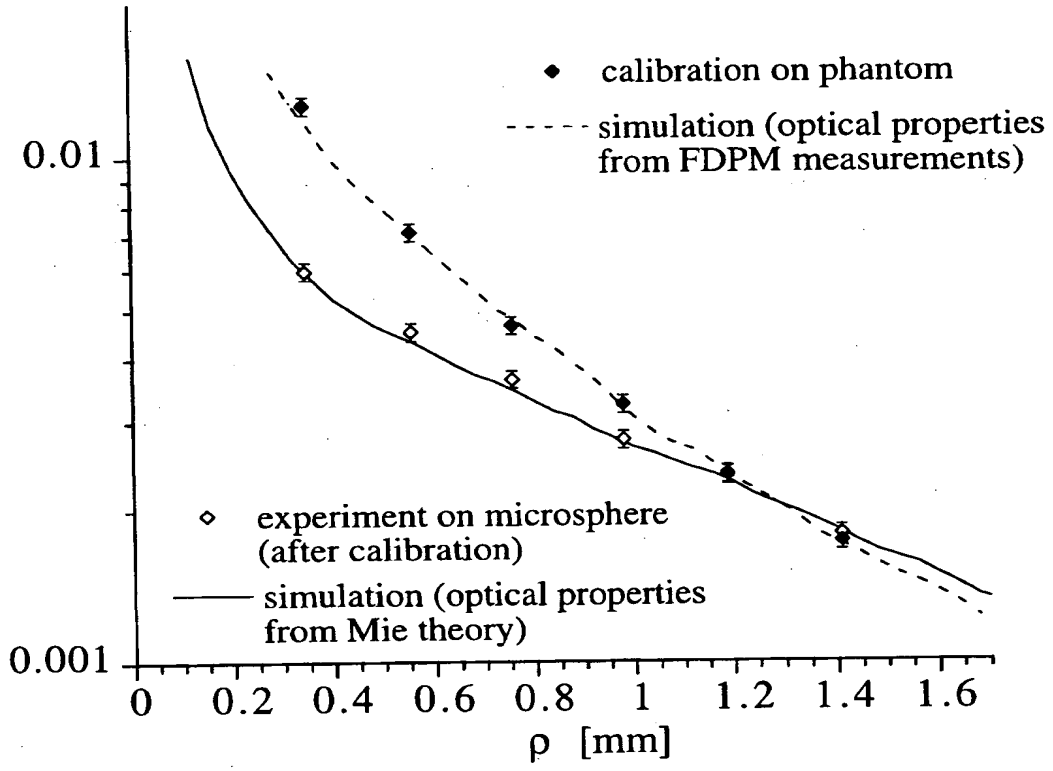

Fig. 9

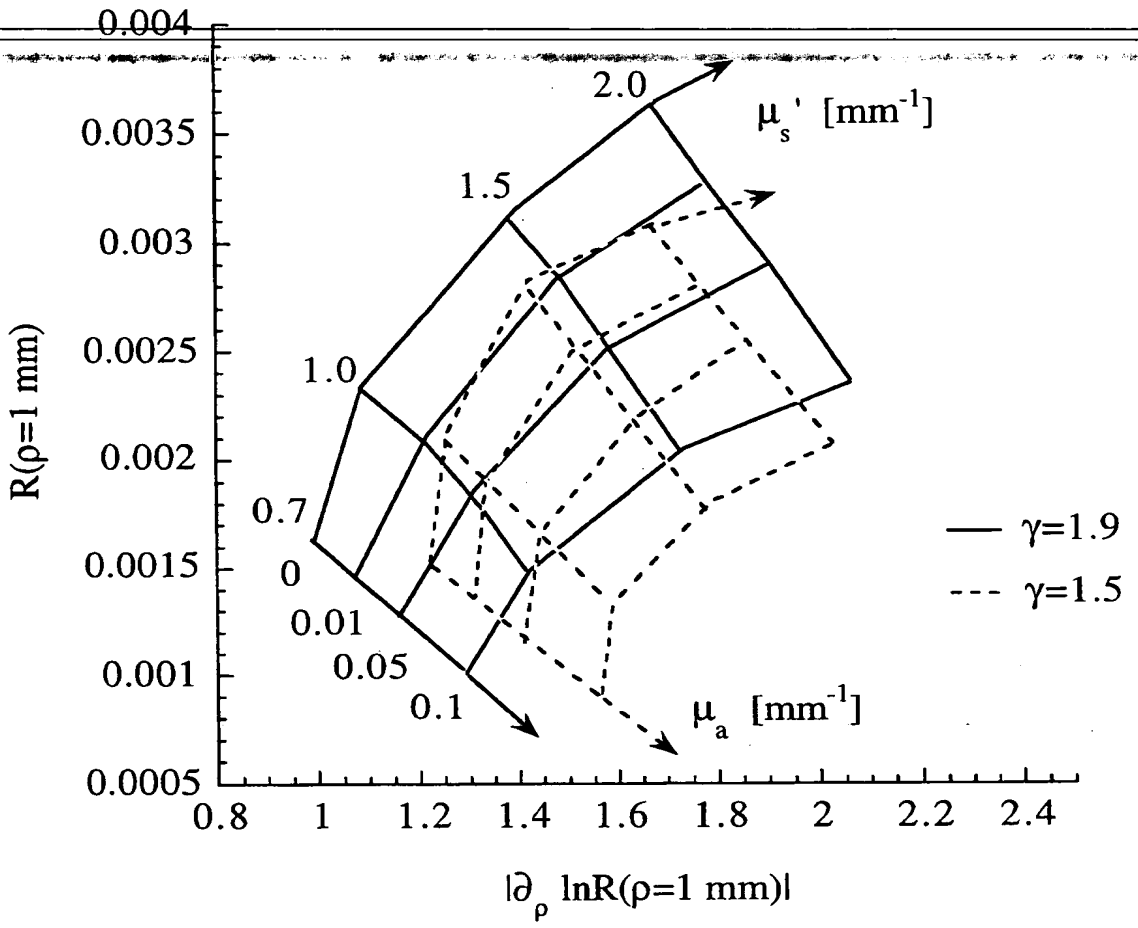

Fig. 10.a

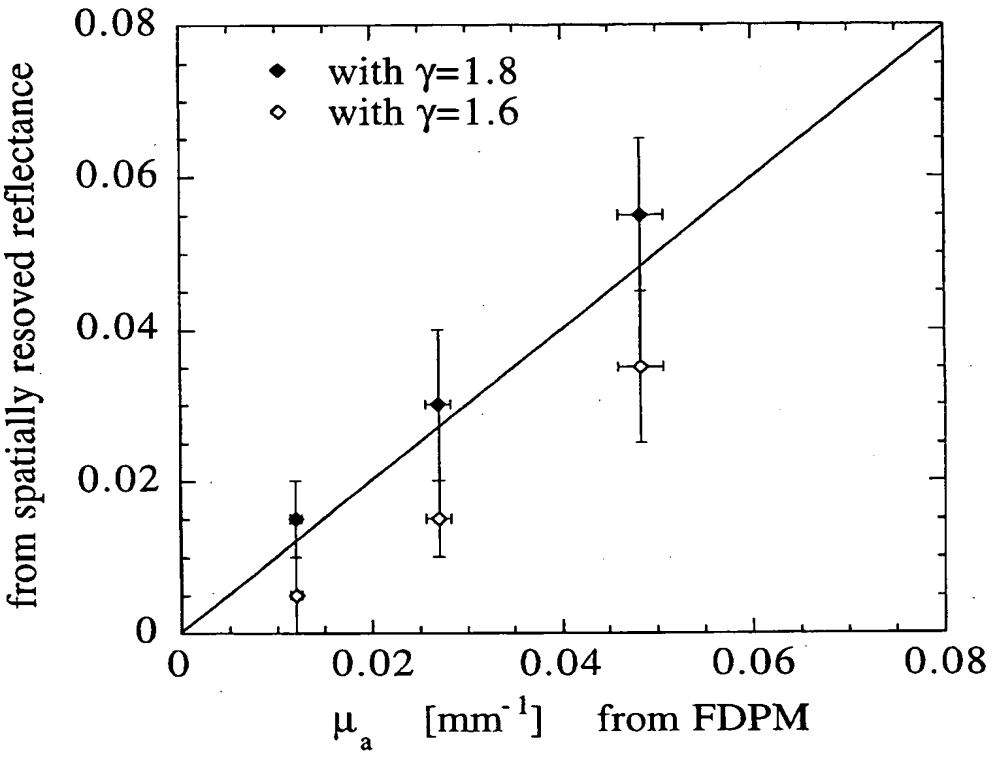

Fig. 10.b

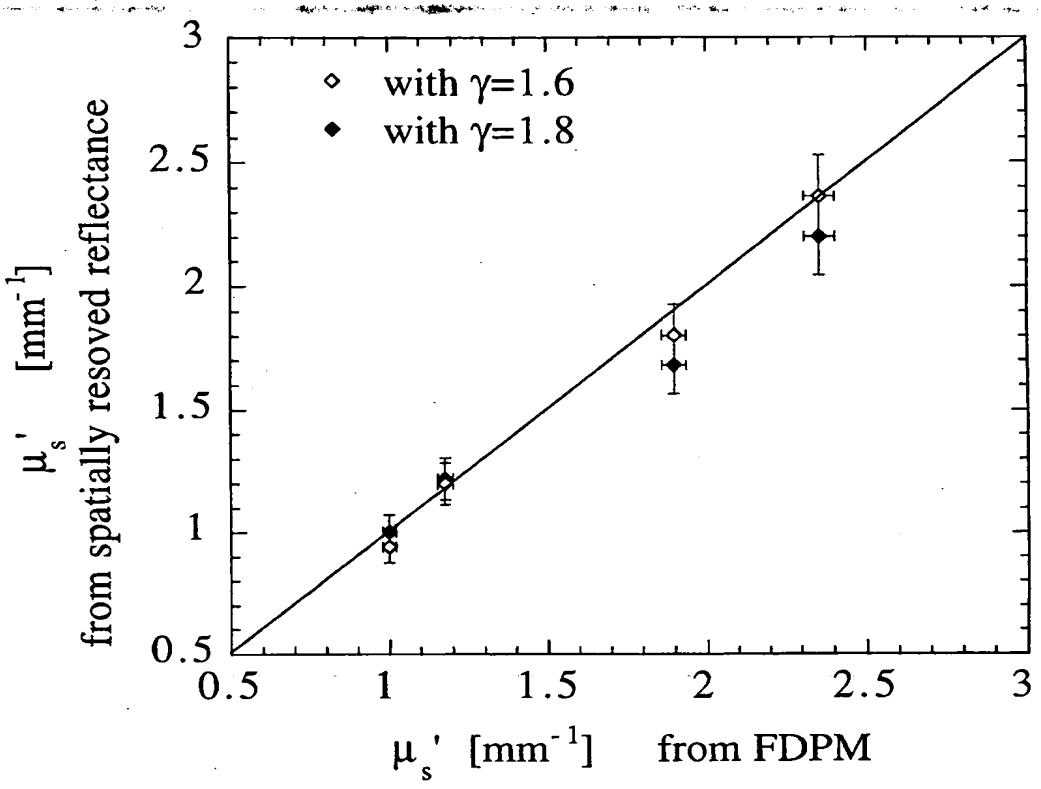
with γ=1.6
with γ=1.8
μs' [mm-1] from spatially resoved reflectance
μs' [mm-1] from FDPM
0.5
1
1.5
2
2.5
3

Fig. 11.a

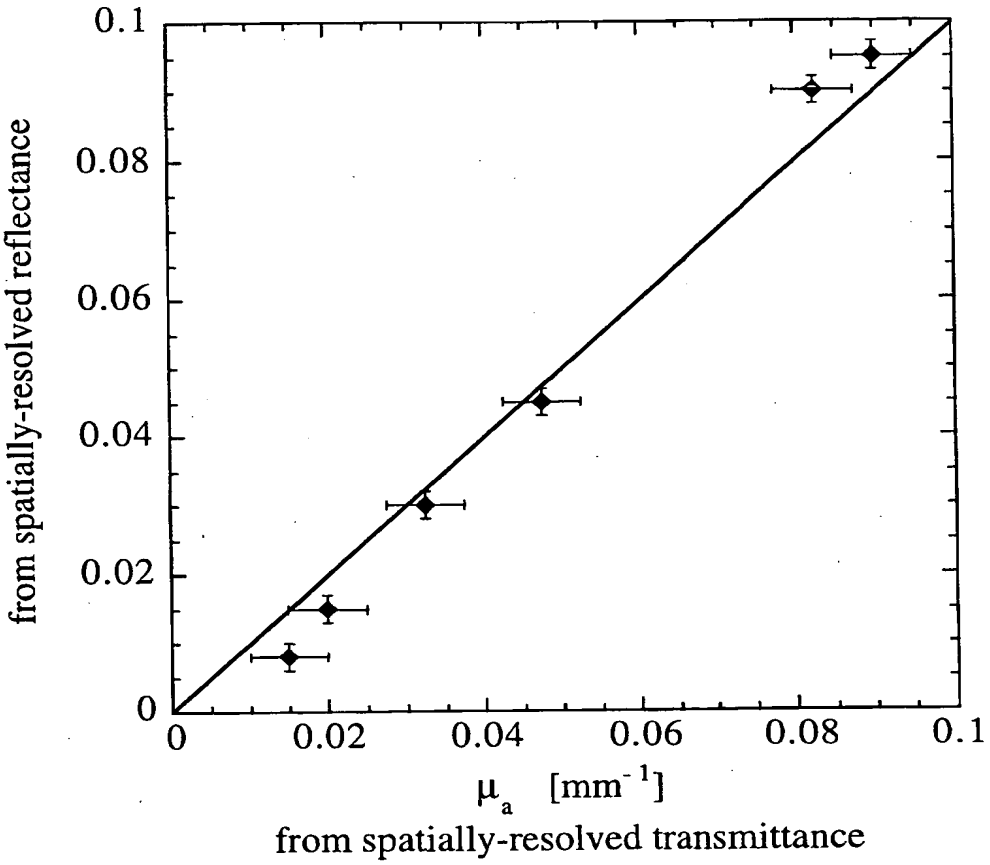

Fig. 11.b

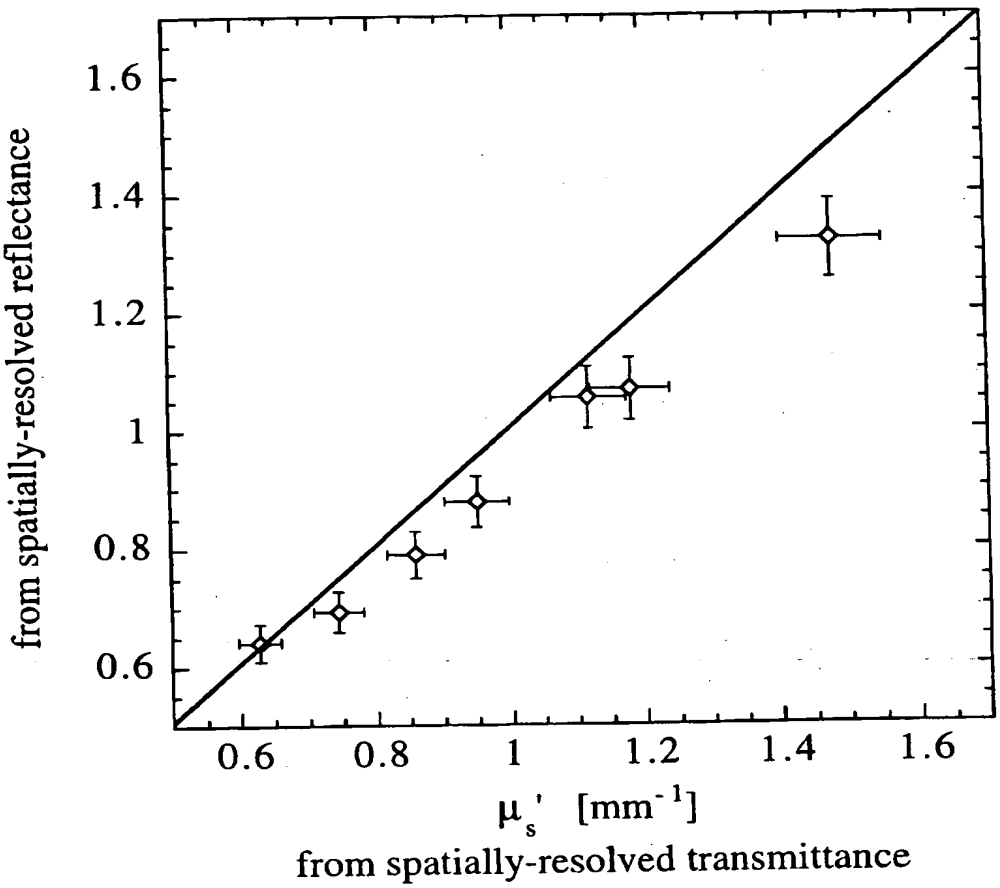

Fig. 12.a.

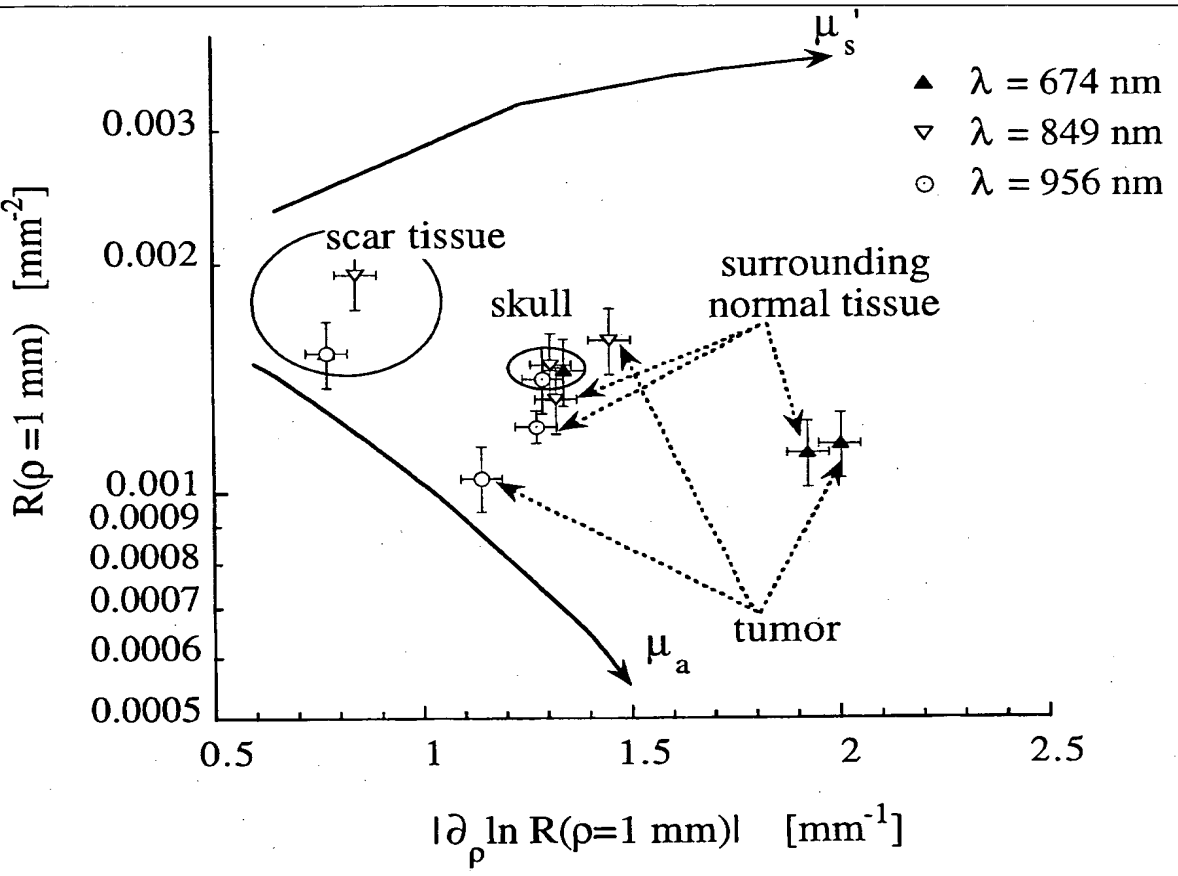
μ s '
λ = 674 nm
λ = 849 nm
λ = 956 nm
scar tissue
skull
surrounding
normal tissue
tumor
μ a
0.003
0.002
0.001
0.0009
0.0008
0.0007
0.0006
0.0005
0.5
1
1.5
2
2.5
R(ρ =1 mm) [mm-2]
|∂ρ ln R(ρ=1 mm)| [mm-1]

Fig. 12.b

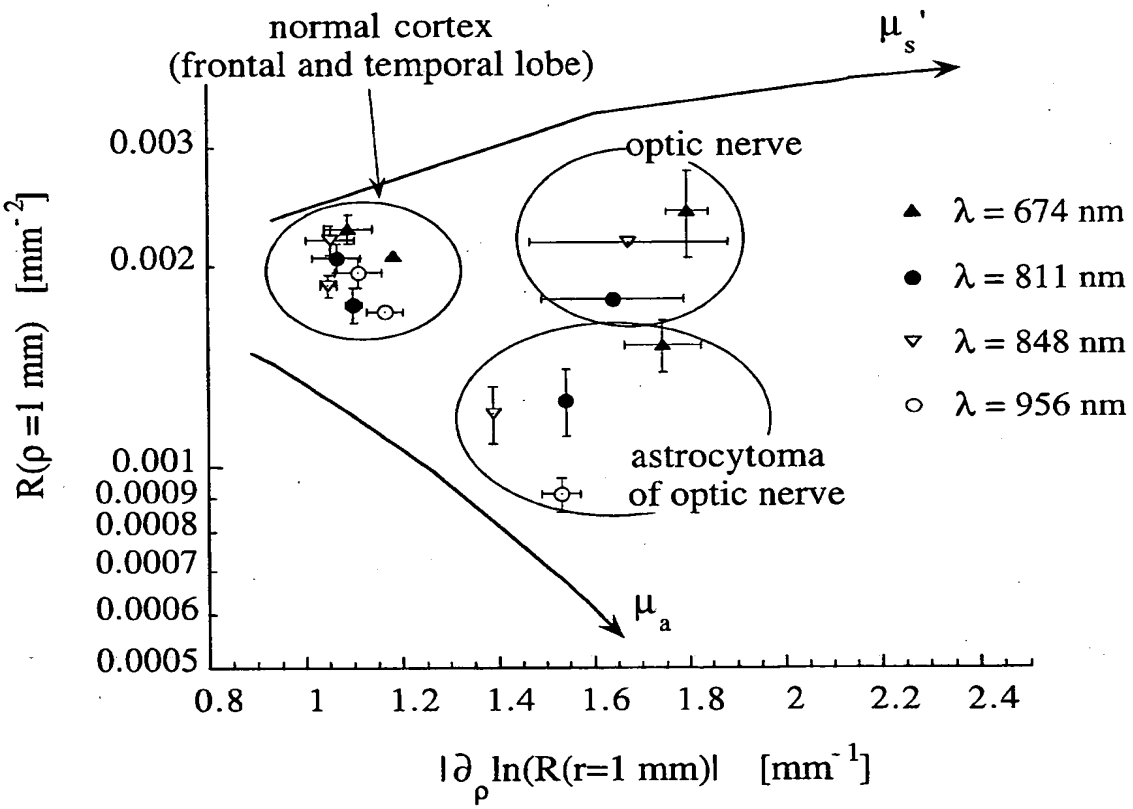
normal cortex
(frontal and temporal lobe)
μ_s'
optic nerve
astrocytoma
of optic nerve
μ_a
λ = 674 nm
λ = 811 nm
λ = 848 nm
λ = 956 nm
R(ρ=1 mm) [mm^{-2}]
0.003
0.002
0.001
0.0009
0.0008
0.0007
0.0006
0.0005
0.8
1
1.2
1.4
1.6
1.8
2
2.2
2.4
$|\partial_\rho \ln(R(r=1\ mm)|$ [mm^{-1}]

Fig. 13.a.

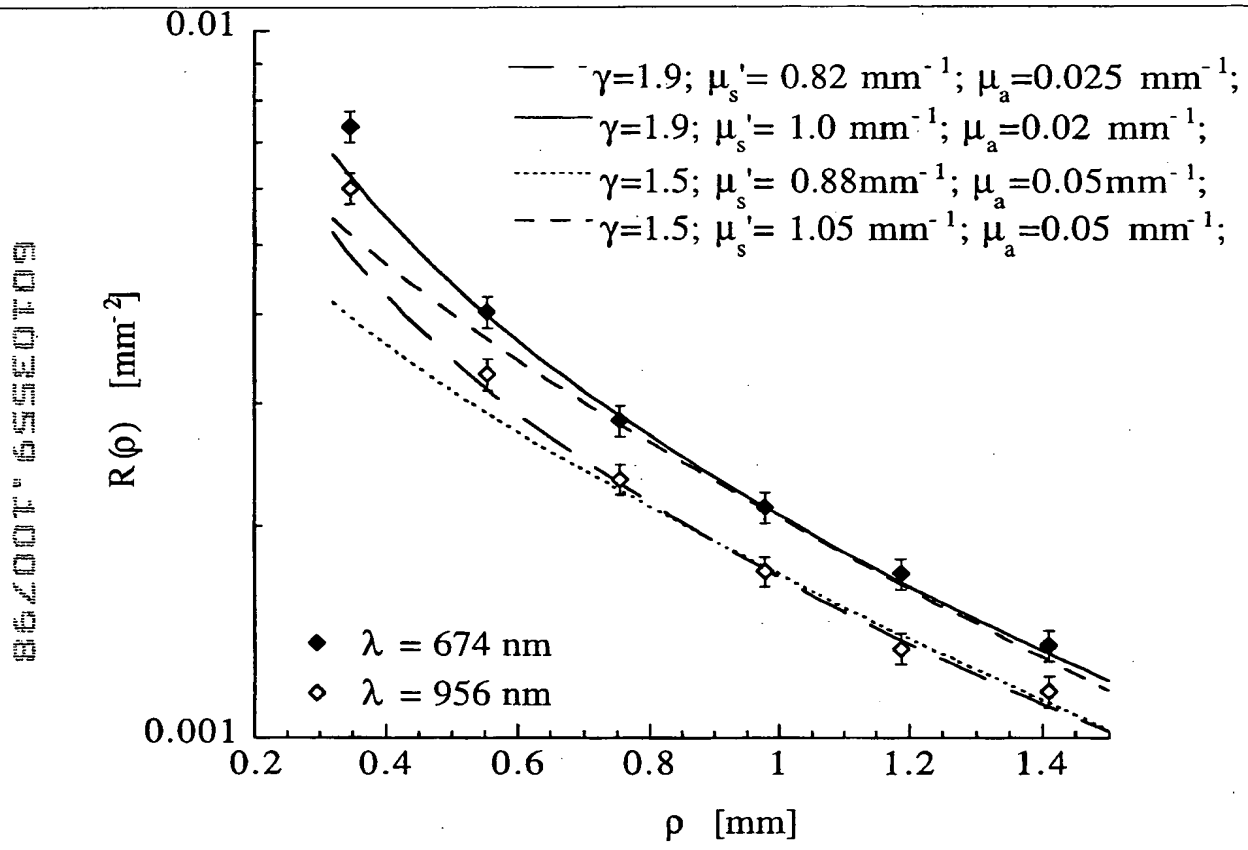
0.01
0.001
0.2
0.4
0.6
0.8
1
1.2
1.4
R(ρ) [mm⁻²]
ρ [mm]
γ=1.9; μs'= 0.82 mm⁻¹; μa=0.025 mm⁻¹;
γ=1.9; μs'= 1.0 mm⁻¹; μa=0.02 mm⁻¹;
γ=1.5; μs'= 0.88mm⁻¹; μa=0.05mm⁻¹;
γ=1.5; μs'= 1.05 mm⁻¹; μa=0.05 mm⁻¹;
λ = 674 nm
λ = 956 nm

Fig. 13.b

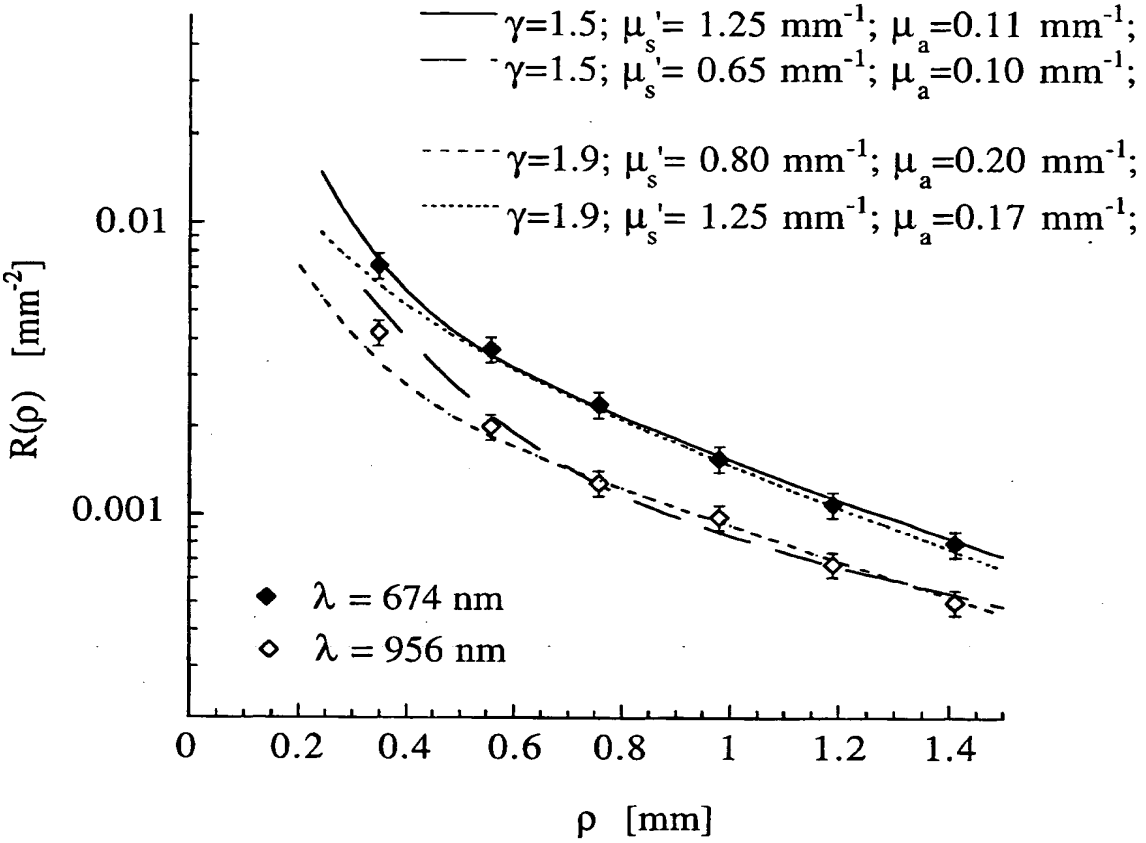
γ=1.5; μs'= 1.25 mm-1; μa=0.11 mm-1;
γ=1.5; μs'= 0.65 mm-1; μa=0.10 mm-1;
γ=1.9; μs'= 0.80 mm-1; μa=0.20 mm-1;
γ=1.9; μs'= 1.25 mm-1; μa=0.17 mm-1;
R(ρ) [mm-2]
0.01
0.001
λ = 674 nm
λ = 956 nm
0
0.2
0.4
0.6
0.8
1
1.2
1.4
ρ [mm]

Table 1

v

type of tissues	wavelength [nm]	probe measurements			from FDPM	
		γ	μ_s' [mm^{-1}]	μ_a [mm^{-1}]	μ_s' [mm^{-1}]	μ_a [mm^{-1}]
cortex (frontal lobe)	674	1.9	1.00±0.05	<0.02±0.01	1.11	0.024
	811	1.9	0.91±0.05	<0.01±0.01	0.79	0.027
	849	1.9	0.92±0.05	<0.01±0.01	0.80	0.024
	956	1.9	0.89±0.05	0. 015±0.01	0.86	0.024
cortex (temporal lobe)	674	1.9	1.00±0.05	0.02±0.01	1.01	0.026
	811	1.9	0.82±0.05	0.02±0.01	0.61	0.035
	849	1.9	0.82±0.05	<0.01±0.01	0.60	0.030
	956	1.9	0.82±0.05	0.025±0.01	0.61	0.033
astrocytoma of optic nerve	674	1.7	1.25±0.10	0.14±0.03	0.96	0.025
	811	1.7	0.95±0.10	0.12±0.03	0.65	0.033
	849	1.7	0.76±0.10	0.09±0.03	0.70	0.028
	956	1.7	0.73±0.10	0.15±0.03	0.71	0.041
normal optic nerve	674	1.7	1.75±0.20	0.06±0.03	N/A	N/A
	811	1.7	N/A	N/A	N/A	N/A
	849	1.7	1.60±0.20	0.08±0.03	N/A	N/A
	956	1.7	1.52±0.20	0.07±0.03	N/A	N/A

Fig.1

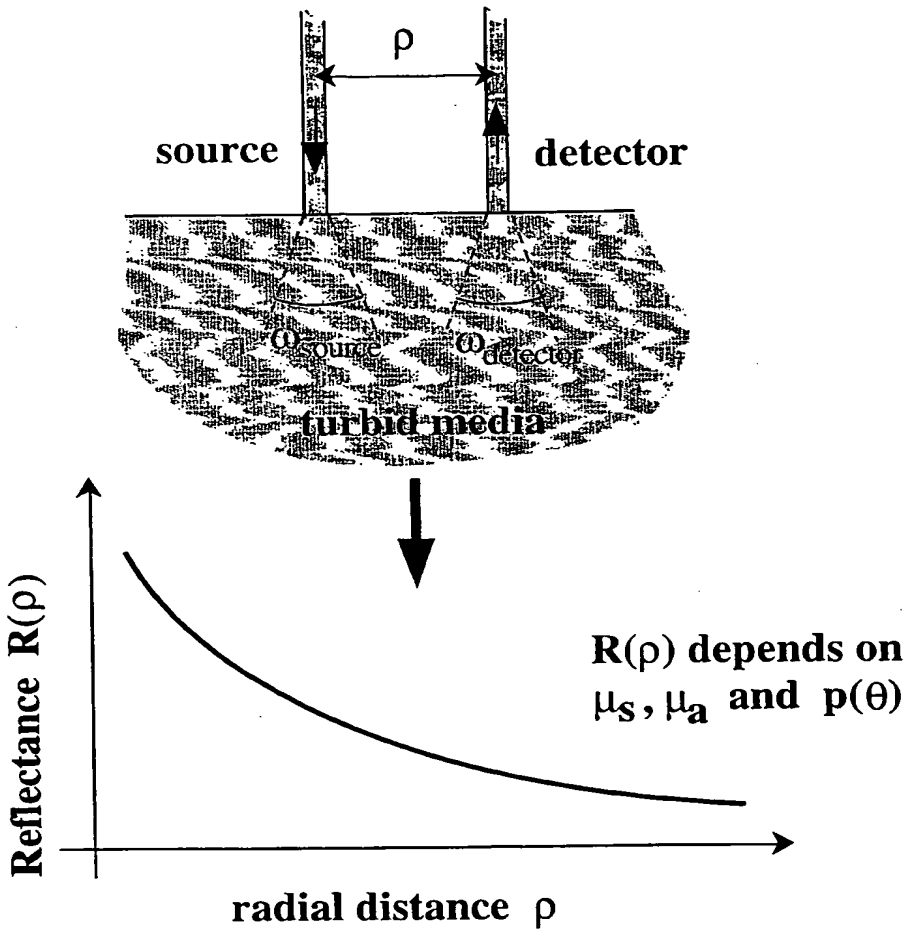
ρ
source
detector
ω_{source}
$\omega_{detector}$
turbid media
Reflectance R(ρ)
R(ρ) depends on
μ_s, μ_a and p(θ)
radial distance ρ

Fig.2

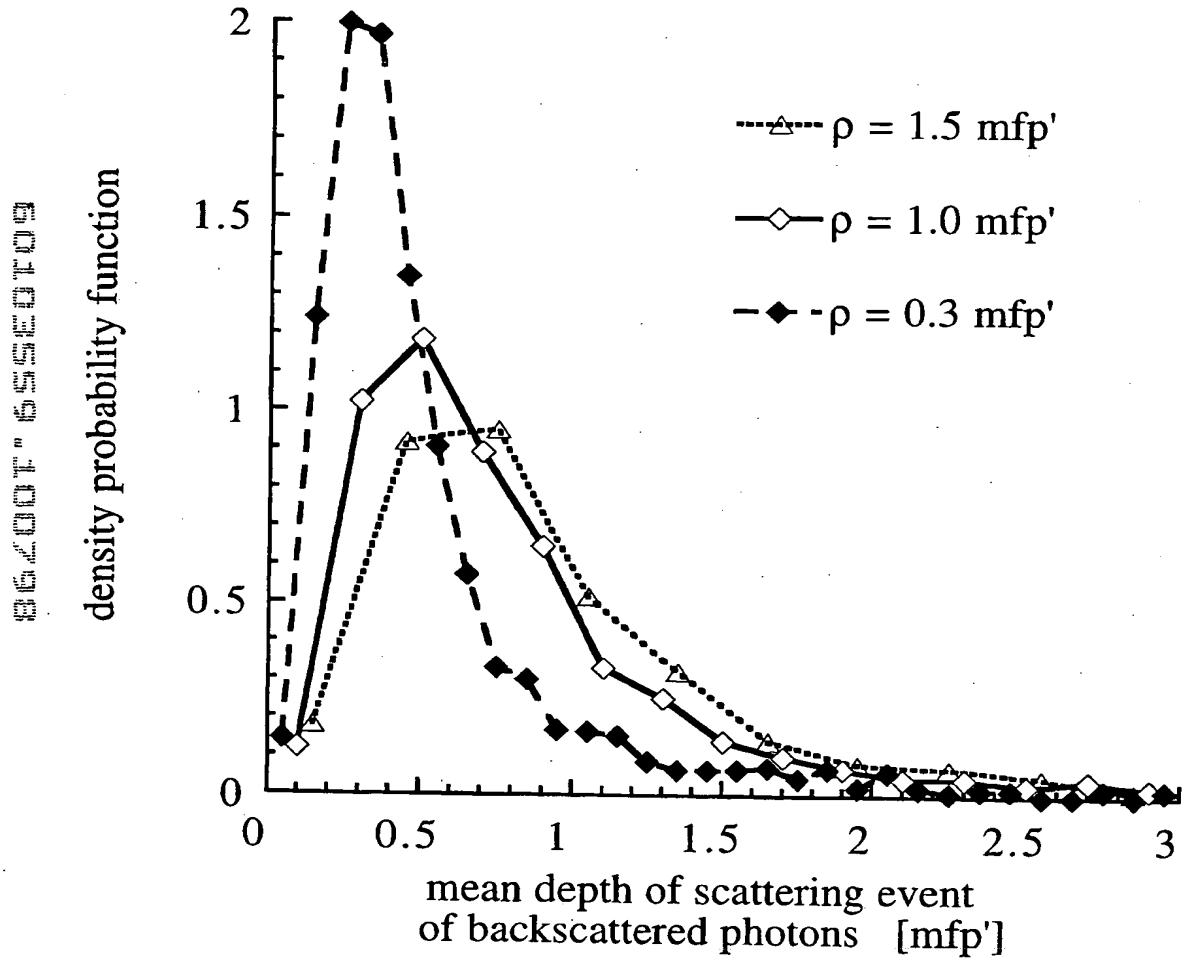
density probability function
2
1.5
1
0.5
0
0
0.5
1
1.5
2
2.5
3
ρ = 1.5 mfp'
ρ = 1.0 mfp'
ρ = 0.3 mfp'
mean depth of scattering event
of backscattered photons [mfp']

Fig. 3

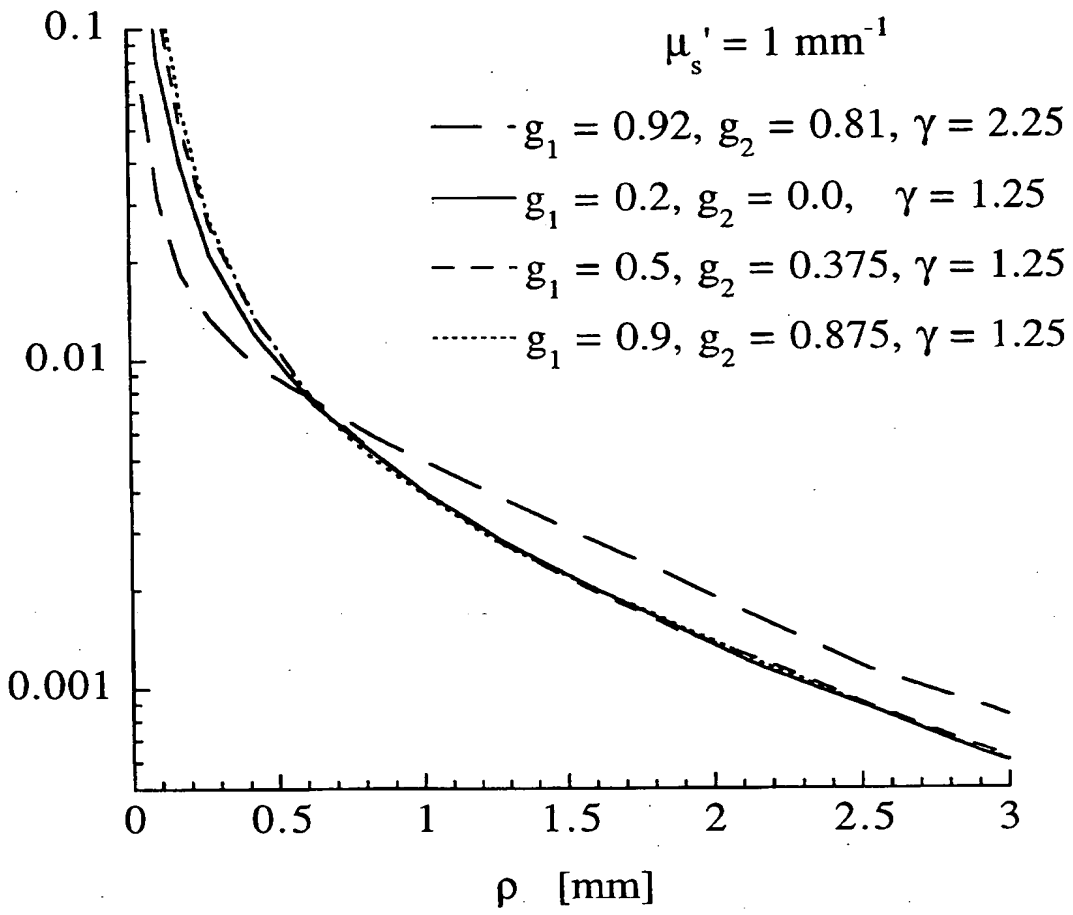
0.1
0.01
0.001
R(ρ) [mm^{-2}]
0
0.5
1
1.5
2
2.5
3
ρ [mm]
$\mu_s' = 1$ mm^{-1}
$g_1 = 0.92, g_2 = 0.81, \gamma = 2.25$
$g_1 = 0.2, g_2 = 0.0, \gamma = 1.25$
$g_1 = 0.5, g_2 = 0.375, \gamma = 1.25$
$g_1 = 0.9, g_2 = 0.875, \gamma = 1.25$

Fig. 4

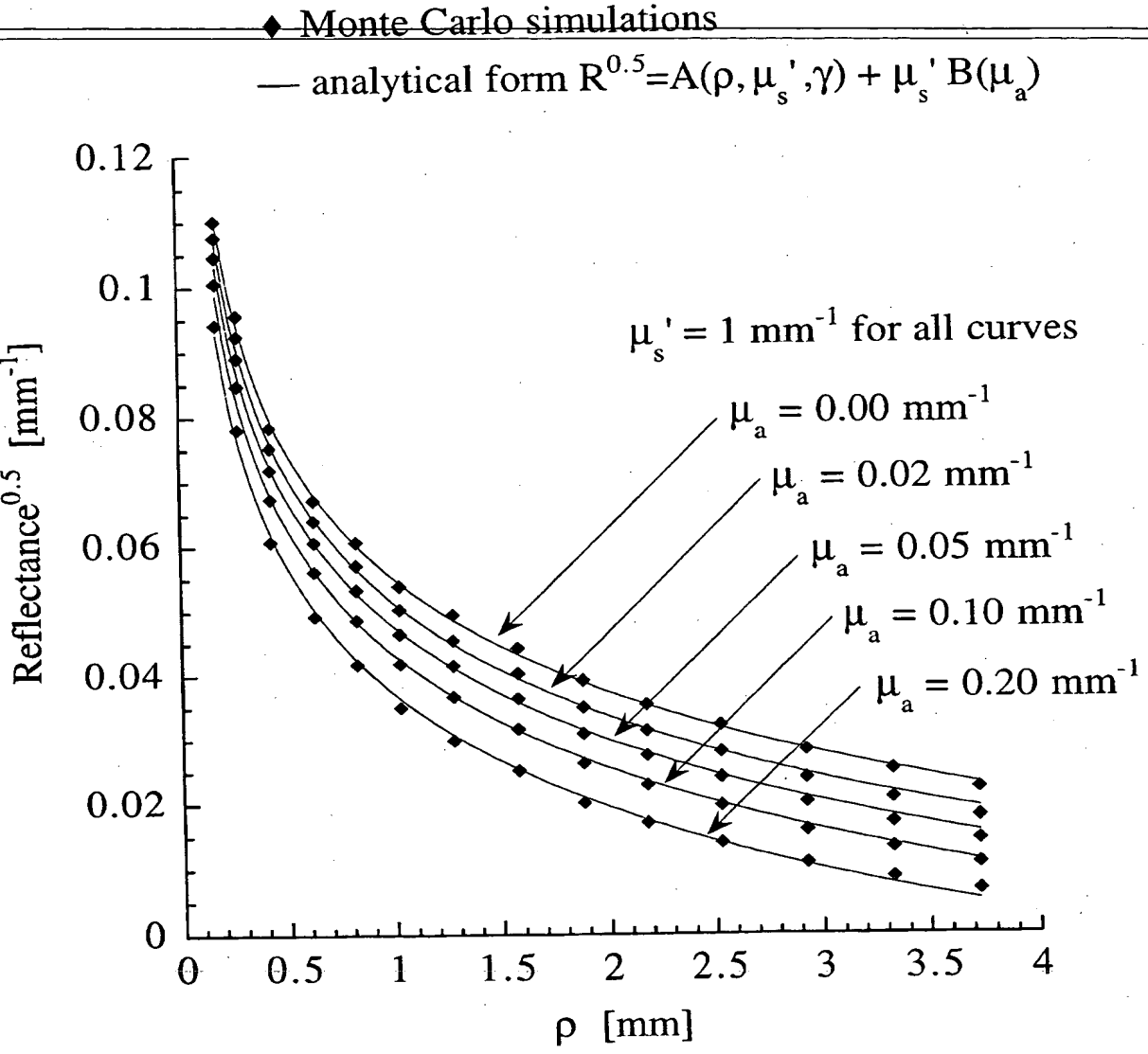
♦ Monte Carlo simulations
— analytical form $R^{0.5}=A(\rho,\mu_s',\gamma)+\mu_s' B(\mu_a)$
$\mu_s' = 1\ mm^{-1}$ for all curves
$\mu_a = 0.00\ mm^{-1}$
$\mu_a = 0.02\ mm^{-1}$
$\mu_a = 0.05\ mm^{-1}$
$\mu_a = 0.10\ mm^{-1}$
$\mu_a = 0.20\ mm^{-1}$
Reflectance$^{0.5}$ [mm^{-1}]
0.12
0.1
0.08
0.06
0.04
0.02
0
0
0.5
1
1.5
2
2.5
3
3.5
4
ρ [mm]

Fig. 5a

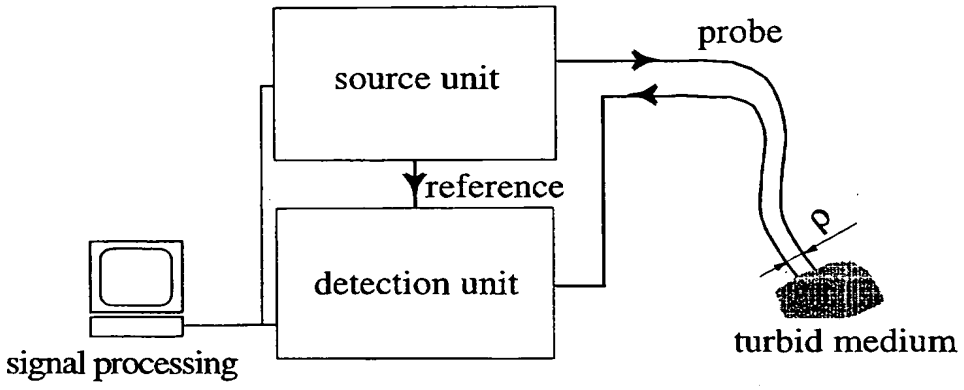
source unit
probe
reference
detection unit
ρ
signal processing
turbid medium

Fig. 5b

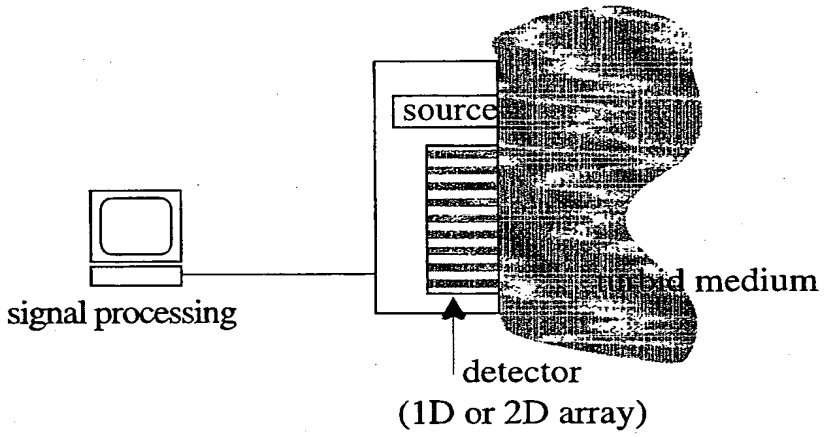
source
signal processing
turbid medium
detector
(1D or 2D array)

Fig. 5c

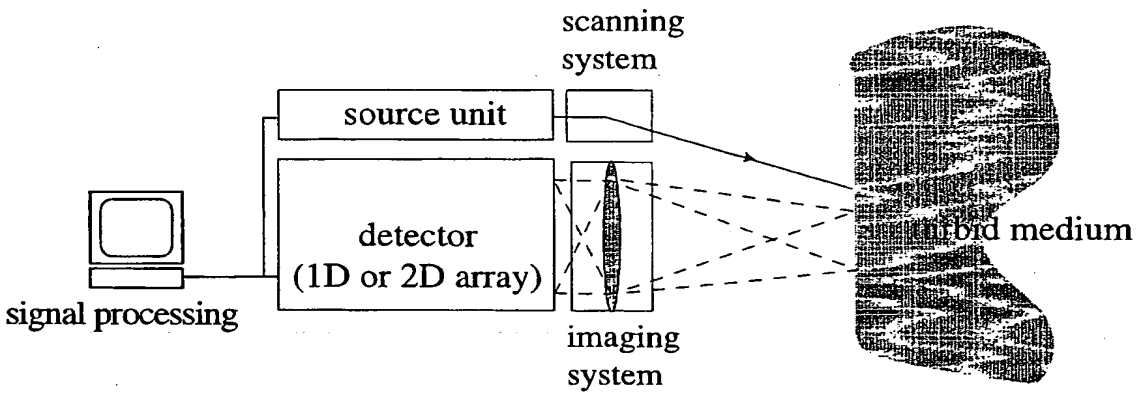
scanning
system
source unit
detector
(1D or 2D array)
signal processing
imaging
system
hybrid medium

Fig. 5d

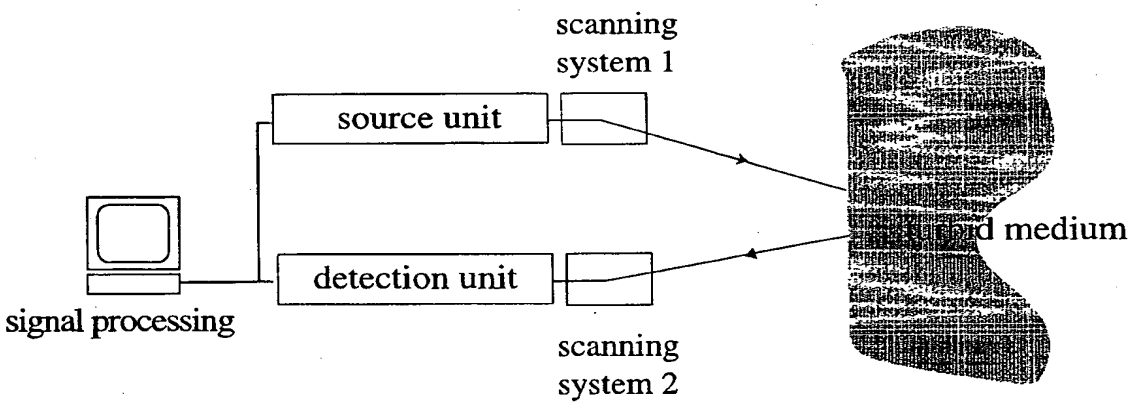
scanning
system 1
source unit
detection unit
signal processing
scanning
system 2
medium

Fig.6a

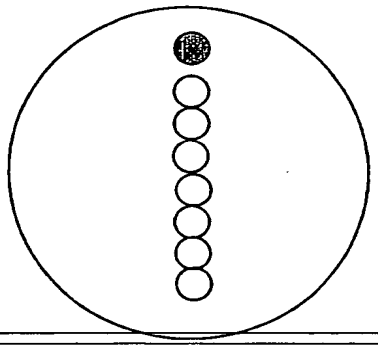

detecting fibers
illuminating fibers
or
illuminating fibers
detecting fibers

Fig. 6b

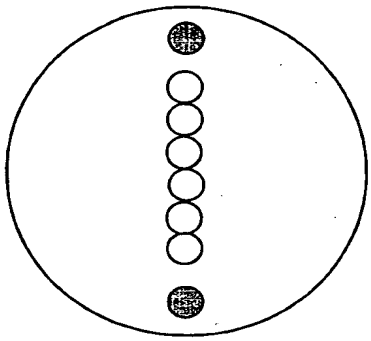

detecting fibers
illuminating fibers
or
illuminating fibers
detecting fibers

Fig. 6c

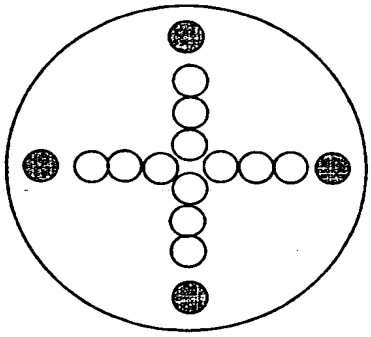

detecting fibers
illuminating fibers
or
illuminating fibers
detecting fibers

Fig.6d

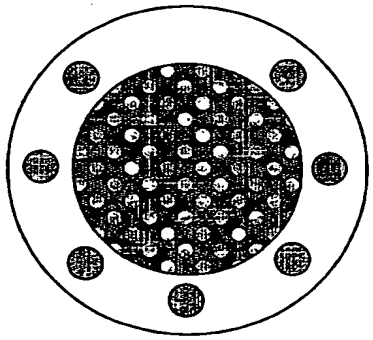

single core fiber (detection or illumination)

multicore fiber (detection or illumination)

Fig. 7

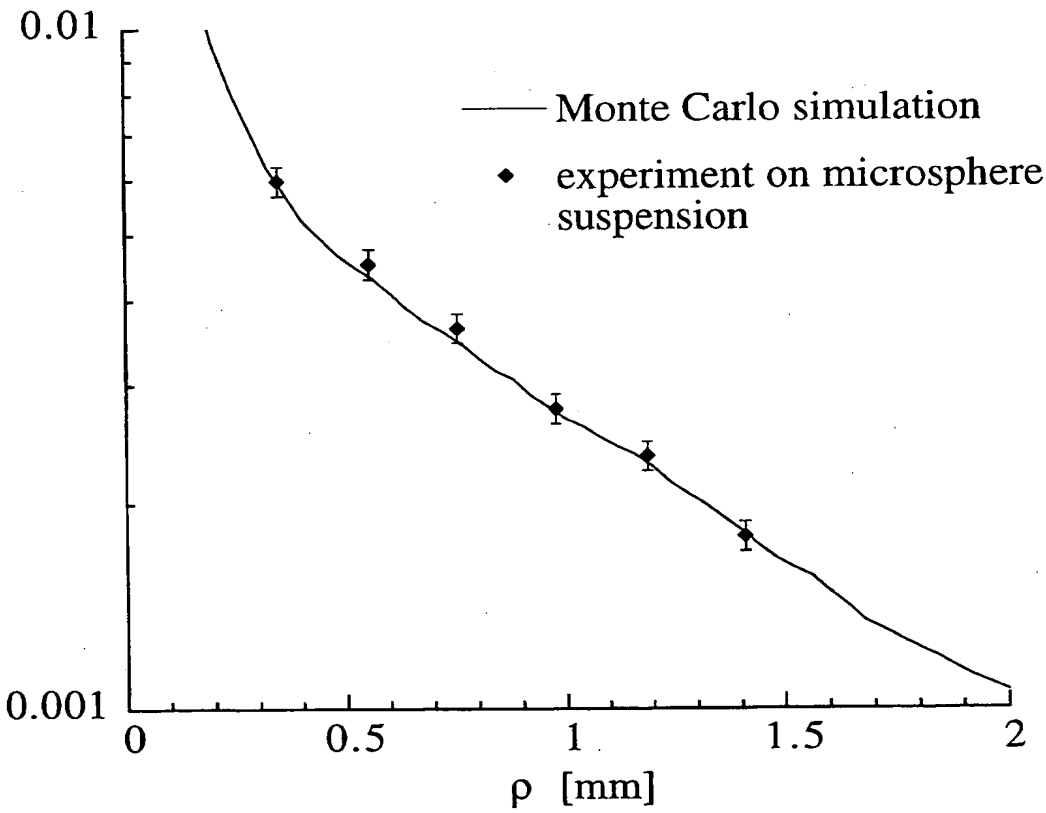
0.01
0.001
0
0.5
1
1.5
2
ρ [mm]
R(ρ) [mm^{-2}]
Monte Carlo simulation
experiment on microsphere suspension

Fig. 8

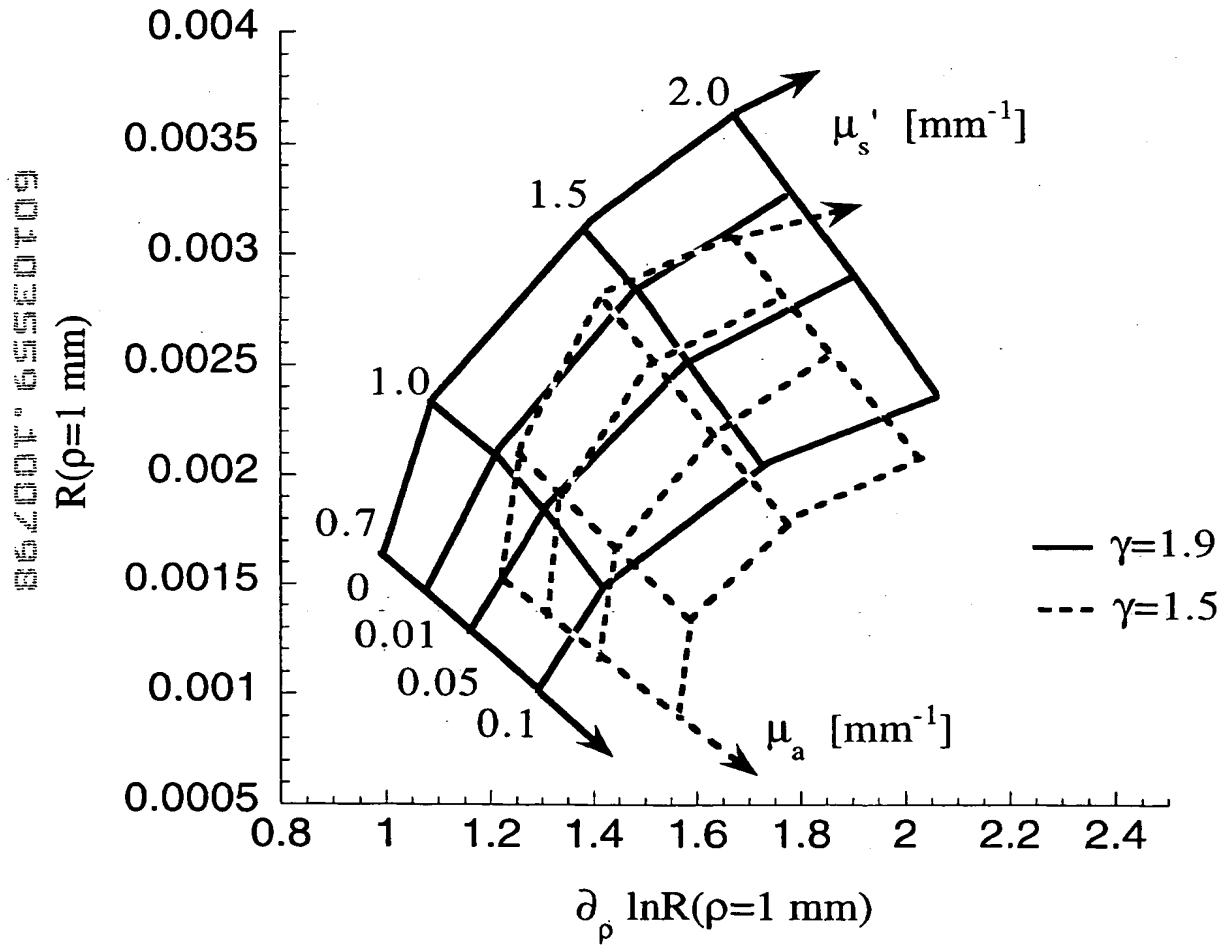
0.004
0.0035
0.003
0.0025
0.002
0.0015
0.001
0.0005
R(ρ=1 mm)
0.8
1
1.2
1.4
1.6
1.8
2
2.2
2.4
∂ρ lnR(ρ=1 mm)
2.0
1.5
1.0
0.7
0
0.01
0.05
0.1
μs' [mm-1]
μa [mm-1]
γ=1.9
γ=1.5

Fig. 9

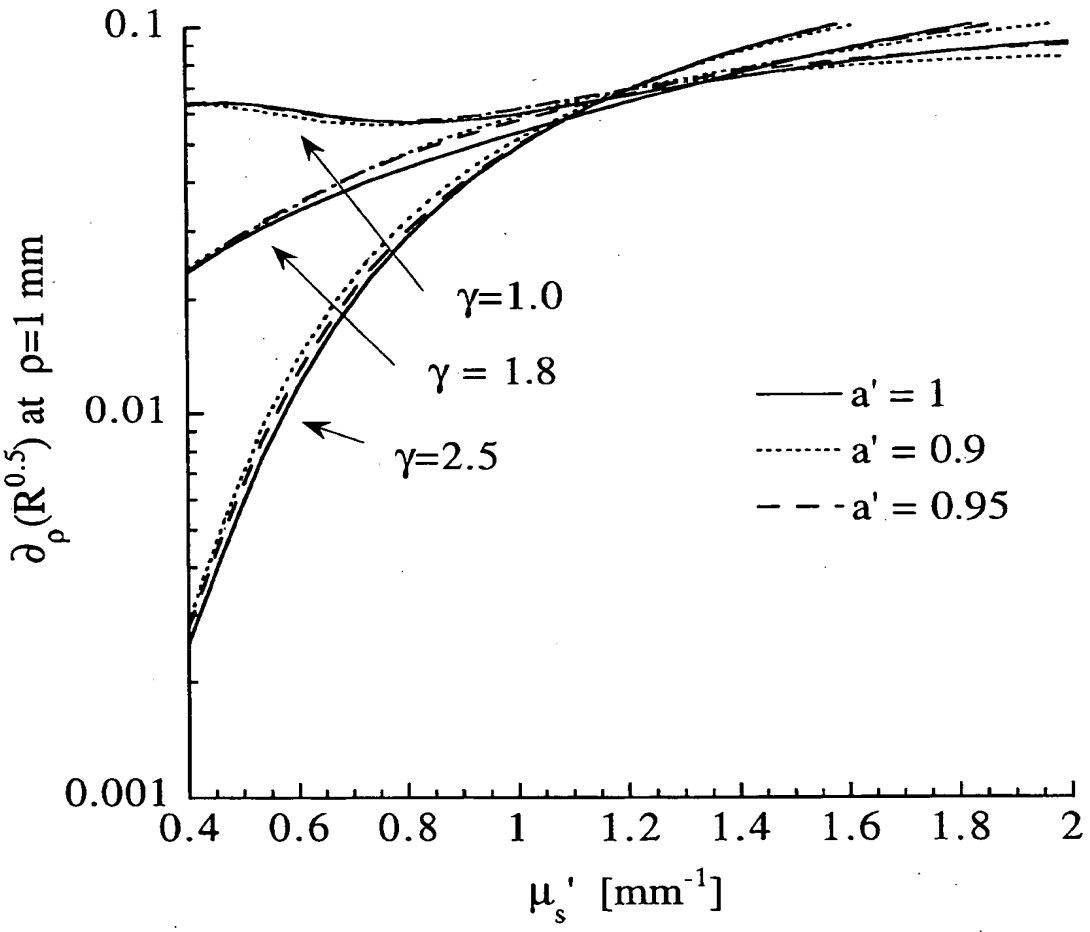
0.1
0.01
0.001
0.4
0.6
0.8
1
1.2
1.4
1.6
1.8
2
$\partial_\rho(R^{0.5})$ at ρ=1 mm
μ_s' [mm^{-1}]
γ=1.0
γ = 1.8
γ=2.5
a' = 1
a' = 0.9
a' = 0.95

Fig. 10

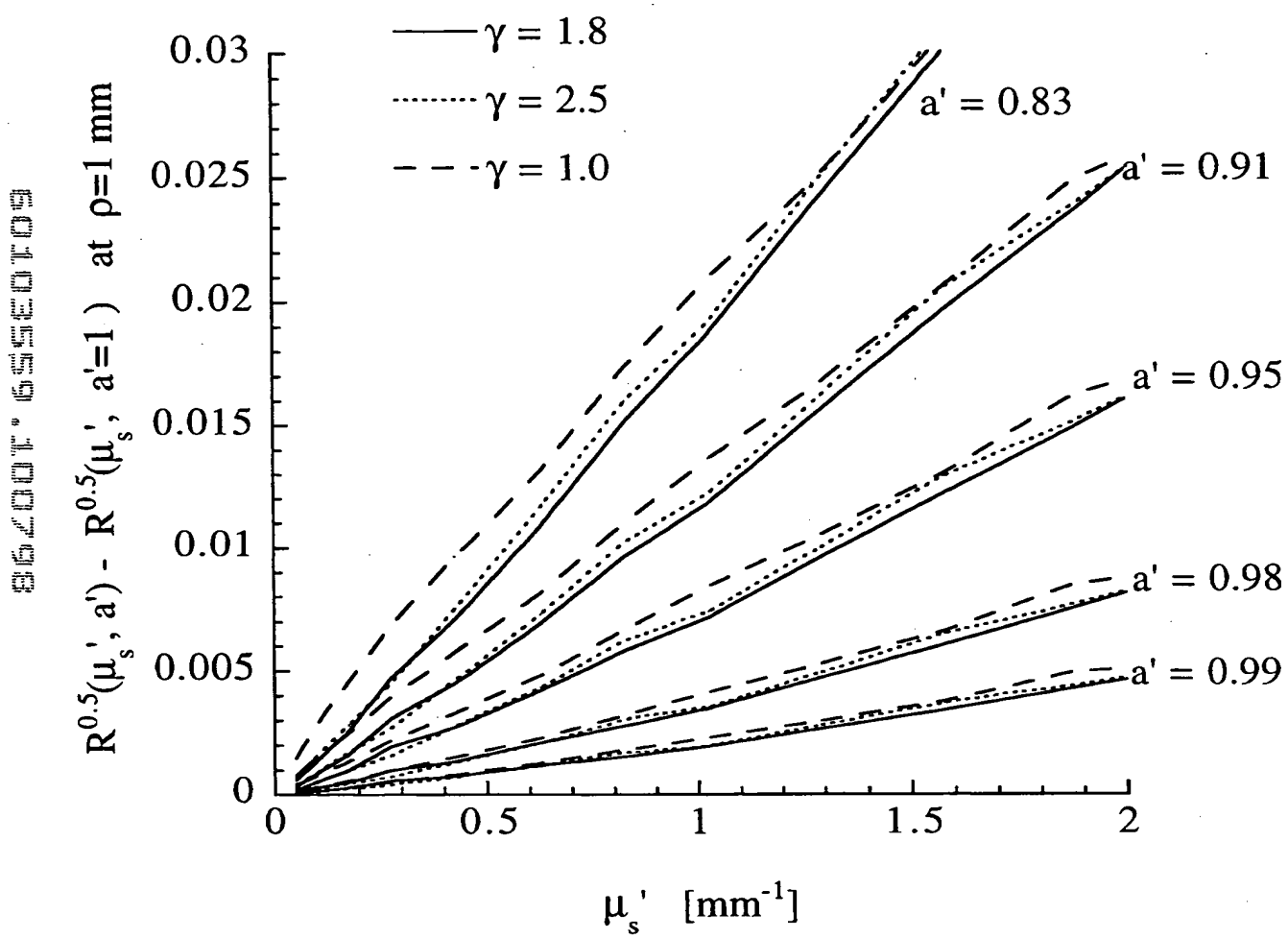
γ = 1.8
γ = 2.5
γ = 1.0
a' = 0.83
a' = 0.91
a' = 0.95
a' = 0.98
a' = 0.99
0.03
0.025
0.02
0.015
0.01
0.005
0
0
0.5
1
1.5
2
$R^{0.5}(\mu_s', a') - R^{0.5}(\mu_s', a'=1)$ at ρ=1 mm
μ_s' [mm^{-1}]

Table 2

v

type of tissues	wavelength [nm]	probe measurements			from FDPM	
		γ	μ_s' [mm^{-1}]	μ_a [mm^{-1}]	μ_s' [mm^{-1}]	μ_a [mm^{-1}]
skull	674	1.9	0.9±0.1	0.05±0.02	1.01	0.036
	849	1.9	0.9±0.1	0.05±0.02	0.82	0.038
	956	1.9	0.85±0.1	0.05±0.02	0.54	0.070
cerebellar white matter	674	1.9	1.35±0.1	0.25±0.05	1.27	0.024
	849	1.9	0.85±0.1	0.095±0.02	0.99	0.018
	956	1.9	0.78±0.1	0.090±0.02	0.75	0.043
medulloblastoma	674	1.9	1.40±0.1	0.26±0.05	1.06	0.021
	849	1.9	1.07±0.1	0.10±0.02	0.78	0.014
	956	1.9	0.4±0.1	0.075±0.02	0.56	0.038
cerebellar white matter with scar tissues	674	2.2	0.65±0.05	<0.02	N/A	N/A
	849	2.2	0.80±0.05	<0.02	N/A	N/A
	956	2.2	0.65±0.05	<0.02	N/A	N/A

PRINT OF DRAWINGS
AS ORIGINALLY FILED

United States Patent & Trademark Office

Office of Initial Patent Examination – Scanning Division

Application deficiencies were found during scanning:

☐ Page(s)_____ of No Declaration were not present for scanning. (Document title)

☐ Page(s)_____ of _____ were not present for scanning. (Document title)

☐ Scanned copy is best available.